Energy Storage and Green Hydrogen Systems in Electricity Markets: A Modelling and Optimization Framework with Degradation and Uncertainty Considerations

by

Pedro Luis Camuñas García-Miguel

A dissertation submitted in partial fulfillment of the requirements for the degree of Doctor of Philosophy in

Electrical Engineering, Electronics and Automation

Universidad Carlos III de Madrid

Advisors:

Dr. Jaime Alonso-Martínez
Dr. Manuel García Plaza

Tutor:

Dr. Santiago Arnaltes Gómez

May 2023

In the midst of winter, I found there was, within me, an invincible summer
- Albert Camus

ACKNOWLEDGEMENTS

Firstly, I would like to express my gratitude to my supervisors Dr. Jaime Alonso-Martínez and Dr. Manuel García Plaza. Also to my tutor Dr. Santiago Arnaltes Gómez and to Dr. Andrés Peña Asensio. Their guidance during these years have allowed me to produce a work I am proud of. With their effort and perseverance, they have taught me how to be a good engineer and researcher.

I would like to acknowledge to Siemens Gamesa Renewable Energy, for the financial aid for this thesis, and to Dr. Manuel García Plaza, which has helped me to carry my work in this company here in Spain and in my international mobility in Hamburg. My gratitude also to Dr. Donato Zarrilli, who welcomed me in Germany and supervised my work abroad, an experience that helped me to grow as a researcher.

Thanks to UC3M colleagues Jesús, Luis, Juan and Francisco, who accompanied me during this hard years. Also to my Siemens Gamesa colleague Jesús, for his kindness and support during my collaboration with the company.

Lastly, I am grateful to my parents, whose efforts in giving me an education have taken me to this point. To my sisters, which helped them. To Irene, whose love and support have allowed me to endure this project. Finally, to Dr. Lucian Mihet, who opened me to the world of R&D, and inspired me to take this path.

PUBLISHED AND SUBMITTED CONTENT

- Journal Papers (5):
  - Title: *Analysis of cost of use modelling impact on a BESS providing arbitrage service.*
    - Authors: Pedro Luis Camuñas, Jesús López merino, Andrés Peña Asensio, Manuel García Plaza and Santiago Arnaltes Gomez.
    - Publication date: June 2022.
    - Journal: Journal of Energy Storage.
    - Publisher: Elsevier.
    - DOI: https://doi.org/10.1016/j.est.2022.104203
    - *This material is partly included in the thesis in Chapters 2 and 3.*
    - *The material from this source included in this thesis is not singled out with typographic means and references.*
  - Title: *A Review on the Degradation Implementation for the Operation of Battery Energy Storage Systems.*
    - Authors: Pedro Luis Camuñas García-Miguel, Jaime Alonso-Martínez, Santiago Arnaltes Gómez, Manuel García Plaza and Andrés Peña Asensio.
    - Publication date: September 2022.
    - Journal: Batteries.
    - Publisher: MDPI.
    - DOI: https://doi.org/10.3390/batteries8090110
    - *This material is partly included in the thesis in Chapter 3.*
    - *The material from this source included in this thesis is not singled out with typographic means and references.*
  - Title: *Impact of risk measures and degradation cost on the optimal arbitrage schedule for battery energy storage systems.*
    - Authors: Pedro Luis Camuñas García-Miguel, Jaime Alonso-Martínez, Santiago Arnaltes Gómez and Jose Luis Rodríguez Amenedo.
    - Journal and publication date: Not published yet.
    - *This material is fully included in the thesis in Chapter 4.*
    - *The material from this source included in this thesis is not singled out with typographic means and references.*

– Title: *Mitigating Degradation Effect and Market Overlapping in Hybrid Farms: An Algorithm for Long-term Benefits.*
  * Authors: Pedro Luis Camuñas García-Miguel, Jaime Alonso-Martínez, Andrés Peña Asensio, Santiago Arnaltes Gómez and Manuel García Plaza.
  * Journal and publication date: Not published yet.
  * *This material is fully included in the thesis in Chapter 5.*
  * *The material from this source included in this thesis is not singled out with typographic means and references.*

– Title: *Modelling and optimization of green hydrogen plant for electricity and hydrogen market participation: case studies and stochastic approaches.*
  * Authors: Pedro Luis Camuñas García-Miguel, Donato Zarrilli, Jaime Alonso-Martínez, Manuel García Plaza and Santiago Arnaltes Gómez.
  * Journal and publication date: Not published yet.
  * *This material is fully included in the thesis in Chapter 6.*
  * *The material from this source included in this thesis is not singled out with typographic means and references.*

OTHER RESEARCH MERITS

- International conference Papers (2):
  - Title: *Analysis of methods to improve energy storage arbitrage benefit considering capacity degradation.*
    - Authors: Pedro Luis Camuñas, Jesús López merino, Andrés Peña Asensio, Manuel García Plaza and Santiago Arnaltes Gomez.
    - Publication date: March 2021.
    - Conference: 2021 22nd IEEE International Conference on Industrial Technology (ICIT).
    - Publisher: IEEE.
    - DOI: 10.1109/ICIT46573.2021.9453614
  - Title: *Numerical Analysis of Renewable Generation Variability for Energy Storage Smoothing Applications.*
    - Authors: Andrés Peña Asensio, Manuel García Plaza, Jesús López Merino, Fernando R Martinez Mendoza, Maciej Marek Niegowski, Pedro Luis Camuñas García.
    - Publication date: March 2021.
    - Conference: 2021 22nd IEEE International Conference on Industrial Technology (ICIT).
    - Publisher: IEEE.
    - DOI: 10.1109/ICIT46573.2021.9453635
- Patents (2):
  - Title: *Optimal energy management system solution to maximize the benefit of a hybrid farm that participates in the electrical and hydrogen markets.*
    - Authors: Andrés Peña Asensio, Manuel García Plaza, Jesús López Merino, Fernando R Martinez Mendoza and Pedro Luis Camuñas García.
    - Date: December 2020.
  - Title: *Method for the reduction of power variability in hybrid power plants with renewable generation sources and energy storage systems with minimum energy storage requirements.*
    - Authors: Andrés Peña Asensio, Manuel García Plaza, Jesús López Merino, Fernando R Martinez Mendoza and Pedro Luis Camuñas García.
    - Date: July 2020.
- Mobility (1):

- Institution: Siemens Gamesa Renewable Energy.
- Location: Hamburg (Germany).
- Responsible: Dr. Donato Zarilli.
- Period: August 2022-December 2022.

ABSTRACT

The increasing penetration of renewable energy in electrical systems requires advances in increasing their controllability. Energy Storage Systems (ESSs) are one of the solutions, since they allow the management of generated energy. Green hydrogen production systems, on the other hand, can utilize electricity to produce hydrogen. This energy carrier which can be sold for revenue generation and can be produced using Alkaline Electrolyzers (AELs).

To coordinate these systems in renewable energy plants, advanced control techniques are needed. Complex processes such as degradation, partial loading and the effect of uncertainties must be considered. These considerations add to the complexity, which can obstruct control process, hence a simplistic formulation is required.

This dissertation addresses this issue by implementing the effect of both ESS and AEL degradation into short-term planning keeping a linear formulation. Moreover, electrolyzer partial loading effect and operational states are also considered. Novel approaches in their inclusion into short-term planning for electricity market participation are proposed, analyzing their long-term economical significance.

Due to the nature of spot electricity markets, which require the commitment of energy delivery beforehand, the uncertainty of renewable source and electricity prices may affect the performance of the system. Various stochastic approaches for short-term optimization are evaluated, with the proposal of novel strategies. The long-term impact of including risk-aware strategies is also analyzed in a simulation framework, whose results indicate that conservative approaches do not necessarily yield better outcomes.

The present study commences with the modelling and formulation of a standalone ESS participating in the day-ahead market. A renewable energy source is incorporated into this model, creating a Hybrid Farm (HF) for multi-market participation. Lastly, a green hydrogen production system is also integrated, allowing the involvement in the hydrogen market. A novel algorithm for operation under uncertainties is proposed, which has been found to outperform a classical Montecarlo approach.

Throughout the research, Python was employed as the programming language of choice. The generated code has been uploaded to a public repository. Real historical data was used to validate the findings and provide a more realistic representation of the systems under study.

CONTENTS

1. INTRODUCTION

This initial chapter begins by conducting a thorough examination of the background information that is relevant to the present dissertation. It explores the recent developments in the field modeling and control of energy storage and green hydrogen systems. Moreover, this chapter highlights the current research gaps and elucidates the motivations behind this work.

Afterwards, the methodology adopted in this research study is clarified. The methods and techniques employed for data collection and analysis are detailed. This chapter concludes with a presentation of the dissertation document outline.

1.1. Background

This section presents the main working principles of electricity markets. It continues with the current state of renewable penetration in electrical systems and thus, these markets. Then, a brief introduction of ESSs and green hydrogen systems is provided. Finally, the state-of-the-art in modeling and control of energy systems is discussed.

1.1.1. Electricity markets

The operation of electricity markets is typically carried out by entities known as market operators. In the majority of liberalized electricity markets, during the opening of the market session, consumers and producers submit their bids to the market operator. The final price for electricity is determined by matching these bids [1].

The market operator plays a crucial role in the functioning of electricity market by coordinating the bids between producers and consumers. They also have the responsibility, in coordination with the Transmission System Operator (TSO) of coordinating the system power flow to ensure stability.

A majority of energy exchanges are typically conducted in the day-ahead market [2]. Within this market, negotiations for hourly energy delivery for the following day take place. These sessions are usually scheduled to occur in the day before delivery.

Intraday electricity markets allow the possibility of trading energy closer to its delivery. Usually market sessions and energy delivery occur within the same day. Iberian spot intraday electricity markets have a pricing mechanism similar to day-ahead markets, which is through discrete auctions. This type of market has gained popularity as renewable penetration has increased, since it allows for greater flexibility [3].

Lastly, real-time markets allow energy trading even closer than intraday markets. Fig-

ure 1.1 depicts an overview of the electricity market sessions and their time before delivery. The Iberian electricity market structure has been used as an example for this illustration.

Figure 1.1: Electricity markets overview.

Another important aspect is deviation management, which occurs when delivered energy differs from the original commitment. A penalty must be paid or a bonus is earned depending in the sign of the deviation and the necessities of the system at the moment. This calculations are made after the delivery.

The market operator is responsible for determining the penalties and bonuses, based on the circumstances of the market when the deviation takes place. These penalties and bonuses encourages producers to make commitments which are able to commit, and must be carefully considered in Energy Management Systems (EMSs) short term planning when participating in electricity markets.

1.1.2. Renewable energy sources in electrical systems

The incorporation of renewable energy sources is paramount in the decarbonization efforts of the economy, as they do not emit carbon dioxide. There are various technologies available for renewable energy generation, including but not limited to hydropower, tidal and geothermal energy. Among them, solar and wind power are the most prevalent technologies, constituting 54.7% of the total installed renewable capacity globally in 2021, according to the International Renewable Energy Agency [4].

EMSs play a crucial role in renewable integration. They aim to optimize the generation and consumption of energy by coordinating the different actors in the system. By improving EMSs effectiveness, profitability of renewable energy projects can be increased, thereby promoting their implementation [5].

Energy generators can generate revenues through electricity markets participation. These markets were designed for deterministic energy sources such as coal or hydropower plants [6]. The integration of wind and solar renewable energy sources, which exhibit a stochastic nature, poses significant challenges from a technical perspective.

Both solar and wind energy sources have the disadvantage of their uncertainty, challenging their participation in electrical markets. Research in the field of EMSs is focused on the development of advanced algorithms that can balance this intermittent nature. This includes the use of forecasting techniques.

1.1.3. Energy storage systems

The term ESS refers to the technology and infrastructure whose purpose is to manage the flow of energy. There are a variety of storage technologies, such as electrochemical batteries, thermal storage and pumped hydro [7]. A wide variety of services can be provided by ESS, some of them are going to be discussed in this subsection.

One of the main advantages of ESSs is their ability to support the integration of renewable sources providing grid stability. For example, they can operate as power supply when renewable energy production has been interrupted or reduced. This gives renewable generators more flexibility and allows them to behave as traditional coal or hydropower plants.

ESSs can assist in the participation of renewable sources in electrical markets, enabling delivery during peak demand or high market prices for increased revenue. This does not only support their integration in electrical systems but also increases renewable energy projects profitability, encouraging their implementation [8].

These systems can also operate independently with the purpose of trading in energy markets, through the process known as arbitrage. This service has raised interest amongst researchers lately.

Fast Frequency Response (FFR) is another service the BESS can provide. It consists in the provision or draw of energy from the grid whenever there is a mismatch between generation and consumption. A review of grid-scale projects of ESSs providing FFR is conducted by authors in [9].

As the capital costs of ESSs tends to be high, multi-stacking services has been proposed as an alternative to increase profitability [10]. A synergy exists between arbitrage and FFR service. This is because frequency response services mainly require power capacity headroom, rather than energy reserves [11].

One of the main challenges of ESSs is their high cost. The investment required for their installation can be substantial in large-scale projects. Furthermore, operation, maintenance and replacement costs can also be important.

Currently, the most widely utilized technology for ESSs is that of pumped-storage hydropower. While there exist a variety of storage technologies, electrochemical batteries have emerged as the most scalable option for grid-scale storage, experiencing significant growth in market adoption in recent years. As for 2021, there are 16GW of grid-scale battery energy storage capacity installed worldwide [12].

Lead-acid batteries are a mature technology which has been widely utilized in the past decades. However, lithium-ion batteries have gained popularity due to their longer lifetime and higher efficiency. Sodium-ion batteries are a newer technology with the potential to outperform lithium-ion in terms of costs, however they are in early development stages [13].

Degradation is a major challenge for electrochemical batteries. It reduces energy storage capacity and power output over time due to repeated charging and discharging cycles. Effective management and understanding of degradation mechanisms is needed to extend battery longevity.

1.1.4. Green hydrogen

Green hydrogen is produced through the electrolysis of water using renewable energy sources. Electrolysis involves the separation of hydrogen and oxygen atoms from water molecules using an electric current. This process emits no pollutants and yields a valuable energy carrier. As such, green hydrogen can play a crucial role in the decarbonization of the economy [14].

Hydrogen is a versatile energy carrier. It can be used as fuel for transportation or in industrial processes. Furthermore, it can be transported through existing natural gas pipelines [15].

The device used for water electrolysis is called *electrolyzer*. The main technologies available are alkaline and proton exchange membrane. Alkaline electrolysis is a more mature technology than proton exchange membrane [16]. A sketch of the hydrogen generation process is present in Figure 1.2.

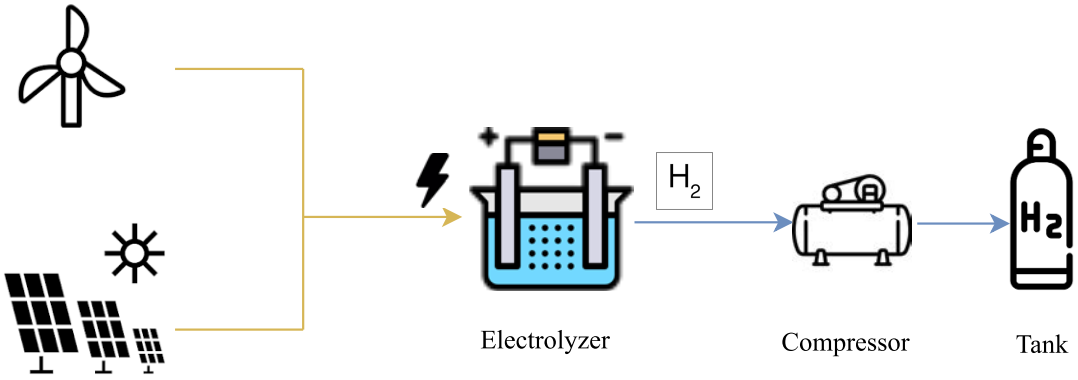

Figure 1.2: Green hydrogen generation process.

The cost of the electrolysis is still relatively high. Research efforts must be put in innovative technologies which can help to reduce the costs of green hydrogen production, in order to stimulate its implementation. Advanced control algorithms may help to reduce such costs by improving its coordination with renewable energy sources.

Intermittent renewable energy sources present challenges for operating electrolyzers, since they are an unstable power supply with inconsistent production rates. To overcome these challenges, advanced energy management strategies and optimized electrolyzer operation are necessary, along with research into more flexible and robust electrolyzer technology. Energy storage systems can also mitigate these challenges by providing a stable energy supply to the electrolyzer.

1.1.5. Modelling and control of energy management systems

An EMS is a technological solution designed to monitor and optimize the production and usage of energy. It can be applied in various settings, including renewable energy systems. Its objectives can vary and may include technical, environmental or techno-economic considerations. Common architectures are centralized, decentralized and hierarchical [17].

The design of control algorithms for EMSs necessitates the use of simulation techniques to model and evaluate a range of possible scenarios. These simulations require the use of digital copies of the systems they will be controlling. Therefore, modelling techniques have been developing in conjunction with control algorithms.

One of the main challenges for EMSs design is dealing with the system complexity. Also, the uncertainties of the input variables, such as renewable resource availability and electricity prices are something to deal with. These uncertainties are considered in this research.

Simulation models employed in this research are designed to capture the key characteristics of the systems under study. Their degree of complexity has been adjusted to meet the requirements of this research. It has been considered that excessively complex models can be counterproductive, especially in long-term process simulations.

1.2. Motivation & contributions

The viability of energy storage and green hydrogen projects is contingent upon enhancing their economic viability. To this end, EMS must optimize their operation in order to maximize project revenues. Thus, it is imperative to have a thorough understanding and effective management of degradation and uncertainties.

The integration of energy storage and green hydrogen projects necessitates the application of advanced control techniques that account for the behavior of constituent components. Additionally, it is crucial to address the uncertainties inherent in renewable energy sources and electrical markets. The utilization of simulation and modeling techniques is fundamental in comprehending the impact of these uncertainties.

Gaps have been found in recent research regarding both modelling and control of such systems. This research aims to fill such gaps by proposing novel modelling and control techniques. Simulation environments have been utilised to validate such proposals.

The main contributions of this work are:

- A new approach for the implementation of Battery Energy Storage System (BESS) degradation into short-term operation.
- Detailed studies in the role of BESS degradation incorporation in short-term operation as a techno-economical process.

- A novel stochastic optimization algorithm for renewable power plants coordinated with energy storage systems & alkaline electrolyzers participating in day-ahead electricity markets.
- A novel algorithm for hybrid renewable-storage power plants participating in multiple energy markets.

1.3. Modelling

The characteristics of the models employed in this research are dependent on their implementation. Since energy is the time-integral of power, the latter is used as input variable. It is considered that active power is constant in a resolution of hourly time periods.

The complexity of the models is constrainted to the desired range of detail for the study. Transitory phenomena, which takes place in the matter of seconds or less, is neglected. This is due to the fact that EMSs operate at relatively low temporal resolutions, such as hours, these phenomena do not have a significant impact on their performance. Therefore only low-resolution processes such as changes in stored energy or hourly hydrogen flows are modeled.

In addition to the modelling of these systems, this research places special emphasis on the degradation processes of both electrochemical batteries and alkaline electrolyzers. Degradation, which refers to a gradual loss of performance over time, is an important process to consider especially in long-term evaluations.

The incorporation of degradation into the models will help to identify the most cost-effective control strategies. This is motivated to the high replacement cost of the technologies considered in this study. This research aims to improve the assessment of the long-term effects of degradation into short-term planning.

1.4. Control

The control of energy systems is examined through the manipulation of inputs, such as active power or input current. The ultimate goal of the implemented algorithms is to optimize energy resource allocation with the aim of maximizing profitability. These algorithms also consider the dynamic behavior of the modelled energy systems.

Such techno-economic objectives are formulated as mathematical programming or optimization problems. This is a well-established approach [18]. Optimization problems are delimited in a solution space which is defined by an objective function. Within this function, techno-economic objectives are formulated to be maximized or minimized.

The solution space is delimited by optimization problems constraints. These constraints are mathematical expressions which have to be satisfied by the problem solution.

They may include physical limitations and are therefore fundamental for defining the system model.

By the use of these constraints formulation, the optimization programs aim to determine this optimal solution which is constrained by the physical limitations of the systems. The proposed control algorithms are tested by using simulation frameworks which include real data and long-term time ranges such as years.

1.5. Data collection

The use of real data for the simulation frameworks is crucial to validate the developed algorithm and models. Real-world data provides a realistic representation of the dynamic behaviour of the systems. By using it, the research can ensure that the developments are robust and can be effectively implemented in real facilities.

The data utilized in this research has been obtained from public sources, with some exceptions. The industrial nature of this research, which has been carried out in collaboration with Siemens Gamesa Renewable Energy, makes compulsory to maintain confidentiality of some of the utilised data, such as wind turbines power curves. Public sources of data, such as electricity prices, are cited whenever such data is introduced.

1.6. Siemens Gamesa Renewable Energy Collaboration

This research has been conducted in collaboration with Siemens Gamesa Renewable Energy. As part of the project *JANO-Joint Action towards Digital Transformation*. Part of the results of this study have been obtained during the development of the aforementioned project.

1.7. Generated code

The different modelling, forecasting and simulation tools developed during this research have been implemented using Python programming language. Due the extension of the generated code, an appendix displaying it has been omitted. However, a public Github repository has been created which contains all the code written during this research:

- https://github.com/Camunatas/PhD_Thesis

1.8. Dissertation outline

The dissertation document is organized as follows: Chapter 2 covers the electrochemical batteries working principles, their modelling and control. The mathematical formulation

of an optimization problem for arbitrage service is presented.

Chapter 3 introduces the degradation process of a battery storage system. A literature review in techno-economic formulations for optimization problems is conducted. A demonstration of the implementation if this process into short-term operation is provided.

In Chapter 4, the previous models are extended to incorporate uncertainties. A brief literature review on stochastic optimization techniques is introduced. A study of risk-management approaches into long-term benefits of a stationary BESS is conducted.

The stationary BESS model is incorporated into renewable power plant model in Chapter 5, conforming a HF model for electricity market participation. Iberian day-ahead and intraday electricity market rules are described. Different market participation strategies are compared in a simulation framework, with the proposal of a novel algorithm for market overlapping mitigation.

Chapter 6 introduces a green hydrogen production system into the HF. It begins describing the Alkaline Electrolyzer (AEL) working principles and a linear formulation for optimization problems. A day-ahead and real-time optimization problem is proposed, which is extended into a two-stage stochastic formulation. A novel bootstrap technique implementation is proposed to overcome the computational burden of the Montecarlo algorithm. A simulation framework is developed to compare both approaches, furthermore, different future hydrogen market and supply chain scenarios are evaluated.

This dissertation concludes with Chapter 7. In this chapter, conclusions and contributions of this research work are presented. Possible future works are also outlined.

2. DEVELOPMENT AND IMPLEMENTATION OF A GRID-CONNECTED BATTERY ENERGY STORAGE SYSTEM MODEL

This research begins addressing the modelling and control of an ESS. Electrochemical batteries are the technology considered, conforming a BESS. Hence, this chapter begins with a definition of the BESS working principles and components.

A literature review on BESS modelling is conducted afterwards. This chapter concludes with the implementation of an EMS algorithm for a grid-connected BESS. The EMS is in charge of generating commitments for trading energy in the day-ahead market.

2.1. Battery energy storage systems operation and components

This section addresses the functioning principles of an electrochemical battery. The components of a battery cell are outlined. The state variables which indicate the performance of an electrochemical battery are defined. Finally, the concept of BESS is introduced.

2.1.1. Electrochemical battery working principles

An electrochemical battery converts electric energy into chemical energy through a series of reactions. These reactions involve the transfer of electrons between two materials generating an electric current which is circulated trough an external circuit. This process is reversible, allowing the storage of electrical energy [19].

A battery is comprised of galvanic cells, where reduction-oxidation or *redox* reactions take place. In these reactions, the oxidation state of the atoms change. This state is a measure of the electrons lost or gained by the atom.

Redox reactions can be divided between oxidation or reduction reactions, depending on the way the atoms are moving. In the oxidation reaction, electrons are emitted, it can be represented as:

$$\text{Anion} \longrightarrow \text{Cation} + e^{-}$$

The anion is the oxidized form of the material, which has lost electrons, increasing its oxidation state and reaching a positive charge. The cation, on the other hand, is the reduced form of the material, which has gained electrons, decreasing its oxidation state and reaching negative charge. The reduction reaction, as opposite to the oxidation, involves the acceptance of electrons, it can be represented as:

$$\text{Cation} + e^- \longrightarrow \text{Anion}$$

These electrons come from the oxidation reaction through an external circuit. The oxidation reaction takes place in the anode, whilst the reduction reaction takes place in the cathode [19].

2.1.2. Battery cell components

A battery cell, illustrated in 2.1, consists in two main components: the electrodes and the electrolytes. An external circuit links both electrodes enabling electron transfer. Ions are transported the membrane connecting both electrolytes.

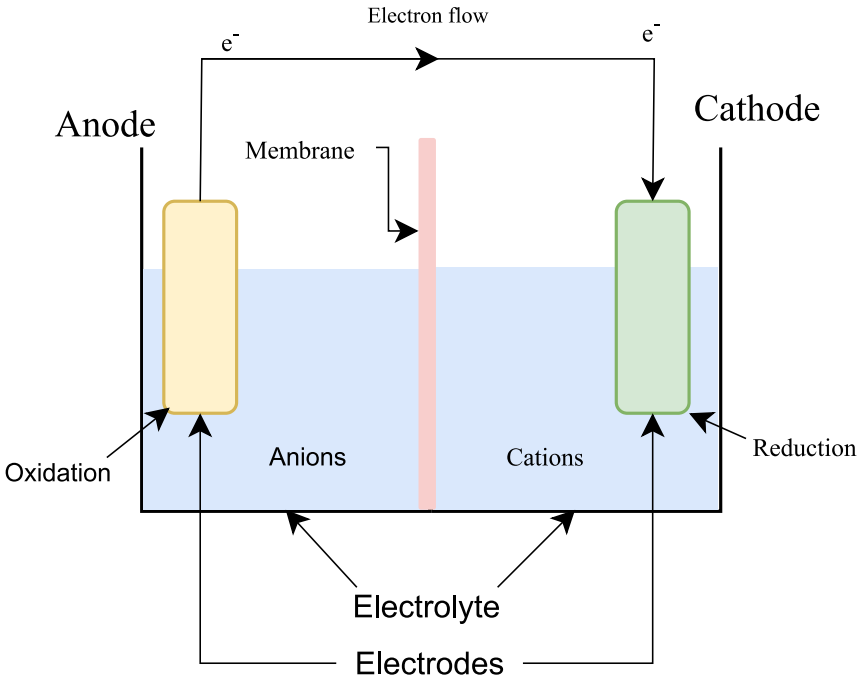

Figure 2.1: Battery cell diagram.

By allowing conductivity, the cell produces a current. The electrolytes contain the dissolved ions which participate in the redox reactions. It also serves as a barrier between both electrodes, preventing short-circuits.

2.1.3. Electrochemical battery performance

The maximum energy it is able to store, the efficiency of the energy conversion and the maximum output power are the most important measures when defining the performance of an electrochemical battery. The properties of the galvanic cells materials and their design directly influence such capabilities.

The amount of ions or *active materials* of an electrochemical battery define the maximum energy the battery can store. Moreover, the electrode surface also affects energy

capacity. The more active materials can be incorporated into the electrode surface, the more electrons can be involved in the redox reactions [20].

The rate of chemical energy converted into electrical energy is defined through the efficiency. This charge loss takes place in secondary processes, such as water electrolysis or heat losses [21].

Electrode materials conductivity and reactivity directly determine maximum output power. An electrolyte with high ionic conductivity allows for efficient ion transportation, increasing output power. The internal resistance of the components also affect the maximum power, its effect increases with battery ageing [22].

These processes directly determine the battery capabilities of providing services. They change during the battery lifetime, until they reach a certain point in which the device has to be disposed [23].

2.1.4. Battery state variables

These variables define the battery characteristics at any given time, the most important ones are:

- Voltage: The electric potential difference between the battery terminals, it is measured in volts (V).
- Current: The flow of electricity through the external circuit between electrodes, it is measured in amperes (A).
- Capacity: It is the amount of energy the battery can store and provide. It can be measured in Ampere-hours (Ah) or Watt-hours (Wh).
- State of Charge (SOC): Is the amount of energy that can be drawn from the battery at any given time, over the capacity, it can be measured in percentage or per unit.
- Power: Is the rate at which electrical energy is circulated. It is measured in watts (W).
- State of Health: The amount of useful life remaining to the device, this concept is extended in Chapter 3.

2.1.5. Battery energy storage systems

A BESS is a specific type of ESS which uses electrochemical batteries. It consists in several key components, the most important being the battery pack, the power converters, and the control systems. It is illustrated in Figure 2.2, where it is connected to a wind farm and an electrical system.

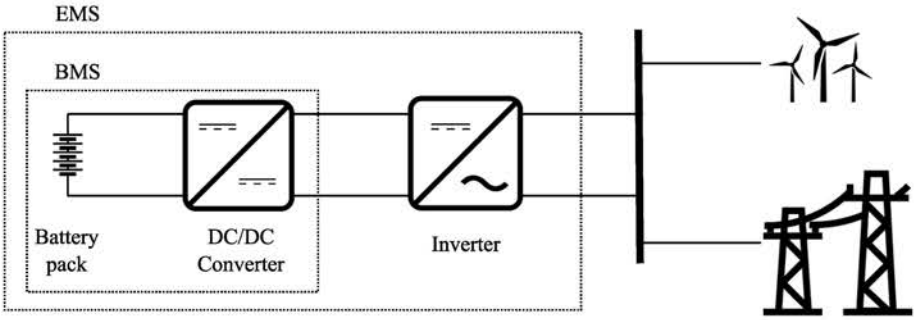

Figure 2.2: Schematic drawing of a BESS.

The battery pack operates in Direct Current (DC), therefore the implementation of an inverter is necessary in order to connect it to Alternate Current (AC) systems, such as the grid. A DC/DC converter serves as interface between the battery and the inverter to regulate the device's voltage and thus controlling its operation.

The inverter allows both the integration of the BESS with energy sources and its connection to the grid. This is because it allows to quickly adjust the output power in response to control setpoints. Furthermore, it has built-in safety and communication features, to ensure a reliable BESS operation.

The control architecture of a BESS comprises two levels: the Battery Management System (BMS) which operates at a lower level, and the EMS which operates on a higher level. The BMS is designed to monitor and control the battery pack. It controls the voltage, current, temperature and state of charge in real-time. It can also optimize performance by balancing the cells and providing diagnostics to higher control levels. Lastly, it provides protection against failures, such as overcharge, excessive temperatures and short-circuits [22].

The EMS receives inputs from the BMS and uses this information to determine the appropriate BESS operation. Besides, it is in charge of coordinating the BESS with other systems. This control architecture, with the power electronics and the battery pack, comprises the BESS.

2.2. Battery modelling

This section covers the most common approaches for electrochemical battery modelling. These models can be categorized attending at their degrees of complexity and accuracy [24]. Three main approaches have been found in the literature: the energy reservoir, the equivalent circuit and the single-particle.

Each type of model has different inputs and outputs. Most control applications use the energy reservoir model, being the latter models less used. In the following subsections, these approaches are defined.

2.2.1. Energy reservoir approach

This model considers the ESS as an energy *reservoir*. The stored energy is the result of the charge and discharge values during a period of time,. This model emulates a liquid tank, and is illustrated in Figure 2.3:

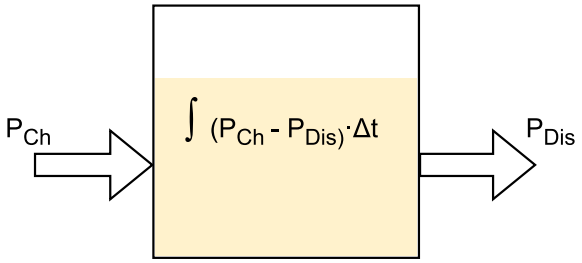

Figure 2.3: Energy reservoir model.

These models are the simplest and the most used for EMS applications due their simplicity and computational efficiency. As input, they receive the charge/discharge powers during a specific time period. Then, the stored capacity is computed in units of energy. In this case, energy is expressed in MWh, as:

$$E(t) = E(t-1) + \left(P_{Ch}(t) \cdot \xi_{Ch} - \frac{P_{Dis}(t)}{\xi_{Dis}} \right), \tag{2.1}$$

where:

- *E(t)*: Stored energy at the end of hour *t (MWh)*.
- *E(t-1)*: Stored energy at the beginning of hour *t (MWh)*.
- $P_{Ch}(t)$: Charging power during hour *t (MW)*.
- ξ_{Ch}: Charging efficiency.
- $P_{Dis}(t)$: Discharging power during hour *t (MW)*.
- ξ_{Dis}: Discharging efficiency.

ESS power is divided between charging and discharging power. This is allows implementing the efficiency in a different way in charging and discharging processes. Its linearity reduces computational complexity.

An important assumption is made in this approach. Since no input voltage is considered, the BMS acts as a black box. Therefore it is feasible only at energy-level control applications.

2.2.2. Equivalent circuit approach

This approach considers the battery as a single circuit, with a voltage source and other elements in series. Equivalent circuit models define stored energy in terms of charge (Ah). It can consider various elements, which can result in different orders of complexity, as depicted in Figure 2.4.

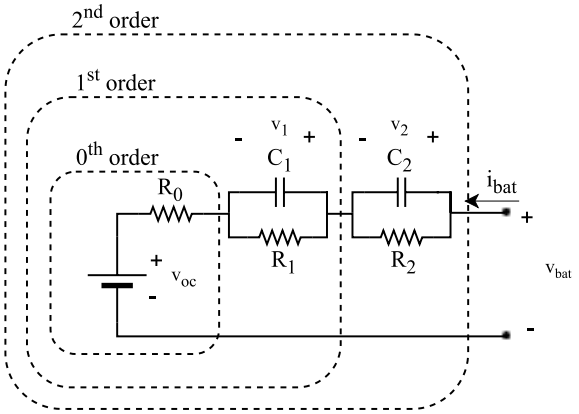

Figure 2.4: BESS equivalent circuit model.

Different terms can be omitted for the simpler models. Depending on the nature of the analysis, each order is more adequate than the others. Whilst the O^{th} is used for steady-state analysis, the 1^{st} and 2^{nd} models are used for short time-steps analysis.

The battery ohmnic resistance is represented with R_o while v_{oc} represents the open circuit voltage, v_{bat} is the voltage in the battery terminals and i_{bat} the battery current. The parallel RC elements represent different chemical reaction dynamics.

Open circuit voltage is proportional to stored charge. For the simplest model, it can be formulated as:

$$v_{oc} = v_{bat} - i_{bat}R_0. \tag{2.2}$$

The open circuit voltage when fully charged and fully discharged must be known, so it can be converted into SOC. This relationship may be not linear and it may depend on the temperature. Offline estimation methods are often utilized to obtain this correlation [25].

2.2.3. Single-particle approach

This approach use the active material concentration in the electrodes (mol/L) as a metric for available capacity. It is illustrated in 2.5. It emulates the ionic conduction and the intercalation in both the anode and cathode.

The ionic conduction consists in the movement of electrons through the external circuit and the electrolyte. Intercalation refers to the insertion of ions in the electrode ma-

terials. The concentration of electrode j as a function of time and particle radius r is represented as c_s.

These models necessitate specific cell construction information for accurate results, which manufacturers may not make available to the controller. Despite this, there are methods for estimating these parameters, which often employ machine-learning models as a basis for estimation [26].

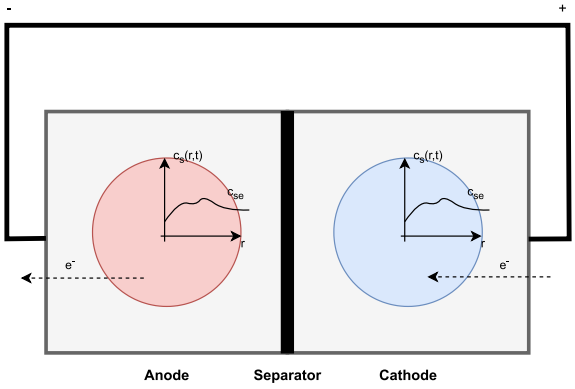

Figure 2.5: Single-particle model.

Single-Particle models consider each electrode as a single entity, providing accurate modeling of transport phenomena, but with less precision at high current levels. This type of model uses Fick's law to represent the mass balance differential equation.

SOC is a measure of the stoichiometry of a battery, wherein one electrode is at its maximum capacity while the other is at its minimum. The stoichiometry at one electrode is always inversely proportional to that at the other electrode. Being the stoichiometry the relationship between the amount of redox reactions reactants and products.

The open circuit voltage of the battery is determined by the surface concentrations of the active materials at the electrodes. When is fully charged, the anode exhibits the maximum active material concentration, while the cathode exhibits the minimum concentration [26].

2.3. Optimization model implementation

This sections demonstrates an implementation of a grid-tied BESS model providing arbitrage service. The formulation is suited for a Mixed-Integer Linear Programming (MILP) model. This is a class of optimization models that combine both continuous and discrete decision variables.

MILP models formulation consists in linear expressions on both constraints and objective functions. The decision variables can be continuous or integer-valued. The latter enables the definition of discrete states for the device, which can be very useful for physical systems modelling.

This subsection is divided into three main parts. The first one introduces the optimization model constraints. The second one describes the objective function. Lastly, a simulation of this implementation is presented.

Model constraints

The constraints of the optimization problem demarcate the solution space to the physical boundaries of the device. They are formulated as follows:

1. The BESS cannot be charged over its nominal power:

$$P_{Ch}(t) \leq P_{Nom} \cdot ND(t), \tag{2.3}$$

   where:

   - $P_{Ch}(t)$: Charging power during hourly period t *(MW)*.
   - P_{Nom}: Nominal power *(MW)*.
   - *ND(t)*: a boolean variable whose value is 1 when it is not discharging at period t.

2. The BESS can't discharge over its nominal power:

$$P_{Dis}(t) \leq P_{Nom} \cdot NC(t), \tag{2.4}$$

   where:

   - $P_{Dis}(t)$: Discharging power during hourly period t *(MW)*.
   - P_{Nom}: Nominal power *(MW)*
   - *NC(t)*: a boolean variable whose value is 1 when it is not charging at period t.

3. Charging power is always positive:

$$P_{Ch}(t) \geq 0, \tag{2.5}$$

4. Discharging power is also always positive. This sign criteria is kept for simplicity on the optimization algorithm:

$$P_{Dis}(t) \geq 0, \tag{2.6}$$

5. The BESS cannot be charged and discharged simultaneously:

$$NC(t) + ND(t) \leq 1. \tag{2.7}$$

6. The resulting BESS power at period t is computed for convenience as follows:

$$P_{Bat}(t) = P_{Dis}(t) - P_{Ch}(t), \tag{2.8}$$

7. The energy stored at the end of the period equals the amount stored at the end of the previous hour and the charged/discharged energy considering efficiencies. Since active power is considered constant during each time period, it can be considered as energy:

$$E(t) = E(t-1) + \left(P_{Ch}(t) \cdot \xi_{Ch} - \frac{P_{Dis}(t)}{\xi_{Dis}}\right), \tag{2.9}$$

where:

- *E(t)*: Stored energy at the end of hourly period *t (MWh)*.
- ξ_{Ch}: Charging efficiency *(%)*.
- ξ_{Dis}: Discharging efficiency *(%)*.

8. The SOC at $t = 0$ is the initial SOC, SOC_{init}, set by the user (by default 0)

$$SOC(0) = SOC_{init}, \tag{2.10}$$

Objective function for energy arbitrage in the day-ahead market

The following objective function seeks to maximize the income:

$$Max\left\{\sum_{t=1}^{24} Price(t) \cdot P_{Bat}(t)\right\}, \tag{2.11}$$

where:

- *Price(t)*: Energy price during hourly period *t (€/MWh)*.
- $P_{Bat}(t)$: Power during hourly period *t (MW)*.

The optimization process outcome is a 24 charge/discharge operations vector, one for each hour of the day. These operations are then submitted to the market operator as hourly bids for the following day. It is assumed that the market accepts all bids.

Implementation results

For simplicity, it is assumed that electricity prices are known before submitting the bids, which may not be the real case. In a more realistic scenario, price forecasting is necessary. This aspect will be addressed in the following chapters, in which the uncertainties of real prices are addressed with an extension of the current implementation.

For this implementation, a battery with the parameters indicated in Table 2.1 is considered. These parameters have been chosen arbitrarily. Hourly Iberian day-ahead market electricity prices for January the 19^{th} 2017 are used as input.

Table 2.1: BESS parameters.

Parameter	Value
Nominal capacity	50 MWh
Maximum power	12.5 MW
Charging efficiency	95%
Discharging efficiency	90%

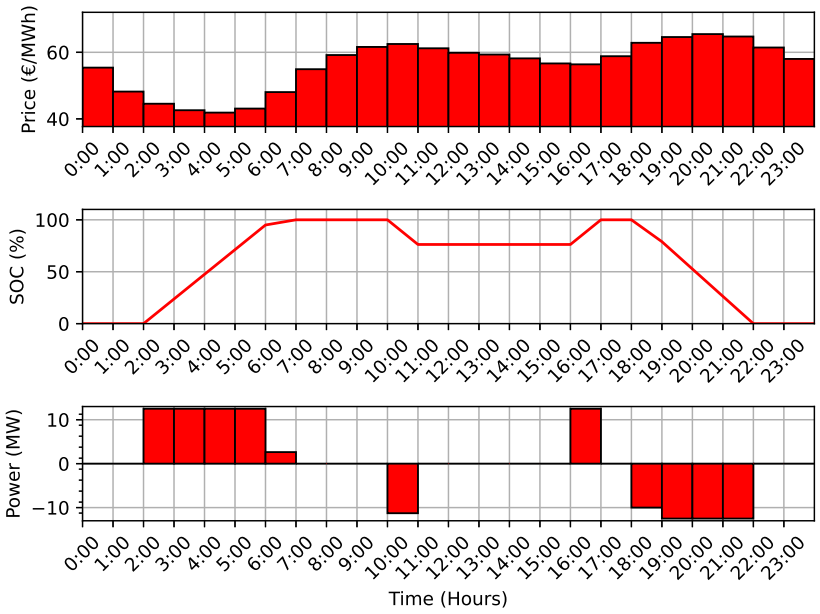

Figure 2.6: Daily arbitrage program.

Results are shown in Figure 2.6. The input electricity prices have been displayed. It is followed by the SOC during the day, and the BESS input powers. It is considered that input power is positive for charging and the opposite for discharging.

As illustrated BESS begins charging during the early hours of the day, specifically from 2:00 to 6:00 AM, when electricity prices are at their lowest. The BESS then marginally discharges at 10:00 AM and recharges at 16:00 PM, taking advantage of the lower afternoon prices. Finally, it fully discharges from 17:00 to 22:00 PM in order to use the peak electricity prices during this time period. The relationship between power and capacity heavily influences this behaviour, since it measures the amount of hours it is capable of be charging or discharging.

2.4. Chapter conclusion

In this chapter, the functioning principles of BESS have been introduced. Different modelling techniques with an example of implementation has been presented. This implementation is the short-term operation of a BESS participating in the day-ahead market.

In the following chapter, the degradation processes of an electrochemical battery are presented. The model implemented in this chapter is extended to consider degradation as a cost in short-term operation, in order to increase long-term benefits by extending battery's useful life.

3. INCORPORATING DEGRADATION EFFECTS IN SHORT-TIME PLANNING

The loss of performance over time is a process usually caused by device usage. Is is very important to consider when defining EMS control strategies. Reducing degradation can extend the device's lifetime, thus increasing long-term benefits.

This chapter addresses the degradation process of electrochemical batteries and its impact on EMS control algorithms. A literature review of different approaches is introduced. Finally, an extension of the optimization formulation introduced in Chapter 2 is proposed, incorporating degradation as a cost in the operation of the grid-connected battery ESS.

The chapter outline is as follows: First, it describes the main factors on electrochemical batteries degradation. Then, a literature review on degradation modelling and its incorporation into short-term planning is carried out. Lastly, the BESS model presented in the last chapter is extended to consider this ageing process.

3.1. Electrochemical batteries degradation

The degradation of an electrochemical battery can carry out a loss of available capacity, efficiency or maximum output power [27]. This can be caused by usage, thus, understanding the mechanisms of degradation and considering them in short-time planning can help to mitigate this performance loss. When degradation is caused by usage, it is named *cycling* degradation, then it is caused by the pass of time, it is named *calendar* degradation.

The deterioration of an electrochemical battery is a multifaceted phenomenon resulting from various factors. The electrodes are particularly susceptible to degradation. The formation of a layer known as the Solid Electrolyte Interphase (SEI) on the negative electrode being identified as a primary contributing factor [28].

The loss of active materials leads to the loss of available capacity. Maximum output power is reduced by a loss of passive films [23]. Cycling degradation can be reduced by controlling different aspects of the operation:

- Cycles Depth of Discharge (DOD) [29].
- Circulated current [30].
- Ambient temperature [31].
- SOC (for calendar degradation) [32].

Temperature has been neglected in control applications with the assumption that the

battery operates in a controlled environment which maintains it at a safe range, this is very common in stationary applications at grid-scale level [31].

3.2. Modelling of battery degradation

This section reviews the degradation models available in the literature. First, it describes the state variable SOH, already mentioned in Chapter 2 which is used to measure the accumulated degradation. Then, it reviews the most common approach for battery ageing modelling.

3.2.1. State of health

The SOH is the most used indicator for battery performance measuring. It can be defined as the proportion of available capacity over its nominal value [33]. Other factors such as maximum output power and efficiency can be utilized in its definition, but capacity is the most used one. A common formulation is (in per unit):

$$SOH = \frac{Cap_{Av}}{CaP_{Nom}} \cdot 100, \tag{3.1}$$

where:

- SOH: State of Health *(%)*.
- Cap_{Av}: Currently available capacity *(MWh)*.
- CaP_{Nom}: Nominal capacity *(MWh)*.

When SOH reaches a certain value, the battery reaches its End of Life (EOL). In some works, EOL is considered when SOH reaches 80% [34], [35]. A SOH of 60% is contemplated in others [36].

This relationship between SOH, EOL and capacity is motivated because when available capacity reaches certain point, it starts fading faster [37].

3.2.2. Literature review on degradation modelling approaches

There is a wide variety of degradation models available in the literature. They differ mainly in their complexity and accuracy, as with the BESS models. More complex models allows a more detailed emulation of the degradation process, however they have a computational burden which may cause trouble during long simulations [38].

Ampere-counter approach

The simplest approach is the Ampere-counter or cycle-counter. It is based on the assumption that the battery can perform a limited amount of full cycles during its lifetime. As input, it receives the energy cycled during a time period [30]-[39]. It can be formulated as follows:

$$\Delta SOH(t) = \frac{|P(t)|}{n_{Cycles} \cdot 2CaP_{Nom}} \cdot 100, \tag{3.2}$$

where:

- $\Delta SOH(t)$: State of health lost during hour t *(%)*.
- $|P(t)|$: Absolute value of the power during hour t *(MW)*.
- n_{Cycles}: Number of cycles before reaching EOL.

Considering that input power has been constant during hour t, it transforms circulated energy in equivalent cycles. Then it computes the relationship between the amount of equivalent cycles during hour t as the fraction of lifetime cycles. It is the simplest approach, but it neglects other degradation factors.

DOD-cycles approach

As described previously, the cycle DOD has an impact in the ageing process. This approach employs the relationship between cycle DOD and lifetime cycles, which is usually provided by the manufacturer [40]-[29]. An example is illustrated in Figure 3.1.

Since it is a non-linear relationship, it is usually transformed into a piecewise linear function, as in [42]. Another strategy consists in using fitting techniques, as in [43], however this approach comes with a loss in accuracy.

A prevalent issue with this methodology is determining the partial cycle DOD. To address this challenge, A Rainflow Counting algorithm can be utilized [44], [45]. This algorithm allows to compute partial cycles into full cycles, enabling the use of this degradation model approach into optimization problems.

Other approaches

The use of an equivalent circuit model allows to a different approach in degradation modelling. As presented in Chapter 2 a voltage source emulating open-source voltage in series with a resistor emulating internal resistance are the most basic elements. This resistor can be employed to model the available power loss over time [46].

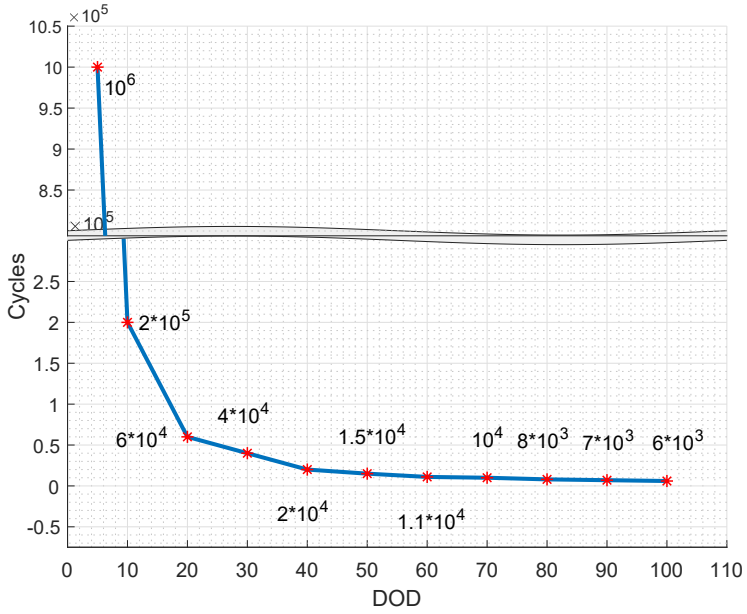

Figure 3.1: Relationship between DOD and useful life [41].

Ultimately, electrochemical-based models are among the less commonly utilized models. In this category, the physics-based Single Particle (SP) model is the most common [47]. Authors in [38] conclude that these models can be very precise, however their complexity is a hindrance for long-term simulations.

3.3. Literature review on battery degradation in optimization problems

The incorporation of degradation into short-term BESS operation is a complex issue that has yet to be fully addressed in the literature. A diversity of strategies have been proposed to consider this process, however, no clear consensus has emerged yet. Furthermore, the topic of degradation in BESS operation has only been briefly discussed in most works.

In this section, a critical literature review of the techno-economical formulations of degradation into short-term operation is performed. A classification of the different approaches is depicted in Figure 3.2. The different categories are presented and discussed separately.

As it can be seen, the main distinction is between the use of constraints in the optimization problem and the use of a cost of use in the objective function. The former utilizes the constraints to consider degradation processes, the latter implements techno-economic effect of degradation in the problem.

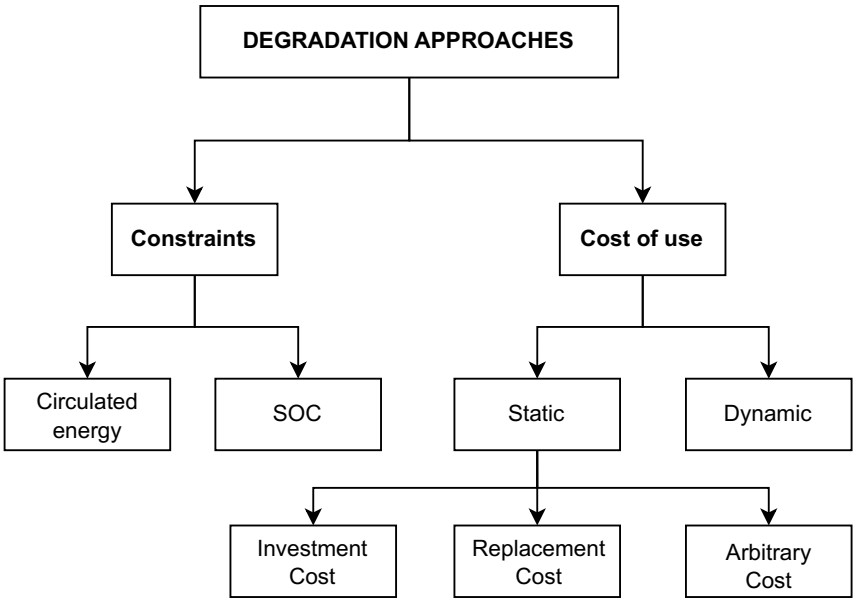

Figure 3.2: Classification of degradation incorporation.

3.3.1. Constrained approaches

From the EMS perspective, BESS control process is carried out by means of a constrained optimization model [48]. Constraints in the form of equalities or inequalities, which enclose the solution space, often represent the physical boundaries of the system. As mentioned in the previous section, DOD and circulated current are some of the main causes of cycling degradation [49].

In the constraints-based strategies, these two magnitudes are restricted in the optimization model constraints, resulting in a reduced degradation. Nevertheless, they are less reliable since the link between the imposed limits and the resulting profits is weaker than in other alternatives. They are less common than the cost of use approaches presented in a later subsection.

Circulated energy restriction

These strategies restrain the circulated energy or current during the optimization period. The premise is to divide the circulated energy by the battery capacity to obtain the number of equivalent cycles. An inequality constraint limits the maximum amount of circulated energy, Equation (3.3) shows the typical expression:

$$EC \leq EC_{Max}, \tag{3.3}$$

where:

- EC: Equivalent cycles during the optimization period.

- EC_{Max} : Maximum equivalent cycles allowed during optimization period.

Authors in [50] present an empirical study of circulated current reduction effect in a BESS performing arbitrage during 14 years. By iterating the circulated current restriction they obtain the amount of cycles a day the BESS should perform for maximum benefits. This approach fails to consider how cycle profitability changes from one day to another.

In [51], cycle and calendar losses are considered. Degradation process is controlled by both oversizing the battery capacity and using a constraint. Afterwards, the constraint is added to the proposed optimization problem limiting daily cycles which is similar to the approach found in [50].

SOC restriction

In this approach, the restriction is applied to the energy stored in the BESS which is limited to a certain level. An example can be found in [32]. This restriction can be formulated as in (3.4):

$$SOC_{Min} \leq SOC(t) \leq SOC_{Max}, \tag{3.4}$$

where:

- SOC_{Min}: Minimum SOC.
- $SOC(t)$: SOC energy during hour t.
- SOC_{Max}: Maximum SOC.

Controlling degradation by setting SOC boundaries during operation presents the same disadvantages as restricting circulated energy. It modifies the operation without considering the service profitability during the optimization period. Nevertheless, the implementations are simple and straightforward.

3.3.2. Cost of use approaches

An alternative to restricting operation in the model constraints is to use the objective function. One advantage of these strategies is that they take into account the optimization problem inputs, which play a crucial role in determining the profitability of the service. The term *cost of use* refers to the way degradation is reflected into the objective function, which is a cost of using battery. For example, in the case of arbitrage of a standalone BESS in the day-ahead market, the objective function can be depicted as [52]:

$$Max\left\{\sum_{t=1}^{24} \pi_{DM}(t) \cdot \left(E_{Dis}(t) - E_{ch}(t)\right)\right\}, \tag{3.5}$$

where:

- $\pi_{DM}(t)$: Energy price during hourly period t *(€/MWh)*.
- $E_{Dis}(t)$: Discharged energy during hourly period t *(MWh)*.
- $E_{ch}(t)$: Charged energy during hourly period t *(MWh)*.

The objective function expressed in (3.5) aims to maximize benefits by purchasing energy at lower prices and selling it at higher prices. By implementing a cost related to cycling degradation, the following expression is obtained:

$$Max\left\{\sum_{t=1}^{24}\pi_{DM}(t)\cdot\left(E_{Dis}(t)-E_{ch}(t)\right)-C\right\}, \tag{3.6}$$

where:

- C: Cost of use *(€)*.

The implementation of this strategy allows for the restriction of BESS operation to instances where the expected profits are greater than the estimated cost of degradation. In situations where the price spread is low, the operation of the BESS will be curtailed until the cost of use is lower than the benefits. This approach enables the flexibility to adjust the impact of degradation in accordance with the profitability. A similar approach is to implement degradation effect as a reward within a reinforcement learning algorithm, such as in [30].

As it can be seen in (3.6), the objective function is expressed in economical units. Expression (3.1) shows how degradation is expressed in a different way. Therefore, a conversion must be made in order to implement it into the objective function. Researchers propose different ways for expressing degradation as an economical quantity. All procedures follow expression (3.7):

$$Deg_{Cost} = \Delta SOH \cdot SOH_{Cost}, \tag{3.7}$$

where:

- Deg_{Cost}: Cost of degradation.
- ΔSOH: State of Health loss.
- SOH_{Cost}: Cost of SOH lost *(€)*.

It is considered that an amount of lifetime expended due to degradation can be understood as an economical cost. The SOH_{Cost} factor quantifies the relationship between this degradation and the resulting cost. Cost of use approaches can be divided into different categories depending on how SOH_{Cost} is defined.

Static approaches

Static approaches are by far the most commonly used in the literature. In this category, the factor SOH_{Cost} is constant throughout the BESS lifetime. This assumes that degradation has the same cost at the start and at the end of life of the system.

Methodologies of this category can be distinguished attending to how the constant factor is obtained. The most common is to consider that it depends on the capital cost. This perspective considers that degrading the battery causes a cost proportional to the investment. Such approach is used, for example, by authors in [53] or [54].

The idea behind using the capital cost is to amortize the investment. However, since current battery prices make arbitrage not profitable [52], considering SOH_{Cost} equal to the investment cost may lead into an excessive degradation cost. When costs of ageing surpass any possible possible profitability, the BESS will never operate. This is the main disadvantage of implementing this degradation cost. It is common in the literature to consider only an arbitrary fraction of the investment cost to solve this issue, as in [43], which is something difficult to justify. Besides this, capital costs are sunk costs and, therefore they should not affect operation.

Another approach consists in using the costs of battery replacement. The idea behind this is that since the investment is already made, the operation should seek to amortize the replacement of the next battery. Unlike using capital cost, this method considers that future payments can affect operation. The method for setting the replacement cost varies between authors.

In [55] the impact of diverse replacement costs in profitability is studied. Authors in [44] propose a method to discount the replacement cost to their present value. This perspective has the disadvantage that future replacement costs are unpredictable. Technical reports such as [56] may give a perspective of how these costs will evolve, but a long-term prediction is always uncertain.

Finally, there are authors which consider that SOH_{Cost} is an arbitrary value. In some works, the degradation cost of use is even used as a fixed penalty unrelated to expected degradation. For example in [57] this penalty is set at 10 \$/MWh. An interesting study is done in [52] in which a parameter sweep for the costs of use is made, to obtain the value which returns the highest Net Present Value (NPV) for the project. In this case, it is uncertain if it will be possible to extrapolate that optimal value to a different system, a different market, or even a different time frame for the same system.

Dynamic approaches

The use of a dynamic cost of use considers that the value of degradation changes during project lifetime. Literature using dynamic approaches is remarkably scarce. An example is found in [58]. In this work a battery is coupled to a generation system, the grid and a

residential customer which acts as a load. Authors of this work consider that the battery looses value during its lifetime. This value is formulated as:

$$V = \frac{\nu}{D}, \tag{3.8}$$

where:

- V: Current battery value *(€)*.
- ν: Cumulative value *(€)*.
- D: Accumulated degradation.

The cumulative value is defined as the overall value added to the system in comparison to the business-as-usual case in which no BESS is present. As the accumulated degradation increases, the cost of use will decrease, resulting in an increased usage of the BESS. The enhancement of the cumulative value is contingent upon the usage conditions. Authors in [58] state that empirical results indicate a convergence of battery value at the first weeks. But it changes with operation conditions, such as users load profile.

3.4. Incorporation of degradation process into short-term operation

This section describes the conventional implementation of degradation cost, utilizing a DOD-cycles based degradation model, which is widely adopted in the literature. The model is applied to the standard optimization problem of a grid-connected BESS participating in arbitrage service.

In this case, the SOH_{Cost} takes the value of the capital costs. To demonstrate the short-term impact of this degradation cost approach in short-term operations, various cases of capital costs are considered.

3.4.1. DOD-based degradation model formulation

For simplicity, it is assumed that the BESS does not undergo more than two cycles per day, as proposed in [24]. This assumption is reasonable, since a typical daily energy price curve has two peaks. However, this method can be extended to accommodate more cycles.

Additionally, it is assumed that no energy is stored for the following day and that the BESS begins and ends its operation in an empty state, thus allowing for the approximation of DOD as SOC. The daily DOD for both cycles is calculated using the amount of energy discharged, as expressed in the following equation. This formulation considers that active power during each time period is constant hence it can be considered as energy:

$$DOD_{Tot} = \Delta SOC_{Tot} = \sum_{h=1}^{24} \frac{|P_{BESS}(t)|}{2 \cdot E_{Nom}}, \tag{3.9}$$

where:

- DOD_{Tot}: Total daily DOD in pu.
- ΔSOC_{Tot}: Total daily SOC variation.
- $P_{BESS}(t)$: BESS power during hourly period *t (MW)*.
- E_{Nom}: BESS nominal capacity *(MWh)*.

It is assumed that the first cycle reaches the maximum daily DOD, given the SOC levels during the cycle. The DOD for the second cycle is calculated by subtracting the energy consumed in the first cycle from the total energy discharged. This approximation allows for a straightforward implementation in a linear optimization problem. The calculation is formulated as follows:

$$\begin{cases} DOD_1 &= SOC_{Max} - SOC_{Min} \\ DOD_2 &= \min(DOD_{Tot} - DOD_1, DOD_1) \end{cases} \tag{3.10}$$

where:

- SOC_{Max}: Maximum daily SOC.
- SOC_{Min}: Minimum daily SOC.
- DOD_1: DOD of first cycle.
- DOD_2: DOD of second cycle.

The SOH loss is computed using equation (3.11), which incorporates the DOD-cycles relationship depicted in Figure 3.1.

$$\Delta SOH = \sum_{c=1}^{2} \frac{1}{N_{Cyc}(DOD_c)}, \tag{3.11}$$

where:

- Δ SOH: SOH lost.
- $N_{Cyc}(DOD_c)$: Cycles at each DOD before End of Life (EOL).

3.4.2. Degradation cost formulation

In this example, capital costs are utilized to quantify the economic impact of degradation costs, as is the most prevalent approach in the literature. Therefore, the degradation cost quantification formulated in (3.7) is applied here. The SOH_{Cost} factor takes the value of the BESS capital costs.

3.4.3. Optimization problem formulation

The optimization model builds on the one outlined in equations 2.3 to 2.10. The degradation process is incorporated as a piecewise constraint using the formulation discussed in the previous subsection.

The objective function is based on expression (3.6), adapted for this specific implementation of the optimization problem. The output of this optimization model is a vector of 24 charge-discharge operations.

$$Max\left\{\sum_{t=1}^{24}\pi(t)\cdot P_{Bat}(t) - Deg_{Cost}\right\}. \tag{3.12}$$

3.4.4. Simulation results

The optimization problem and degradation cost approach outlined above are used in a simulation of a single day of arbitrage operation. The parameters of the BESS are provided in Table 3.1.

To demonstrate the effect of various capital costs on short-term operation, multiple costs of use are implemented for the same day in the simulation. These costs, represented in €/kWh of nominal capacity, are incorporated into the simulation using expression (3.7). Additionally, the scenario of zero capital costs, which effectively eliminates costs of use, is also considered as a base case in the evaluation.

Table 3.1: BESS parameters.

Parameter	Value
Capacity	10 MWh
Nominal power	5 MW
Efficiency	95%

The simulation utilizes historical electricity prices from the Iberian day-ahead market, specifically the prices from April 4th, 2018. The results of the simulation are depicted in Figure 3.3 and take into account the SOC in various simulation cases.

As depicted in the figure, the market price exhibits two peaks. In the scenario where degradation costs are not taken into account, the BESS carries out two full cycles, utilizing these peaks. As capital costs increase, the cost of battery degradation also increases. As a result, the optimization algorithm reduces the depth of the cycles for two reasons: First, to widen the price spread so that the profit exceeds the degradation cost, and second, to decrease the degradation as shown in Figure 3.1.

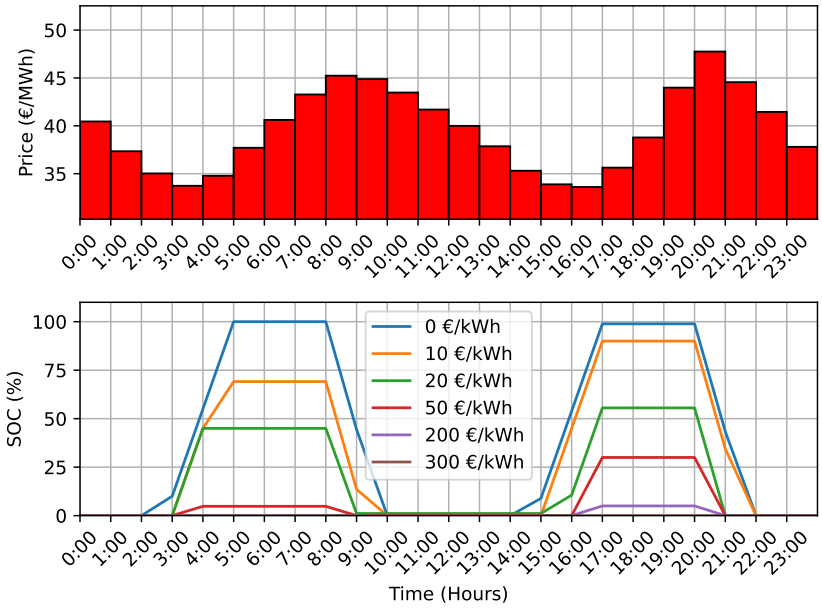

Figure 3.3: Daily operation results for different capital costs.

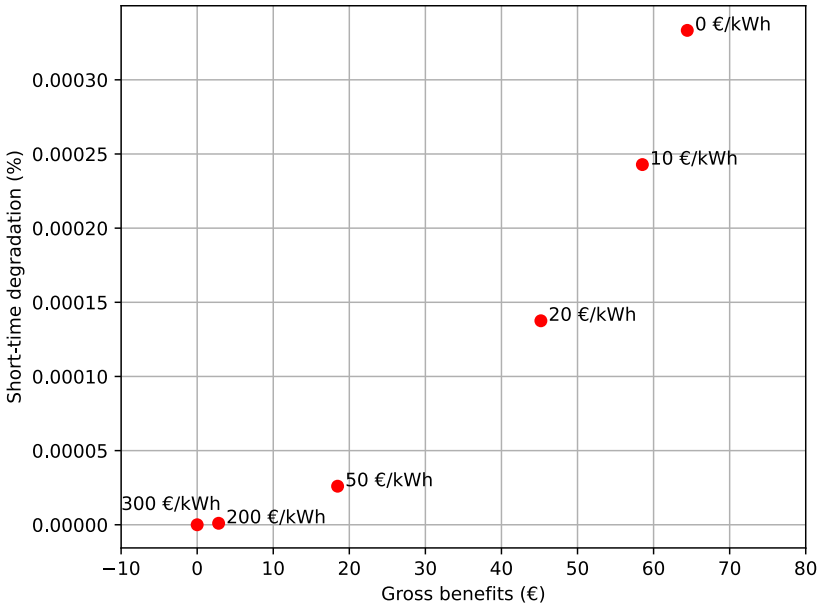

Figure 3.4: Degradation vs gross benefits.

When the capital cost reaches 50 euros per kilowatt-hour, the BESS prioritizes cycling during the second peak pricing period, which has a wider range of prices. However, when

the capital costs reach 300 euros per kilowatt-hour, the degradation costs become too high to generate a profit, resulting in the system not operating. This serves as an example of the potential inefficiency of overestimating degradation costs in control applications.

The relationship between short-term degradation and gross benefits attained with varying capital costs is illustrated in Figure 3.4. As capital costs decrease, degradation increases exponentially while gross benefits increase linearly. This can be observed by the trend in the figure.

3.5. Chapter conclusion

Different degradation factors caused by both battery operation and the pass of time have been introduced in this chapter. An example of their implementation in the model developed in Chapter 2 has been presented. Different magnitudes of degradation costs and their effect in short-term operation have been analyzed.

Up to this point, the assumption of perfect foresight has been taken. As outlined in the introductory chapter, market participation requires to make decisions with price or renewable resource uncertainty. The incorporation of these uncertainties is introduced in the following chapter.

4. INCORPORATING UNCERTAINTIES IN BATTERY ENERGY STORAGE SYSTEMS PERFORMING ARBITRAGE

When participating in electricity markets, price/quantity bids must be submitted without prior knowledge of the electricity prices. Usually, forecasting tools are used to obtain a prediction of such inputs. In previous implementations, the assumption of perfect price foresight was made for simplicity.

When an optimization problem does not consider uncertainties, it is called *deterministic*, since they use deterministic forecasts. *Non-deterministic* optimization problems, on the other hand, incorporate uncertainties into their formulation and use probabilistic forecasts. This chapter addresses both strategies.

The first section serves as introduction to EMS optimization approaches considering uncertainties. Afterwards, the forecasting tool used in this research is presented. This chapter concludes with a study of the relationship between degradation and uncertainties in short-term planning, and its outcome in long-term projects.

4.1. Energy systems optimization with uncertainty

Mathematical programming models can be classified into two categories: deterministic and non-deterministic. Deterministic models consider inputs as fixed, while non-deterministic models take into account that inputs may be uncertain. Since inputs for power system optimization, such as commodity prices or renewable energy generation, are often unknown in advance, it is necessary to consider uncertainties in the optimization process.

This section introduces the concepts of stochastic and robust optimization. Then, the Montecarlo method, which is widely applied in this kind of problems, is presented.

4.1.1. Stochastic vs robust optimization

When a decision with an uncertain parameter is made, the outcome is uncertain. The range of possible outcomes can be described as a Probability Density Function (PDF) [59]. Depending on the available data of this PDF, optimization under uncertainty techniques can be divided between stochastic and robust [60].

In stochastic optimization approaches, the search for the optimal solution is affected by the randomness of the outcomes [61]. If the objective is to maximize the solution, the problem can be formulated as follows:

$$f(x_{Opt}) \geq f(x) \text{ for all } x \in S, \tag{4.1}$$

where f is the objective function, x_{Opt} is the optimal configuration and S is the space of all solutions. This solution space is considered as finite, because it is assumed that the realizations of the uncertain parameter con be predicted by using historical data [59]. As the dimension of S increases, the problem becomes harder to solve [61]. This occurs when more than one random parameter is present, for example wind speed and electricity prices.

On the other hand, robust optimization only considers the worst possible outcome. It only requires the range of possible outcomes from the uncertain parameter[59].

Robust optimization approaches can produce over-conservative results, which may cause issues in energy systems optimization [62]. Stochastic optimization approaches, on the other hand, are viable when data can be predicted, using forecasting tools. This is the case of renewable energy sources and electricity prices [63].

While some works, such as [59] consider hybrid approaches, in this work only stochastic optimization strategies are considered. This is motivated because the uncertain parameters realizations can be estimated using forecasting tools and that risk-management strategies can be applied under these approaches [64].

4.1.2. Montecarlo method

Montecarlo method is a statistical algorithm which consists in repeatedly sampling uncertain values [65]. When applied to mathematical optimization, it allows to generate a set of possible outcomes for a given problem [66]. Recent advances in computational processes have allowed to apply this method in more complex problems [67].

The set of possible outcomes is generated by solving a deterministic version of the problem under different realizations of the uncertain parameters. This set is then transformed into a PDF by using a Kernel Density Estimator (KDE). This is a non-parametric method which positions a kernel function at every data point in the set and sum them to estimate the PDF [68].

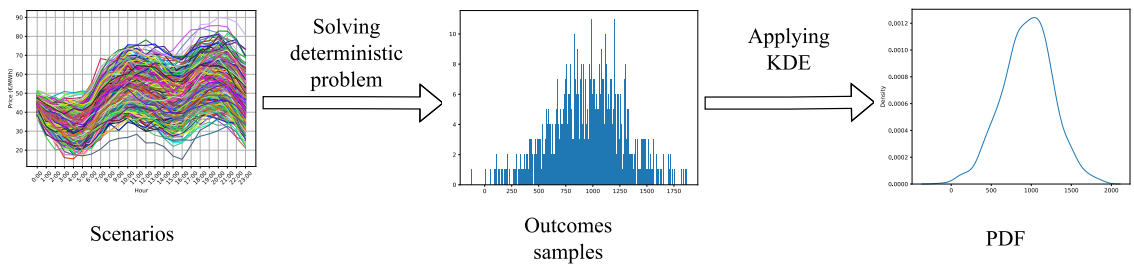

Figure 4.1: Scheme of Montecarlo method for optimization problems.

The process of generating this PDF with a Montecarlo method in an optimization

problem is illustrated in Figure 4.1. A set of input scenarios is used to generate a set of outcomes samples by solving a deterministic version of the mathematical program under each scenario. A KDE is then applied to the set of outcomes to generate a PDF.

This method can be applied to a variety of optimization problems, from financial modeling to engineering design. However, it is important to note that the accuracy of the results is dependent on the number of simulations performed, and as such, a large number of simulations are necessary to reduce the level of uncertainty in the results. Additionally, different scenario algorithm reduction techniques can be used to further improve the results, but their feasibility depends on the complexity of the problem [69].

4.2. Time-series forecasting with SARIMA

This section introduces the Seasonal Autorregresive Integrated Moving Average (SARIMA) model. SARIMA is commonly used for analyzing and forecasting time-series data with seasonal patterns. It is used in this research for input parameters predictions.

4.2.1. Deterministic forecasting

Hourly energy prices can be represented as time series, with each value showing a strong dependence on previous values and the hour of the day. A widespread forecasting technique is the Seasonal Average Auto Regressive Integrated Moving Average (SARIMA) model. It consists in the combination of a Moving Average (MA) and Auto-Regressive (AR) forecasting model.

An AR model of order n predicts the future value of a timeseries as a function of the n past values. A MA model of order q predicts the future value of a timeseries as a function of the past q error terms. The MA model can capture auto-correlation, while the AR model can capture partial correlations. These models are combined into an ARMA model, which is typically used for time series forecasting when the series is stationary.

The training data used for each daily price prediction is chosen to be the 100 previous days. Using a wider time series for the training data may result in over-fitting and negatively impact the model performance. Historical data from the Iberian Market from 2015 to 2020 are shown in Figure 4.2.

It can be seen that the time series changes its stationarity over time, therefore a differentiation is required, making an ARIMA model necessary. This model consists of an ARMA model with a differentiating component "I". Since the time series presents a linear average trend, a differentiation order of 1 is needed, this stationarizes the time series and allows the AR and MA components to catch the correlations within its values.

The value of the energy price for a given hour has a relationship with the values on the same hour for previous days, as it follows daily consumption patterns. However, season-

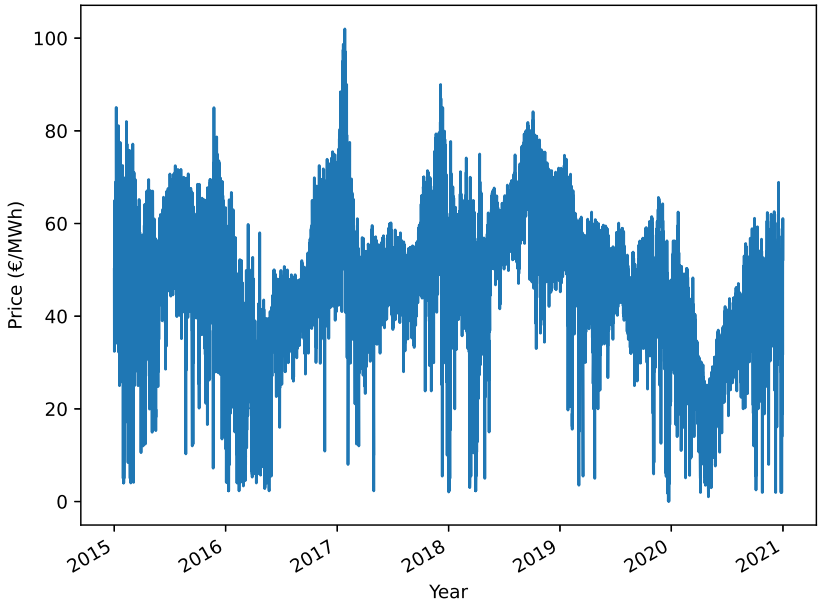

Figure 4.2: Electricity prices from 2015 to 2021.

ality on longer periods, such as years, is less clear as depicted in Figure 4.2. Therefore, daily seasonality can be considered to improve the prediction performance by using a SARIMA model. The SARIMA model has three additional components which are the seasonal counterparts of the regular ARIMA model. The AR component of the SARIMA model is described by equation (4.2):

$$\phi(Y) = \phi_1 Y_{t-1} + \phi_2 Y_{t-2} + ... + \phi_n Y_{t-p}, \tag{4.2}$$

where:

- Y_{t-n}: Value at n lags.
- ϕ_n: Coefficient used to fit the model.
- n: AR order, usually denoted as p.

The seasonal counterpart of the AR component is very similar:

$$\Phi(Y^S) = \Phi Y^S_{t-1} + \Phi Y^S_{t-2} + ... + \Phi Y^S_{t-P}, \tag{4.3}$$

where:

- Y^S_{t-n}: Value at n seasonal lags (n $\cdot$ 24h).
- Φn: Coefficient used to fit the model.
- n: Seasonal AR order, usually denoted as P.

The MA component is described by equation (4.4):

$$\theta(Y) = \theta_1\xi_{t-1} + \theta_2\xi_{t-2} + ... + \theta_D\xi_{t-d}, \tag{4.4}$$

where:

- θ_n coefficient of past lag n prediction error.
- ξ_n: error of past lag n prediction error.
- n: MA order, usually denoted as d.

This component has also its seasonal counterpart similarly as:

$$\Theta(Y^S) = \Theta_1\xi_{t-1} + \Theta_2\xi_{t-2} + ... + \Theta_D\xi_{t-D}, \tag{4.5}$$

where:

- Y_t: Error prediction.
- Θ_n coefficient of past n seasonal lag prediction error (n $\cdot$ 24h).
- ξ_n: error of past seasonal n lag prediction.
- D: Seasonal MA order, usually denoted as D.

Differentiation orders are denoted as d and D for the regular and the seasonal differentiation respectively. The order of SARIMA model components is notated as (p,d,q)(P,D,Q). The authors in [70] statistically show that a SARIMA with order $(2, 1, 3)(1, 0, 1)_{24}$ is appropriate for forecasting such prices, and the same order is used here, it is worth noting that a seasonal period of 24 has been chosen, day-ahead market electricity prices follow daily cycles.

Coefficient	**Value**
ϕ_1	0.0175
ϕ_2	0.9825
θ_1	0.0921
θ_2	-0.9853
θ_3	-0.1065
Φ_1	0.9854
Θ_1	-0.8960

Table 4.1: SARIMA model coefficients.

The fitting is performed by using the Limited-memory BFGS (L-BFGS) algorithm. This iterative algorithm uses only a limited amount of memory to store the history of past iterations. It has the advantage of using limited computer memory, making it suitable for this application. The parameters obtained by this technique are presented in Table 4.1.

As an example, a deterministic forecast for April the 16^{th} 2018 is shown in Figure 4.3.

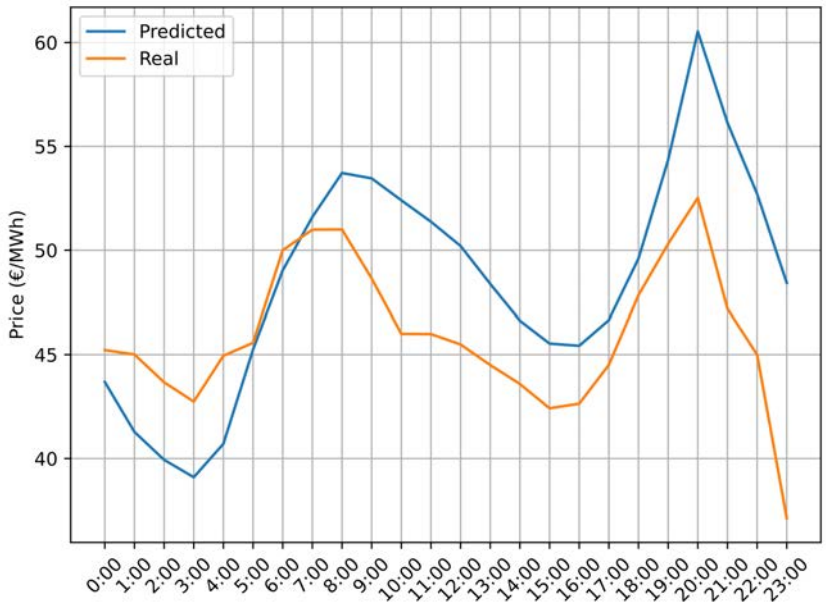

Figure 4.3: Day-ahead forecasting example for April the 16^{th} 2018.

4.2.2. Probabilistic forecasting

A SARIMA model gives as outcome not only a point forecast but also the variance of such prediction. When the model is fit as in previous subsection, it can be used to sample different realizations, thus creating different scenarios [71].

The Montecarlo method uses this feature. This process is useful for estimating the probability density of future events. Since Montecarlo estimation is based on a finite number of simulations, it is subject to a certain level of error, therefore it is common to simulate a large number of paths in order to reduce the error.

A draw of 1000 scenarios is created from the SARIMA model presented previously. The generated price paths are shown in Figure 4.4 for January 19th, 2017 as an example. They represent possible future prices and must be taken into account in the bidding strategy.

Since forecast errors tend to increase with time, it can be observed that the scenario dispersion is lower for the early hours and the results diverge for the latter ones. Other works such as [72] propose the inclusion of a scenario reduction algorithm. However, these methods can decrease Montecarlo method accuracy.

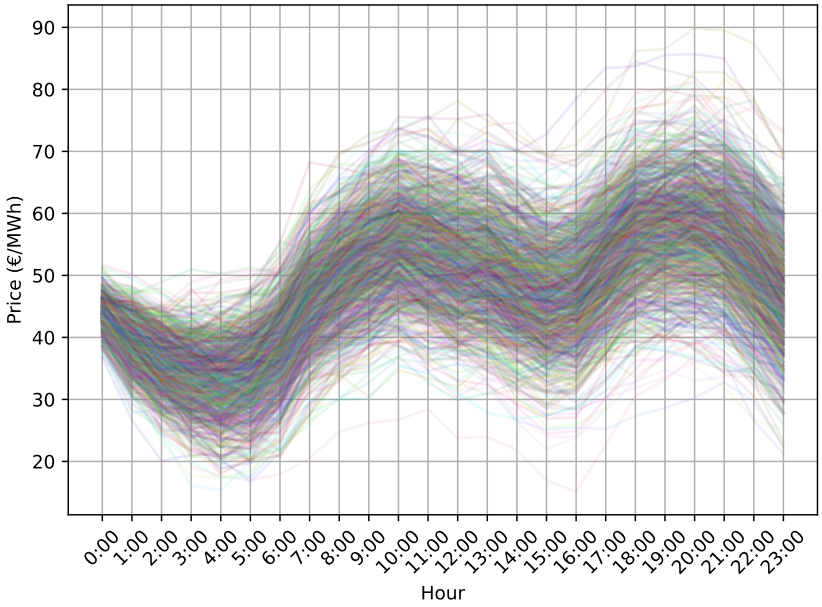

Figure 4.4: Generated scenarios.

4.3. Two-stage stochastic optimization

This approach involves considering two stages in the decision-making process. In the first stage, decisions are made considering the uncertain parameters are known, this is attained with deterministic forecasts. In the second stage, the outcome of the first-stage decisions based on the uncertain parameters realizations is considered as a cost.

A PDF generated in a Montecarlo simulation is used to obtain a distribution of the second-stage costs. It allows the effective optimization of energy systems under uncertainty [60]. These two-stage models can be extended into multi-stage models, which can be useful when rolling forecasts are available and updated hourly [73].

Depending on how the risks of first-stage decisions are considered in second-stage costs, different approaches can be found. This section introduces the risk-neutral and risk-aware strategies. Examples found in the literature are used to present the formulations under each approach.

4.3.1. Risk-neutral approaches.

Risk-neutral stochastic optimization problems aim to maximize the total expected benefits without regard of first-stage decisions risks. An example of this can be found in [74], in which an optimization algorithm is used for maximizing day-ahead market profits of a wind farm with a hybrid energy storage system, consisting of batteries and hydrogen fuel cells as ESSs.

The model input includes wind power and electricity prices scenarios. Day-ahead

power commitments are generated in the first stage, which are used as input for the second stage real-time operation. Both ESSs are used for reducing deviations. The objective function of the optimization problem, which aims to maximize profits, is formulated as follows:

$$Profit_{Da} = \sum_{i=1}^{n} \sum_{sw=1}^{NS} \pi_{sw} \sum_{sp=1}^{NS} \pi_{sp} \cdot P_d^{i,sw} \cdot \lambda_{Da}^{i,sp} , \tag{4.6}$$

where:

- $Profit_{Da}$: Day ahead market expected profits.
- i: Index for hourly interval.
- sw,sp: Index of the wind power and prices scenarios, respectively.
- π_{sw}, π_{sp}: Probability of each wind power and price scenario, respectively.
- $P_d^{i,sw}$: Delivered power to the network for hour i and scenario sw.
- $\lambda_{Da}^{i,sp}$: Day-ahead market price at hour i and scenario sp.

As shown, the algorithm has to go through all price scenarios for all wind power scenarios, which increases the computational burden exponentially when more uncertain parameters are considered, a common issue in stochastic optimization problems already mentioned in a previous section. This approach assumes that the scenarios have different probabilities, which is the case when a scenario reduction algorithm has been applied to the original Montecarlo samples [69].

Hourly power commitments are used as decision variables in this approach. The optimization model searches for the hourly schedule that provides the maximum number of benefits of all scenarios combined. An alternative approach is to use the schedule that yields the highest mean of profits, a method named Sample Average Approximation [60], which is described more in detail in the next section. Both strategies consider all situations to be equal, which neglects extremely adverse scenarios that may be unlikely but not avoidable.

4.3.2. Risk-aware approaches.

These models incorporate risk management into the optimization framework by adding a risk-awareness term to the objective function [75]. The most common term is the Conditional Value-at-Risk (CVaR), also known as Expected Shortfall (ES). This term is a variation of the Value-at-Risk (VaR) which has the drawback of not providing any information about the size of costs exceeding the threshold [60].

The CVaR $_{1-\beta}$ is defined as the mean of the values of all realizations of a random variable above the $1-\beta$ quantile. This metric provides information about the size of the probability density function tail. By adding this term to the objective function, it takes adverse scenarios into account.

Authors in [75] present a stochastic formulation for a hybrid plant participating in the day-ahead market. This approach includes the CVaR in its objective function, which is formulated as follows:

$$\max \Big(\gamma E(S) + (1-\gamma) CVaR_{1-\beta}(S) \Big), \tag{4.7}$$

where:

- *E(S)*: Expected value (mean) of the schedule.
- $CVaR_{1-\beta}(S)$: Conditional value at risk of the schedule for a confidence level β.
- γ: Exogenous parameter $0 < \gamma < 1$.

As shown, an exogenous parameter can be used to modulate the impact of the second term into the solution. Changing its value modifies the algorithm robustness, modifying the impact of risks into the operation.

4.4. Analysis of risk measures impact in a standalone BESS performing arbitrage

The optimization techniques described above are tested in this section. A simulation framework is presented to test the final outcome of each strategy. The simulation framework consists in a project of a standalone BESS providing arbitrage service in the Iberian day-ahead market from 2016 to 2020.

The BESS model formulated in Chapter 2 is utilized. Different cases of optimization strategies are implemented under the same conditions. Results after five years are extrapolated for the remaining project life, which is considered to end when the BESS EOL is reached. This extrapolation is made in order to have a more complete evaluation of the different strategies considered.

This section begins presenting the implementation of the SARIMA model for first stage and second stage samples generation. Stochastic optimization formulations are proposed afterwards, adapted for the current application. Lastly, the simulation framework and results are described.

4.4.1. First stage and second stage samples generation

For each day, a set of 1000 electricity price scenarios as the one illustrated in Figure 4.4 is utilized. Each scenario is used as input for the MILP model for a BESS doing arbitrage

considering degradation costs presented in Chapter 2, based in a DOD-cycles degradation model. A hourly power schedule is generated for each scenario.

This process is repeated until 1000 power schedules are generated. Figure 4.5 illustrates a cluster of such schedules generated for January the 19^{th} 2017. The width of the dots represents the frequency with which the algorithm schedules that power level during that hour under varying price scenarios.

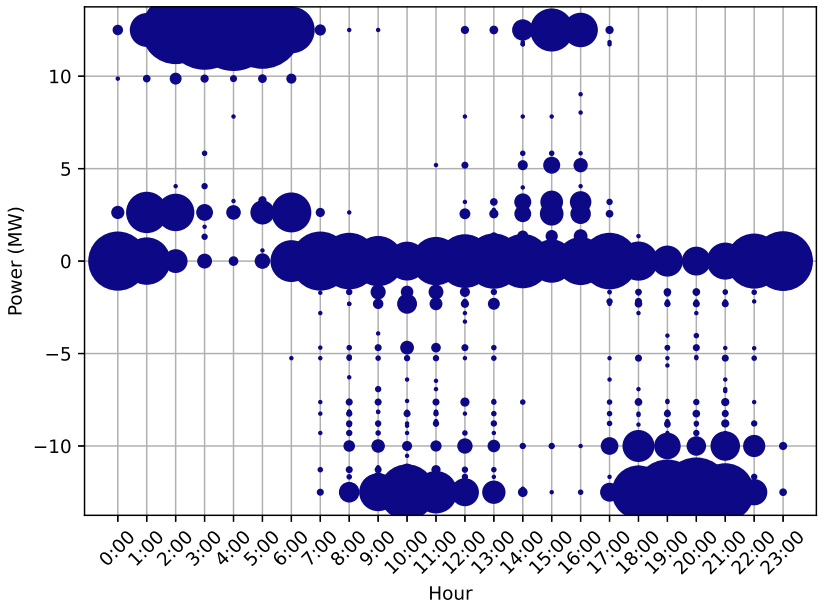

Figure 4.5: Charging and discharging programs on 1000 generated schedules.

As it can be observed, it is common to do a full power charge at the early hours of the day. Additionally, it can be seen that it is less frequent for the algorithm to utilize the midday valley in prices, potentially due to the low price spread during these hours. There are also a lot of situations in which the BESS is not participating in the market, since powers are kept at 0.

For generating the second-stage costs, the outcome of each schedule is calculated under each scenario. This process generates a sample of 1000 expected benefits for each schedule. A Kernel Density Estimation can be employed to estimate the probability density function for the profits of each scenario [76].

As an example, the distribution of profits under Schedule number #256 is presented in Figure 4.6 for January 19th, 2017. This schedule was chosen at random. The 5th and 95th percentiles are also shown.

These percentiles are utilized as confidence levels for the risk-aware stochastic strategies.

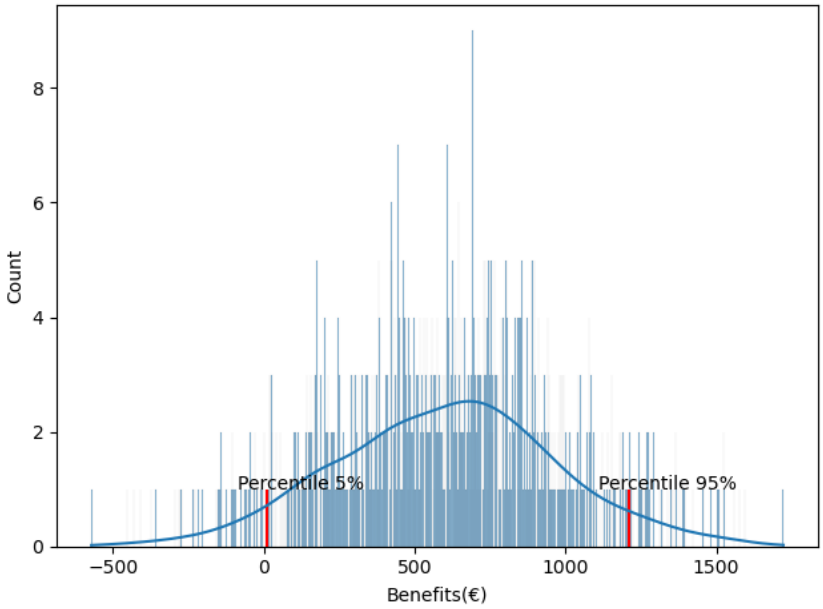

Figure 4.6: Second stage samples of Schedule #256.

4.4.2. Stochastic approaches

Different strategies are implemented in order to compare the effect of risk management in long-term profits. The same sample generation process is used in each case. Risk-prone, risk-aware and risk-neutral strategies found in the literature are considered. A combination of these is proposed.

Sample Average Approximation

The Sample Average Approximation (SAA) is a risk-neutral method that evaluates the mean of the samples [77]. The average profit is calculated for each schedule. The candidate which yields the highest average profit is selected, a formulation for this implementation is presented as follows:

$$\max\left(\frac{1}{n}\sum_{j=1}^{n=1000} x_{ij}\right), \tag{4.8}$$

where:

- n: Number of scenarios.
- x_{ij}: Net profit of power schedule i under price scenario j *(€)*.

Figure 4.7 illustrates the means of all power schedules for January the 19^{th} 2017.

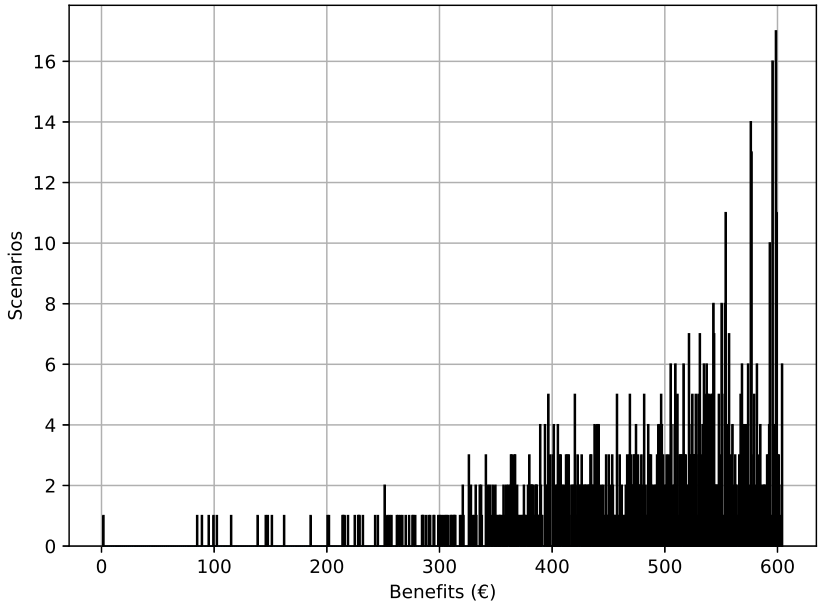

Figure 4.7: Mean of benefits for each schedule.

The histogram in Figure 4.7 shows that many schedules have average profits close to the maximum. Since the SAA method only considers the distribution mean, it is possible that there are other important distinctions between schedules with similar means that should be considered. For example, some schedules may be more risky due to skewed or thick-tailed distributions, while others may have similar means but present thicker right tails, which could represent opportunities to gain higher profits.

Conditional Variance or Expected Shortfall approach

The use of the Expected Shortfall (ES) results in a risk-aware approach. This strategy punishes candidate solutions which demonstrate high chance of poor outcomes, reflected in the left tail of their distribution. The expected shortfall for a continuous probability distribution can be obtained as follows:

$$ES_\beta(X) = -\frac{1}{\beta}\int_{-\infty}^{-VaR_\beta(X)} xf(x)\,dx, \tag{4.9}$$

where:

- $ES_\beta(X)$: Expected shortfall for percentile β.
- X: probability distribution.
- $VaR_\beta(X)$: Value at risk or of percentile β.
- x: values of the distribution X.

- *f(x)*: Probability density for value x.

Given that the profit distribution for each schedule is discrete and all price scenarios are assumed to have equal probability, the expected shortfall is the mean of profits that fall below the β percentile. To favor distributions with lower risk, the expected shortfall is added to the mean in this selection strategy, as expressed in (4.10). A multiplicative factor K is included to adjust the impact of the expected shortfall on risk assessment. The objective function for this approach is formulated as:

$$\max\left(\frac{1}{n}\sum_{j=1}^{n=1000} x_{ij} + K \cdot ES_{\beta}(X_i)\right), \tag{4.10}$$

where:

- x_{ij}: Net profit of power schedule i under price scenario j.
- X_i: profit distribution for schedule i.
- K: Multiplicative factor.

Expected Tail Return

Additionally, it may be beneficial to favor schedules with thick right tails in order to gain higher profits. A measure of the impact of the right tail, similar to the expected shortfall, is the Expected Tail Return (ETR):

$$ETR_{\beta}(X) = -\frac{1}{\beta}\int_{-VaR_{\beta}(X)}^{+\infty} x f(x)\, dx, \tag{4.11}$$

where:

- $ETR_{\beta}(X)$: Expected tail return for distribution X and percentile β.

The ETR, in this case, is the average of the values that exceed the β percentile. Similar to the approach used for the expected shortfall, a multiplicative factor is added to the mean of profits, in this case to account for the right tail of the distribution. The objective function for this approach is formulated as:

$$\max\left(\frac{1}{n}\sum_{j=1}^{n=1000} x_{ij} + K \cdot ETR_{\beta}(X_i)\right). \tag{4.12}$$

ETR & ES combined Approach

Lastly, for the sake of completeness, a combination of both expected shortfall and expected tail return is proposed. The objective function for this approach is as follows:

$$\max\left(\frac{1}{n}\sum_{j=1}^{n=1000} x_{ij} + K \cdot (ETR_{\beta}(X_i) + \cdot ES_{\beta}(X_i))\right) \tag{4.13}$$

4.4.3. Simulation results

The strategies formulated above are compared in a simulation from January the 1^{st} to December the 31^{th} 2020. Battery degradation is implemented, hence the available battery capacity fades from one day to the next. Simulation outcomes are extrapolated until the end-of-life (EOL) of the project to obtain the final results for each strategy.

Simulation framework description

The power schedules presented to the market session for each BESS are generated using six different strategies:

- The Expected Shortfall (ES) strategy, which takes into account the risk of low profits by adding the expected shortfall to the mean of the profits as defined in (4.10).
- The Expected Tail Return (ETR) strategy, which favors schedules with a thick right tail by adding the expected tail return to the mean of the profits as defined in (4.12).
- A combination of the ES and ETR strategies, which takes into account both risk and opportunity by adding both the expected shortfall and the expected tail return to the mean of the profits as defined in (4.13).
- The Sample Average Approximation (SAA) strategy, which selects the power schedule that yields the highest average profit as defined in (4.8).
- A deterministic approach, in which the direct forecast is used to obtain the final power schedule.
- The ideal case, as a benchmark, in which perfect price foresight is considered.

The degradation model outlined in Chapter 2 is employed to compute degradation caused by the real operation on a daily basis. It is important to consider calendar degradation in addition to cycles, as the expected lifespan of a LFP battery is around 6000 cycles. Research in [78] shows that LFP cells experience a 5% capacity loss when stored at 25°C and 50% SOC over a period of 900 days. This value is used in the current study, taking into account that the BESS has a thermal management system and SOC is kept at 0% at

the start and end of each day. By combining this with the daily usage-induced capacity loss, a mean of 0.0056% daily capacity loss by calendar aging is obtained, which will result in lower profits from arbitrage due to degradation.

Five year simulation results

The parameter K is initially set to 1, but varying it does not significantly affect the comparison of different approaches. Figure 4.8 illustrates the accumulated cash flow after 5 years for each strategy. It can be observed that all strategies display seasonal patterns, corresponding to the warmer months with lower price spreads and reduced BESS operation. Initially, it may appear that the ETR approach yields better results than the others, the deterministic approach yields similar results to the SAA and ES&ETR strategies, and the ES approach yields substantially worse results.

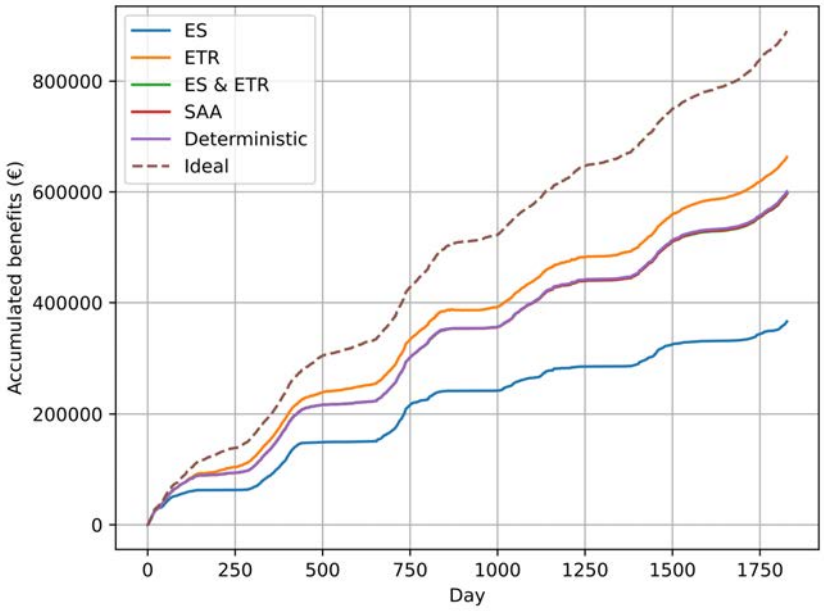

Figure 4.8: Accumulated benefits after 5 years.

As shown in Figure 4.9, the different strategies result in varying levels of battery degradation. The seasonal patterns observed in Figure 4.8 are not present as calendar degradation continues to occur even when the BESSs are not in operation. The ETR approach results in a more aggressive use of the battery, prioritizing power schedules with the potential for higher income, often resulting in more full daily cycles than when using other strategies, even more than in the ideal scenario where prices are known. However, it is not possible to determine from this simulation alone whether the increased degradation is outweighed by the higher income. Similarly, the use of ES as a risk measure results in both lower income and degradation, making it difficult to compare with other approaches. It is important to note that this simulation alone does not provide enough information to determine if the higher income from ETR compensates for the higher degradation.

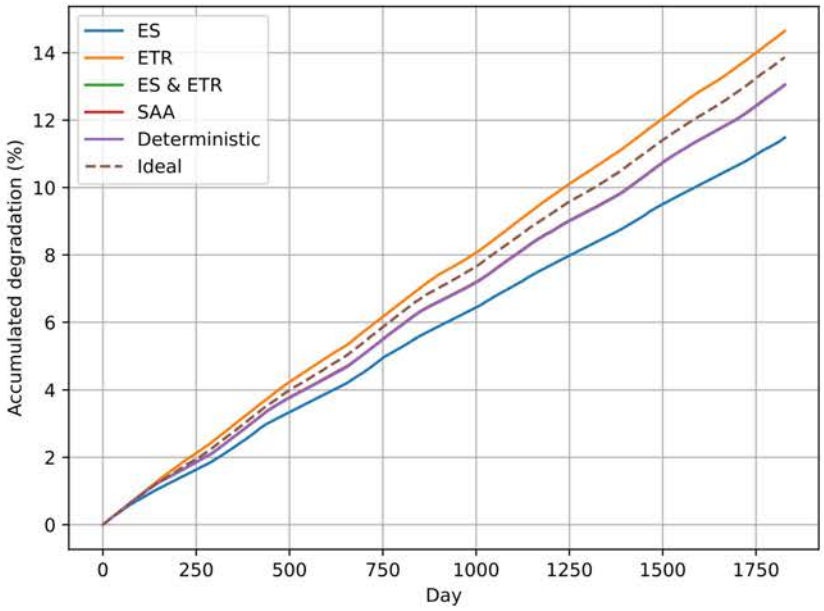

Figure 4.9: Accumulated degradation after 5 years.

The simulation results indicate that the Direct approach using the point forecast and the SAA approach yield similar outcomes in terms of income and degradation. This suggests that there is no benefit to using the SAA approach, which involves a higher computational effort through Montecarlo analysis. The results imply that the system does not have any non-linearities or characteristics that are not captured by the ARIMA forecast. Therefore, the Direct approach using the point forecast is sufficient for forecasting the prices.

Full project extrapolation

In order to evaluate the impact of each strategy in a project, an extrapolation is made of each simulation case, until the BESS reaches its end of life, defined as when the capacity reaches 80% of its nominal value. This is done by taking into account the average net income per MWh of the current available capacity and the average daily capacity loss over a 5-year simulation using real data.

The extrapolation method chosen is based on the average net income per MWh of the current available capacity and the average daily capacity loss over the 5-year simulation with real data. Other methods of extrapolation were tested, such as repeating the available prices data, but no significant differences were found.

The simulation is run twice, once without incorporating the degradation costs into the daily optimization and once by including them. The accumulated cash flow for both cases is presented in Table 4.2.

Table 4.3 shows the end of life (EOL) time for each case. This allows for a comparison

	With degradation cost	Without degradation cost
Ideal	1.24 M€	1.17 M€
ES	0.61 M€	0.81 M€
ETR	0.88 M€	0.79 M€
ES & ETR	0.88 M€	0.81 M€
SAA	0.88 M€	0.81 M€
Deterministic	0.88 M€	0.82 M€

Table 4.2: Accumulated cash flow with each strategy.

of the impact of the implemented degradation model on the long-term analysis.

	With degradation cost	Without degradation cost
Ideal	7.21 years	6.05 years
ES	8.72 years	6.67 years
ETR	6.83 years	6.14 years
ES & ETR	7.67 years	6.12 years
SAA	7.67 years	6.13 years
Deterministic	7.67 years	6.14 years

Table 4.3: EOL time for each strategy.

The results reveal substantial variations in accumulated cash flow and end-of-life time between the evaluated strategies, particularly in regards to degradation costs, with variations of 30% in BESS lifetime. To assess these outcomes, a comparison of the Net Present Value (NPV) of the cash flows using a 7% discount rate is conducted, as depicted in Figure 4.10 and Table 4.4.

The results indicate that the evaluated strategies are able to achieve approximately two-thirds of the theoretically optimal NPV, represented in the results as *Ideal*. There is likely potential for improvement in forecasting through the use of more advanced algorithms.

	With degradation cost	Without degradation cost
Ideal	0.99 M€	0.97 M€
ES	0.47 M€	0.67 M€
ETR	0.71 M€	0.66 M€
ES & ETR	0.69 M€	0.67 M€
SAA	0.69 M€	0.68 M€
Deterministic	0.70 M€	0.69 M€

Table 4.4: NPV with each strategy.

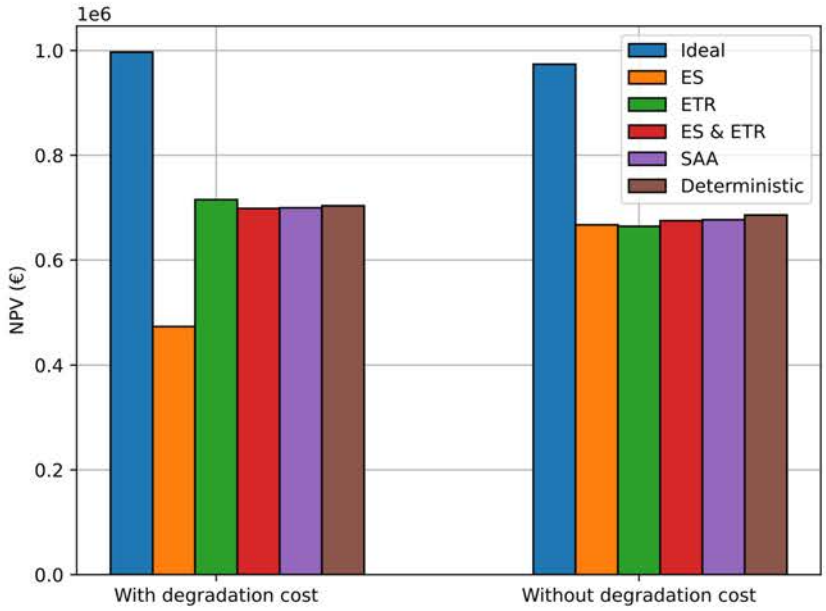

Figure 4.10: NPVs with each strategy with and without considering degradation costs.

When degradation costs are excluded from the optimization process, the resulting NPV and battery lifetime are relatively similar across all strategies. The only significant difference is observed for the ES strategy, which results in higher accumulated cash flow but at the expense of longer end-of-life time. These variations appear to balance each other out, resulting in similar NPV.

The effect of including degradation costs in NPV is dependent on the optimization strategy employed. Using the ETR approach results in a 7.5% increase in NPV, highlighting the potential of including such costs in the objective function to enhance project value. However, utilizing the ES approach leads to a 30% decrease in NPV, illustrating how consideration of degradation costs can negatively impact project profitability when utilizing a risk-averse optimization approach. The remaining strategies result in almost insignificant increases in NPV, but with an extension in battery lifetime, requiring more time to reach a similar NPV.

Inclusion of degradation costs results in similar NPV for all strategies except for the ES approach. The ES strategy becomes even more conservative, resulting in reduced accumulated cash flow due to the increased weight of calendar aging, and a greatly extended end-of-life time, resulting in a reduction in NPV. For the remaining strategies, the most notable difference is found when using ETR, where the NPV is comparable to the others, but achieved in a significantly shorter time frame due to more aggressive utilization of the battery. This may be of interest when payback time is a concern.

The results presented were obtained with a fixed value of K=1. To evaluate the impact of this parameter, a sweep analysis was conducted and the results are depicted in Figure 4.11. The ETR strategy exhibits a small peak at around K=0.5, yielding an NPV of 0.73

M€, which is 4.3% higher than the Deterministic approach. Conversely, the NPV for the ES strategy decreases as K increases, as it leads to a more conservative use of the battery. Notably, the effect of increasing K is relatively insignificant for the ES & ETR strategy.

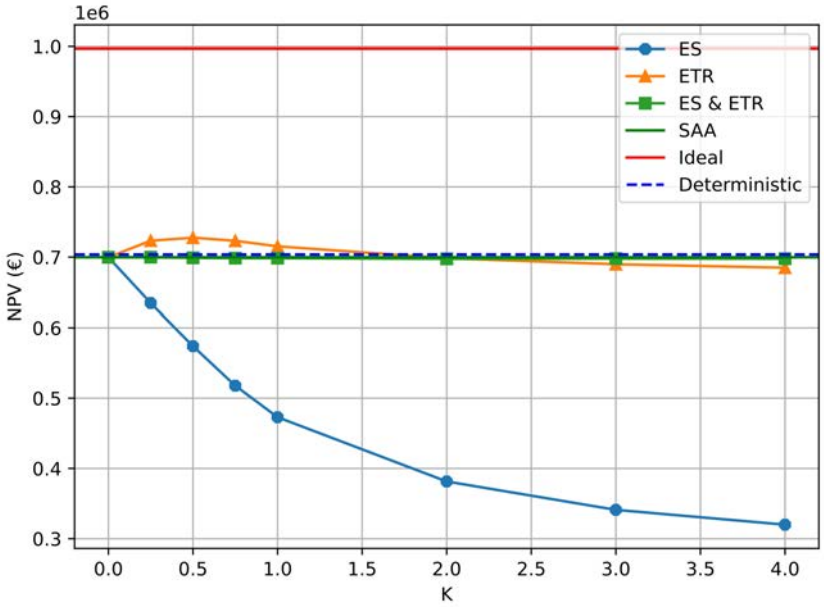

Figure 4.11: NPVs considering degradation with various values of K.

The results indicate that a conservative approach, such as the use of the ES strategy, results in the worst outcome compared to other strategies. Therefore, there is no justification for a risk-averse approach to battery operation, especially given that daily market participation consists of a series of relatively small bets, resulting in minimal risk for each transaction. This is an assumption made in the literature, and this conclusion is one of the contributions of this work.

Furthermore, the results demonstrate that implementing a risk-prone approach to battery operation that incorporates degradation costs, such as the ETR strategy, leads to a higher NPV (approximately 4.3% higher) and a shorter project timeline, which could be beneficial.

4.5. Chapter conclusion

In this chapter, different risk-aware stochastic approaches have been implemented, with the proposal of a new one. It has been concluded that a conservative approach does not yield better results. A risk-prone approach improves results, but the exogenous parameter which modulates it must be chosen correctly.

In the next chapter, the BESS model is incorporated in a renewable power plant, conforming an HF. This increases complexity and opens the BESS to new applications. The operation of this system in multiple electricity markets is analyzed.

5. ENERGY STORAGE SYSTEMS IN HYBRID FARMS

This chapter introduces a renewable generation system to the ESS, conforming a Hybrid Farm. The operation is extended from the day-ahead electricity market to include intraday spot markets. A progressive optimization algorithm is formulated and different market participation strategies are compared with the proposal of a novel approach which mitigates the effect of market overlapping.

Firstly, Iberian electricity markets rules are introduced, this region has been chosen for illustration purposes since it is consistent with other ones. Afterwards, the HF model formulation for optimization applications is presented. Then, the proposed stochastic optimization algorithm for multi-market participation is described. This chapter concludes with an implementation of this model in the Iberian electricity markets. A study is conducted in the effects of multi-market participation.

5.1. Iberian electricity market rules

Before each market session opening time, the EMS needs a forecast of electricity prices and wind power generation for its decision-making process. Since the forecast accuracy depends on the time horizon, it is necessary to consider each market session opening hour. Deviations costs rules must be take into account, since they reflect the impact of forecasting errors.

This section briefly introduces the rules for Iberian day-ahead and intraday spot markets. Due the small volume of energy traded in continuous markets, they are neglected in this study. This section concludes with the description of deviation management rules applied by the Iberian market operator.

5.1.1. Day-ahead market

The majority of energy traded in the Iberian electricity markets is located in the day-ahead market. In 2020, it accounted for 74% of the total [79]. Hence, it is the most important market for arbitrage operation. The Iberian day-ahead market session takes place every day of the year at 12:00 CET.

The price and volume of energy is determined for each hour of the following day by the intersection of demand and supply. Market agents submit their offers through the market operator OMIE *(Operador del Mercado Ibérico de Energía)* [80]. As a result, the EMS has to submit 24 hourly offers for the following day, using price and generation forecasts generated 12 to 36 hours prior to delivery time.

5.1.2. Intraday markets

Intraday spot markets accounted for 14% of the energy traded in 2020. Since six times more energy is traded compared to intraday continuous markets, only the former ones are considered in this research [79]. In Table 5.1, the closing times and delivery hours of the market sessions are shown.

Table 5.1: Intraday market sessions in 2018.

Session	**1**	**2**	**3**	**4**	**5**	**6**
Closing time	18:50	21:50	1:50	4:50	8:50	12:50
Delivery hours	22(D-1)-23	0-23	4-23	7-23	11-23	15-23

The closing times in Table 5.1 are the deadlines for submitting offers to the market operator. Decisions must be made before this time. The delivery hours in the table are the hours during which the energy negotiated in each intraday market session will be delivered on day D.

Since Session 1 and 2 cover the same hours, Session 1 is neglected as Session 2 has a closer opening to the delivery. Intraday markets allow agents to correct their schedule on the day-ahead market. This can be done by purchasing energy during hours when a deviation from the day-ahead program is expected. Arbitrage can also be performed to gain additional liquidity. Both options are considered in the simulation cases.

5.1.3. Deviation adjustment mechanism

This mechanism is applied by the market operator the day after delivery. Depending on the state of the electrical system at each hourly period, it calculates the economical penalties or bonuses to the producers. The amount to be paid or receives depends on the state of the system when the deviation occurs.

A penalty must be paid to the operator if the deviation is downwards while a bonus is received if the deviation is upwards. These amounts also vary depending if the deviation was against of each the system. This results in a four different deviation costs for each hour.

The absolute value of a deviation during an hourly period t can be formulated as follows:

$$\lambda(t) = |E_D(t) - E_c(t)|, \tag{5.1}$$

where:

- $\lambda(t)$: Deviation during hourly period t *(MWh)*.
- $E_D(t)$: Delivery during hourly period t *(MWh)*.

- $E_c(t)$: Commitment during hourly period *t (MWh)*.

If the deviation is upwards and in favor of the system, the additional energy is remunerated at the day-ahead price during hourly period *t*, therefore the bonus is calculated as:

$$\beta(t) = \lambda(t) \cdot \pi_{DM}(t), \tag{5.2}$$

where:

- $\beta(t)$: Bonus obtained during hourly period *t (€)*.
- $\pi_{DM}(t)$: Day-ahead price during hourly period *t (€/MWh)*.

If the deviation is upwards and against the system, the additional energy is remunerated at less than the day-ahead price during hourly period *t*, this bonus is calculated as:

$$\beta(t) = \lambda(t) \cdot \pi_{DM}(t) \cdot (1 - \lambda_{Coef}(t)), \tag{5.3}$$

where:

- $\lambda_{Coef}(t)$: Coefficient for deviations against the system during hourly period *t*.

If the deviation is downwards and in favor of the system, the energy deficit is charged at the same price as the day-ahead price during hourly period *t*, therefore the penalty is calculated as:

$$\rho(t) = \lambda(t) \cdot \pi_{DM}(t), \tag{5.4}$$

where:

- $\rho(t)$: Penalty during hourly period *t (€)*.

If the deviation is downwards and against the system, the energy deficit is charged at more than the day-ahead price during hourly period *t*, therefore the penalty is calculated as:

$$\rho(t) = \lambda(t) \cdot \pi_{DM}(t) \cdot (1 + \lambda_{Coef}(t)). \tag{5.5}$$

The total deviation costs, is formulated as follows. As it can be seen, it can be negative, this is caused when more energy is available than commited:

$$\lambda_{Cost}(t) = \rho(t) - \beta(t), \tag{5.6}$$

where:

- $\lambda_{Cost}(t)$: Deviation costs during hourly period *t (€)*.

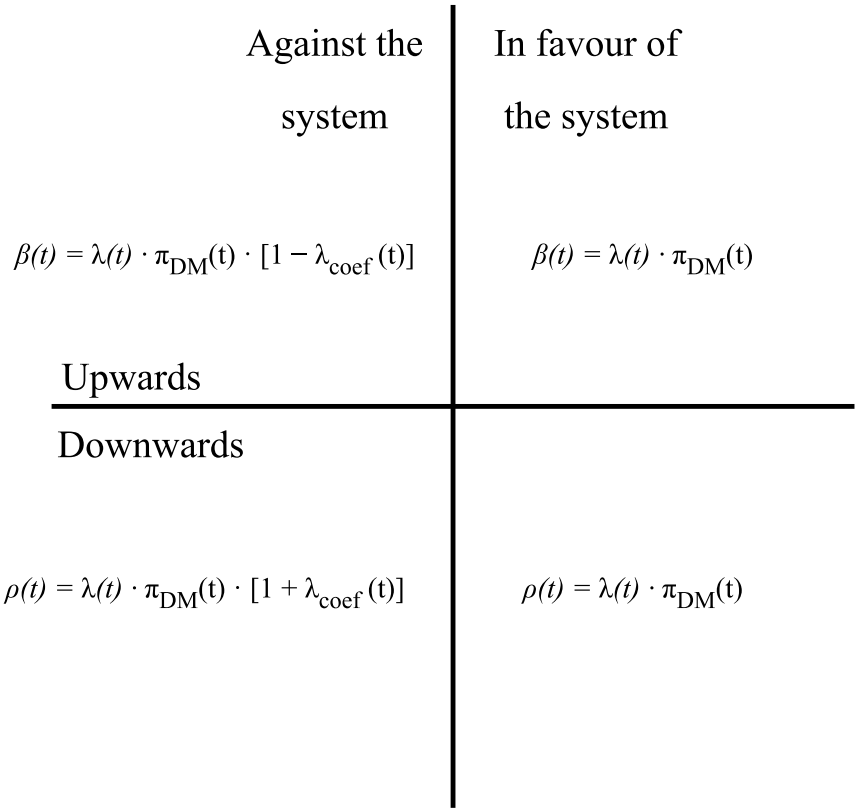

Figure 5.1: Deviation costs calculation.

This is summarized in Figure 5.1. The four expressions are illustrated. As it can be seen, the calculation of the bonuses and penalties is almost identical when the deviation is against or in favor of the system, with the sign of $\lambda_{Coef}(t)$ switched.

The coefficient $\lambda_{Coef}(t)$ represents the system's vulnerability to deviations against it. A higher coefficient means a higher penalty needs to be paid. As seen in (5.3), if the coefficient is greater than 1, the bonus for upwards deviations can be negative, which implies a penalty. During the same hourly period, if downwards deviations are against the system, upwards deviations are in favor of the system, and vice versa. The deviation coefficient is determined by the system operator and it is the same for both types of deviations.

5.2. Hybrid farm model

The HF model receives as input a deterministic forecast of electricity prices and wind power. A three-level control architecture is implemented into the EMS for both committing energy and managing the ESS, this control system is described in a following section. Daily profits are calculated using the formulation presented in the previous section. A sketch of the plant configuration is shown in Figure 5.2.

In this chapter, the input generation process is presented. Then, the Wind Turbine Generator (WTG) and the control architecture is described. Lastly, the daily profits calculation process is introduced.

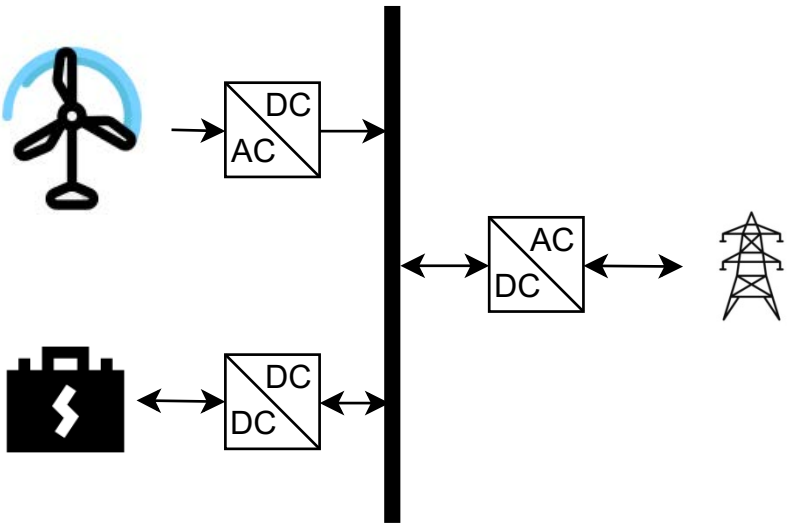

Figure 5.2: HF configuration.

5.2.1. Model inputs

Model inputs are deterministic forecasts obtained using the SARIMA model presented in Chapter 4. For each input, the SARIMA model is fitted and trained diversely. Both models are trained with real historical data.

Wind power

Wind power forecasts are obtained with a two-stage approach as in [81]. First, hourly wind speed is forecasted using a SARIMA, then, such prediction is fed into a function with the power curve of a Gamesa G128 WTG. The optimization and EMS models receive directly the forecasted and real wind power hourly values.

Wind speed historical data is taken from Sotavento experimental park on Galicia, Spain [82]. This particular park was chosen due to its publicly available data and its location within the Iberian market region. The data has a resolution of one hour and the measured wind speed for the year 2018 is presented in 5.3.

Hourly wind speed forecasts are required during the opening hours of market sessions. The first forecast is at 12:00h, when the day-ahead market commences, and subsequent forecasts are generated during the opening hours of intraday market sessions. For real-time operations, actual measured wind speed data is utilized. The SARIMA model employed has an order of $(2,0,3)(2,1,3)_{12}$. The configuration process for the model is not covered in this work. Figure 5.4 illustrates the 2018 average Mean Absolute Percentage Error (MAPE) of the wind speed forecasts generated during different market sessions. It is observed that the prediction error tends to decrease, motivated by the increasing proximity between the market session and the last of the delivery hours.

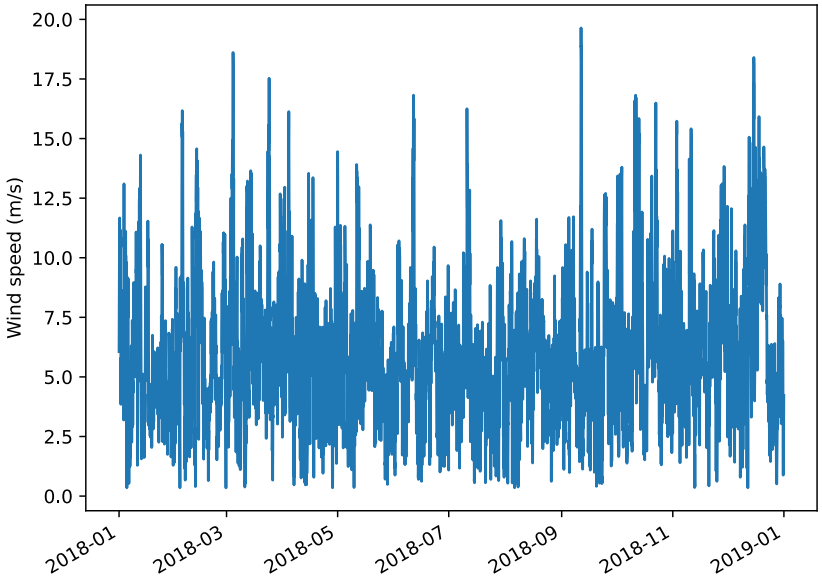

Figure 5.3: 2018 hourly wind speed historical data.

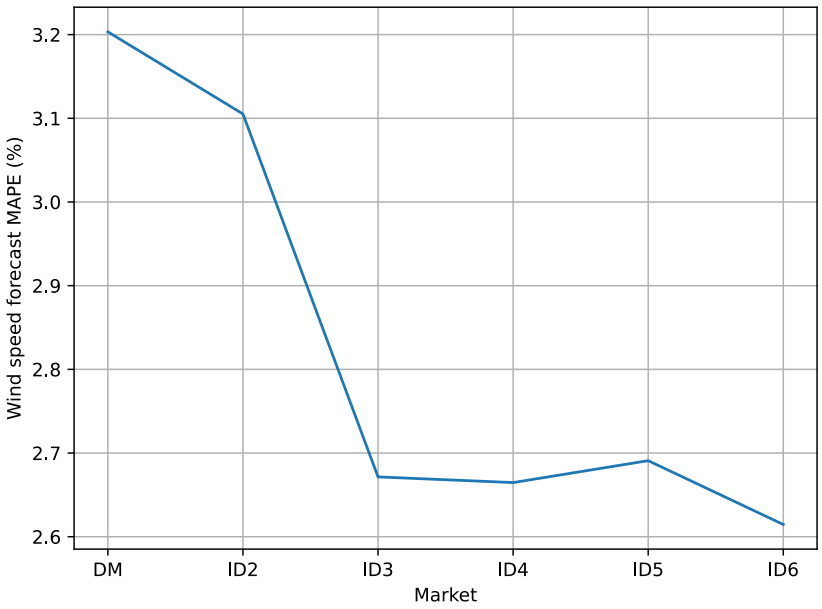

Figure 5.4: Average MAPE of each wind speed forecast for 2018.

Electricity price forecasts

The 24 hourly prices for the next day are predicted at 12:00h of the previous day. The SARIMA model with order $(2,1,3)(1,0,1)_{24}$ presented in Chapter 4 is used here. For simplicity, perfect foresight of intraday prices is considered.

Deviation prices

The hourly deviation coefficients derived from 2018 historical data are used to calculate final deviation costs. However, a deviation coefficient is required for the optimization model of intraday market offerings. Since deviation coefficients are only known after the delivery period has ended, a forecasting technique for predicting the direction (favorable or unfavorable) of deviation is required, but it is outside the scope of this paper. Therefore, a deviation coefficient of 21%, the average of 2017, is considered when participating in the intraday market.

5.2.2. Hybrid farm components parameters

Wind turbine generator

The WTG is a single Gamesa G128 WTG with a nominal power of 4.5 MW. The power curve is taken from [83]. Only a WTG is considered for convenience. Generator converter efficiency is considered as part of the power curve characteristic.

ESS

The storage system is composed of a 10MWh/2.5MW Lithium Iron Phosphate (LFP) battery, this is a 4h ESS which is a requirement from the Renewable Economic Regime [84].Its round-trip efficiency is assumed to be constant at 90% as in [85]. Calendar and cycle degradation models presented in Chapter 3 are also implemented in this study. Table 5.2 defines this latter degradation model:

Table 5.2: Calendar degradation results at 25^{o}C [78].

SOC (%)	**Capacity lost** (%)
0	0.002
50	0.0055
100	0.012

5.2.3. Control architecture

The EMS control architecture is divided in three levels. Each one operates with different inputs and in different time windows. A sketch of the architecture is illustrated in Figure 5.5:

The tertiary level operates in advance, and is responsible for the offering strategy in various energy markets. The optimization models for market scheduling are applied at this level.

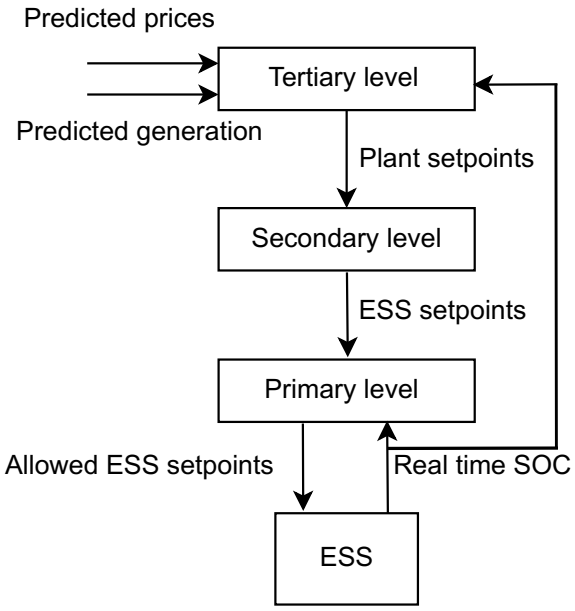

Figure 5.5: EMS control levels.

As input, the tertiary level receives prices and wind powers forecasts. It also receives the BESS SOC in real-time. After generating the commitments, it sends plant setpoints to the secondary level.

The secondary control level operates in real-time, at the beginning of each hour, and is in charge of generating the ESS setpoints. Real-time generation and commitments produced in the third level are used as input. The ESS setpoints calculation is formulated as follows:

$$P_{ESS}(t) = P_{Com}(t) - P_{Gen}(t), \tag{5.7}$$

where:

- $P_{ESS}(t)$: ESS setpoint during hourly period t *(MW)*.
- $P_{Gen}(t)$: Measured generation during hourly period t *(MW)*.
- $P_{Com}(t)$: Commitment during hourly period t *(MW)*.

As shown, when an upward deviation is anticipated, the ESS will receive a setpoint to charge the excess. Conversely, when a downward deviation is expected, a discharging setpoint is generated.

Lastly, the primary control level manages the energy storage system, it receives charge-discharge setpoints from the secondary level and adjusts them based on the real-time SOC. If the ESS is not able to cover the missing energy, a downward deviation will occur during that hour. If the ESS is unable to store the excess energy, then an upward deviation will occur.

5.2.4. Daily profits calculation

Daily profits are calculated following Iberian market rules. Daily earning are formulated in (5.8). Daily losses are formulated in (5.9).

$$Earnings = \sum_{h=1}^{24} \Big(E_{DM,C}(t) \cdot \pi_{DM}(t) + E_{ID,C}(t) \cdot \pi_{ID}(t) \Big), \tag{5.8}$$

$$Losses = \sum_{h=1}^{24} \Big(P_{\varphi}(t) \cdot \pi_{ID}(t) + \lambda_{Cost}(t) \Big), \tag{5.9}$$

where:

- $Earnings$: Daily earnings *(€)*.
- $E_{DM,C}(t)$: Energy commitment on day-ahead market during hourly period *t (MWh)*.
- $\pi_{DM}(t)$: Day ahead market real price during hourly period *t (€/MWh)*.
- $E_{ID,C}(t)$: Energy commitment on intraday markets during hour *t(MWh)*.
- $\pi_{ID}(t)$: intraday market real price during hourly period *t (€/MWh)*.
- $\lambda_{Cost}(t)$: Deviation costs during hourly period *t (€)*.
- $Losses$: Daily losses *(€)*.
- $P_{\varphi}(t)$: Power purchased on intraday market during hourly period *t (MW)*.

Downwards deviations can be corrected in intraday markets in two ways:

- By purchasing the expected energy deficit in the intraday market ($P_{\varphi}(t)$).
- By using stored energy to cover the imbalance.

The optimization algorithm chooses how to correct expected deviations deviation depending on intraday market prices and deviation costs at each hour.

5.3. Progressive optimization algorithm

Since market sessions occur at different hours, the optimization algorithm for multi-market participation has to be divided into different stages. This approach is known as progressive optimization [86]. At each market session opening hour, a stage of the optimization problem is solved using as input not only wind speed and electricity prices forecasts but also the solution of the previous stage.

A sketch of this process is presented in Figure 5.6. The process starts when the Daily Market (DM) market bidding is solved, generating an hourly power schedule vector P_{Sch}. This vector is updated, by each Intraday Market (ID) and SOC Emptying (SE) optimization algorithm, and sent to secondary control level in real-time throughout the day. Each time these algorithms are utilized, as a result, the P_{Sch} is updated.

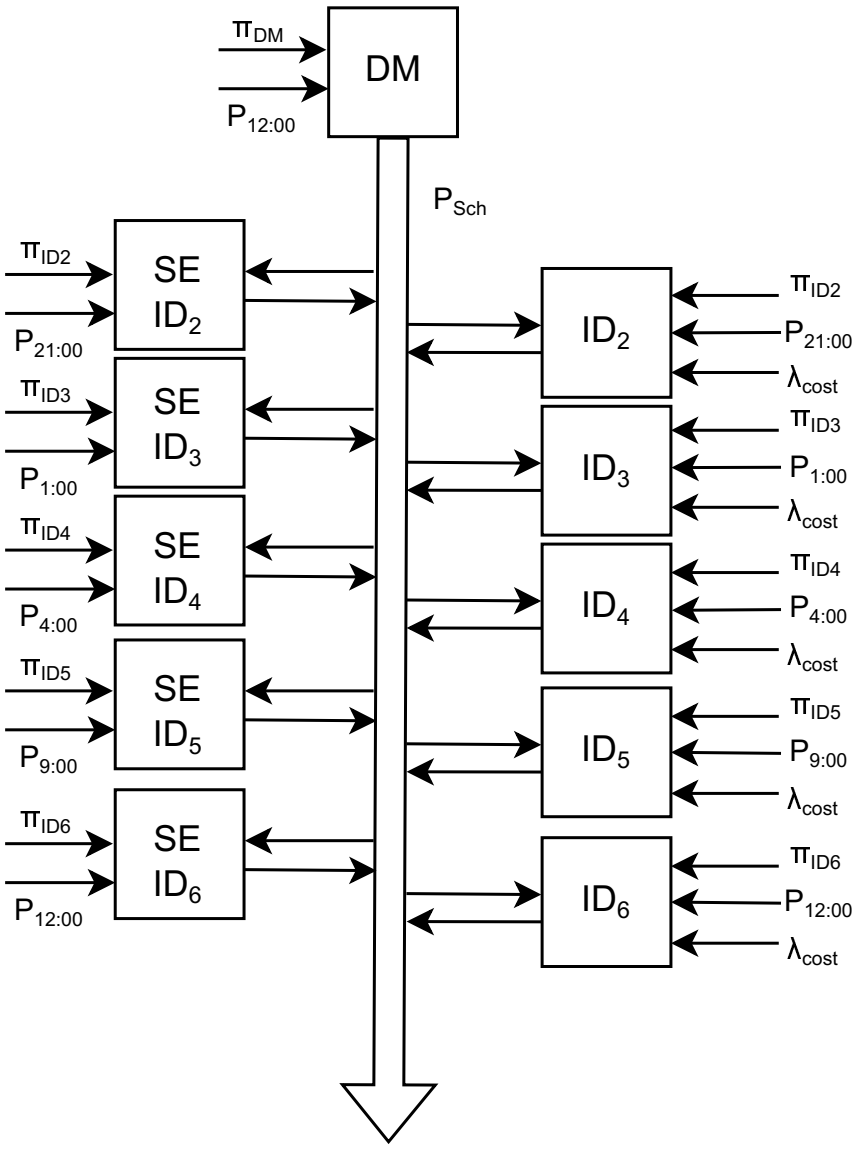

Figure 5.6: Daily optimization process.

This section presents the formulation of the optimization algorithms. It begins by introducing the day-ahead market operation, followed by the intraday market ones. Lastly, an algorithm based in controlling intraday market participation splitting the ESS is proposed.

5.3.1. Day-ahead market offering

The inputs for the day-ahead market offering include the price and power generation forecasts for the next day generated at 12:00 PM, the actual ESS nominal power and capacity, and other plant parameters. The constraints of the standalone BESS optimization model are used here.

Since a new component is added, the HF power flow must be defined. Since the WTG is considered a black box, only this new constraint is needed. It is formulated as follows:

$$P_{Gen}(t) = P_s(t) + P_{Ch}(t), \tag{5.10}$$

where:

- $P_{Gen}(t)$: Total generation power during hourly period t *(MW)*.
- $P_s(t)$: Generation power sent directly to the grid during hourly period t *(MW)*.
- $P_{Ch}(t)$: Generation power sent to the storage system during hourly period t *(MW)*.

The objective function aims to generate a vector of hourly commitments for the day-ahead market. It will use the ESS to allocate generated energy in the most profitable hours. It is defined as:

$$Max\left\{\sum_{h=1}^{24} \pi_{DM}(t) \cdot \Big(P_s(t) + P_{Dis}(t)\Big)\right\}. \tag{5.11}$$

As it can be seen, ESS does not purchase energy from the market. As per the regulations of the Renewable Energy Economic Regime [84], ESS is not allowed to purchase energy from electricity markets when operating in hybrid plants.

5.3.2. Intraday market offering

Intraday markets participation allows to correct deviations from the day-ahead market schedule. Downwards deviations can be corrected by purchasing energy in the market. Upward deviations can be corrected by generation excess.

The optimization algorithm takes as input the day-ahead market schedule, wind power forecasts, deviation costs, real-time SOC and intraday market prices. Each intraday market session occurs three hours before delivery, as shown in Table 5.1. The expected SOC at the start of delivery is communicated by the tertiary control level.

Constraints from day-ahead scheduling are repeated here. However, new ones are added to manage deviations. They are formulated as follows:

1. Upwards deviations are defined separately from downwards deviations:

$$\lambda_{\uparrow}(t) = P_{PCC}(t) - P_{sch}(t), \tag{5.12}$$

where:

- $\lambda_{\uparrow}(t)$: Upward deviation during hourly period *t (MW)*.
- $P_{PCC}(t)$: PCC power during hourly period *t (MW)*.
- $P_{sch}(t)$: Scheduled power during hourly period *t (MW)*.

2. Downwards deviations are formulated as:

$$\lambda_{\downarrow}(t) = P_{sch}(t) - P_{PCC}(t), \tag{5.13}$$

where:

- $\lambda_{\downarrow}(t)$: Downward deviation during hourly period *t (MW)*.

3. Downwards deviations are considered as always positive, to separate both types:

$$\lambda_{\downarrow}(t) \geq 0. \tag{5.14}$$

4. The same happens with upwards deviations:

$$\lambda_{\uparrow}(t) \geq 0. \tag{5.15}$$

As it can be seen, when one type of deviation takes place, the other is equal to zero.

5. Hourly deviation costs are:

$$\lambda_{Cost}(t) = \lambda_{\downarrow}(t) \cdot \rho(t) - \lambda_{\uparrow}(t) \cdot \beta(t). \tag{5.16}$$

Deviation penalties and bonuses are calculated from expressions (5.3) to (5.5). The intraday optimization uses real day-ahead market prices, since they are already available at the time of the intraday market sessions. Due the complexity of forecasting deviation coefficient, it is set at 21%, which the average from 2017 and all deviations are considered to be against the system. Historical deviation coefficients are used to calculate real benefits.

6. Internal power flow constraint depicted on (5.10) is modified:

$$P_{Gen}(t) = P_s(t) + P_{Ch}(t) + P_{Del}(t) + P_{Curt}(t), \tag{5.17}$$

where:

- $P_{Del}(t)$: Generated power used to cover deviations during hourly period *t (MW)*.

- $P_{Cur}(t)$: Generation power curtailed during hourly period *t (MW)*.

Generated power is allocated to either cover expected deviations or maximize profits in the intraday market.

7. The constraint regulating stored energy results:

$$E(t) = E(t-1) + \Big(P_{Ch}(t) \cdot \xi - \frac{P_{Dis}(t) + P_{Dis,s}(t)}{\xi}\Big), \tag{5.18}$$

where:

- $P_{Dis,s}(t)$: ESS power sold during hourly period *t (MW)*.

This split of discharged power into two parts, one used to cover deviations and one used for arbitrage, is similar to the division of generated power.

8. If arbitrage on intraday market is disabled, the following constraints are applied:

$$P_{Dis,s}(t) = 0. \tag{5.19}$$

$$P_{s}(t) = 0. \tag{5.20}$$

9. PCC output power is computed as follows:

$$P_{PCC}(t) = P_{Del}(t) + P_{Dis}(t) + P_{\varphi}(t). \tag{5.21}$$

The intraday market purchased power is not physically received by the plant and serves to fulfill commitments on the day-ahead market in case of deviations. It is therefore not included in the PCC output power constraint, which measures expected deviations. The exchanged power is part of the scheduled power vector input for the subsequent intraday market optimization, as shown in the constraints represented by expressions (5.12) and (5.13).

The objective function is defined in (5.22), it aims to minimize expected deviations and maximize profits by energy trading .

$$Max\Bigg\{\sum_{h=1}^{ID_{len}} \pi_{ID}(t) \cdot \Big(P_{s}(t) + P_{Dis,s}(t) - P_{\varphi}(t)\Big) - \lambda_{Cost}(t)\Bigg\}, \tag{5.22}$$

where:

- ID_{len}: intraday market length.

The hourly commitment vector is updated using the outputs of the intraday market optimization problem:

$$P_{S\,ch,new}(t) = P_{S\,ch,prev}(t) - P_{\varphi}(t) + (P_{s}(t) + P_{Dis,s}(t)), \tag{5.23}$$

where:

- $P_{Sch,new}(t)$: New hourly schedule *(MW)*.
- $P_{Sch,prev}(t)$: Previous hourly schedule *(MW)*.

5.3.3. State of charge emptying algorithm

As previously discussed, the secondary control level sends generated energy to the grid when the ESS is full and hourly commitments are fulfilled, leading to an upward deviation. The market operator only pays for excess energy at the day-ahead market full price when the deviation is in favor of the system, as described in equations (5.2) and (5.3). This can result in a missed opportunity to sell energy at higher prices when the deviation is against the system.

Moreover, the highest calendar degradation occurs when the ESS is at full capacity, as shown in Table 5.2. A novel optimization algorithm is proposed which involves selling part of the stored energy on the nearest intraday market when the ESS SOC exceeds a the threshold. This service differs from intraday market arbitrage in:

- It operates simultaneously with the intraday market optimization process.
- It only manages energy above a certain threshold, effectively splitting the ESS.
- It is limited to offering energy only in the first hours of each intraday market, to prevent overlap with the next one.

For illustration purposes, in Figure 5.7 the operating hours of the proposed service are shown, marked in blue over the delivery hours of intraday market, which are marked as white bars. As it can be seen, the first hours of each intraday market are not repeated in the following ones, hence no market overlapping occurs when operating here.

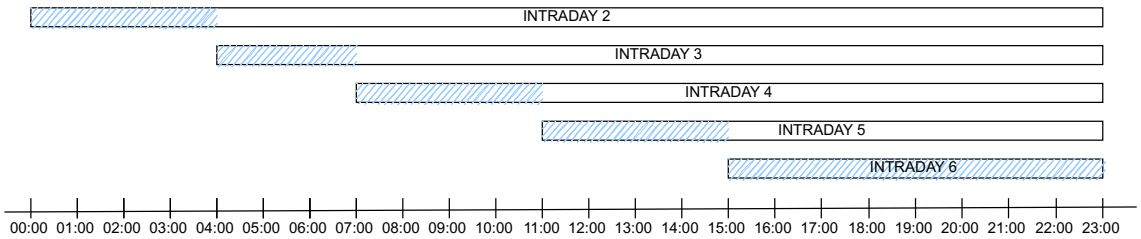

Figure 5.7: SE service operating hours.

This service splits the ESS into two Virtual Energy Storage Systems (VESS), one for profit generation and the other for deviation reduction. The stored energy is divided with a threshold of 75% set for the SE service. This value was determined through testing various values in the study and was found to be the optimal balance between profits and deviation reduction.

$$SOC = SOC_i - SOC_{SE}, \tag{5.24}$$

where:

- SOC_{SE}: SOC threshold *(%)*.
- SOC_i: Initial SOC *(%)*.

The SE service is managed as an optimization problem identical to the one for intraday market participation, but limited to the first hours of the next intraday market. The variables used for deviation coverage are disabled as the objective of this service is solely profit generation. The objective function is:

$$Max \sum_{h=1}^{SE_{len}} \pi_{ID} \cdot P_{SE}(t)\Big), \tag{5.25}$$

where:

- SE_{len}: SE length for the next intraday market .
- $P_{SE}(t)$: Power sold during hourly period *t (MW)*.

As evident, the goal is to sell available energy at the most expensive hours. The scheduled power vector is updated as in (5.23).

$$P_{Sch,new}(t) = P_{Sch,prev}(t) + P_{SE}(t). \tag{5.26}$$

5.4. Market participation strategies

In this section, different case studies are presented, each showcasing a different approach to using the ESS on the HF. Each case involves simulating the HF with the respective approach operating during 2018 in the Iberian electricity markets. The aim is to compare and assess whether revenue-stacking is more efficient than focusing on individual services, and the performance of the proposed service.

At the end of each day, accumulated degradation and SOC serve as initial value for the following day's operation. The average daily profits and degradation under each scenario are used in a full project extrapolation for a comprehensive view of the different cases.

5.4.1. Simulation cases

The simulation use cases are the following:

- Ideal: Perfect foresight of prices and power generation; operates only in day-ahead market.
- DM: The plant only participates in the day-ahead market, the ESS is used for covering deviations in real time.
- DM + SE: Similar to the *DM* case, but the SE service is also enabled.
- DM + ID: Similar to the *ID* case, but the plant also trades energy in the intraday markets.
- ID: Only participates in intraday markets for covering deviations.
- SE: Only participates in intraday markets to cover deviations and performs SE service.
- CF: Similar to the *DM* case, but the ESS does not participate in the day-ahead market optimization.

5.4.2. Simulations results

The simulation was conducted using the same input data in each case. Expected profits were calculated by summing the expected earnings from day-ahead and intraday market commitments. Real profits were calculated as the difference between daily earnings equation (5.8) and daily losses (Equation 5.9) using historical data of electricity prices and deviation coefficients. Figure 5.8 displays the accumulated profits and costs for each scenario and Table 5.3 shows the numerical results.

Table 5.3: Numerical results.

Case	Expected profits (M€)	Deviation costs (M€)	Purchases costs (M€)	Real profits (M€)
Ideal	0.614	0	0	0.614
DM + ID	1.677	0.031	1.309	0.336
ID	1.671	0.029	1.305	0.338
DM	0.488	-0.277	0.256	0.509
DM + SE	0.581	-0.201	0.276	0.507
SE	0.568	-0.195	0.255	0.508
CF	0.482	-0.27	0.244	0.509

The results indicate that expected profits increase with intraday market arbitrage, as anticipated. These profits are calculated based on the delivery of all committed energy to the market, resulting in higher profits in scenarios with intraday market participation as

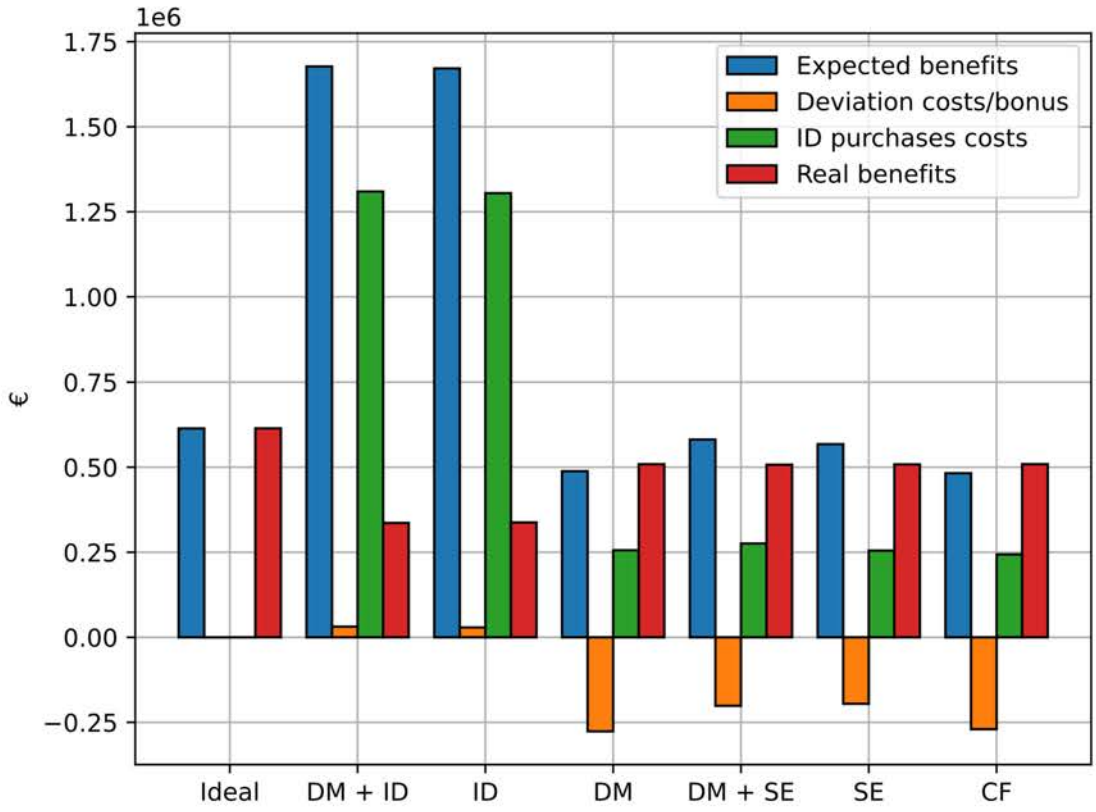

Figure 5.8: Simulations results.

all expected energy excess can be sold. The worst expected outcomes occur in scenarios without intraday market participation and similar results are observed when the ESS performs capacity firming.

The deviation costs are negative in almost all scenarios, indicating that upward deviations are more frequent. Purchasing energy in the intraday market effectively avoids downward deviations. The fewer services the ESS provides, the greater the negative deviation costs, suggesting that the ESS tends to be fully charged most of the time, leading to upward deviations.

Purchases in the intraday market are the primary source of profitability loss. These costs are significantly higher when selling energy in the intraday market is enabled. The fact that intraday market purchases occur when the ESS cannot cover expected deviations highlights that increased ESS involvement in markets can have negative effects.

Committing more energy to various markets increases the risk of having to make corrections by purchasing energy in the intraday market. The best results seem to be achieved by letting the ESS operate solely on the day-ahead market or providing capacity firming services. As shown in Figure 5.9, intraday market participation has resulted in the need to cover up to 40% of committed energy through intraday market purchases.

Figure 5.10 displays the accumulated degradation. In the scenarios where the ESS

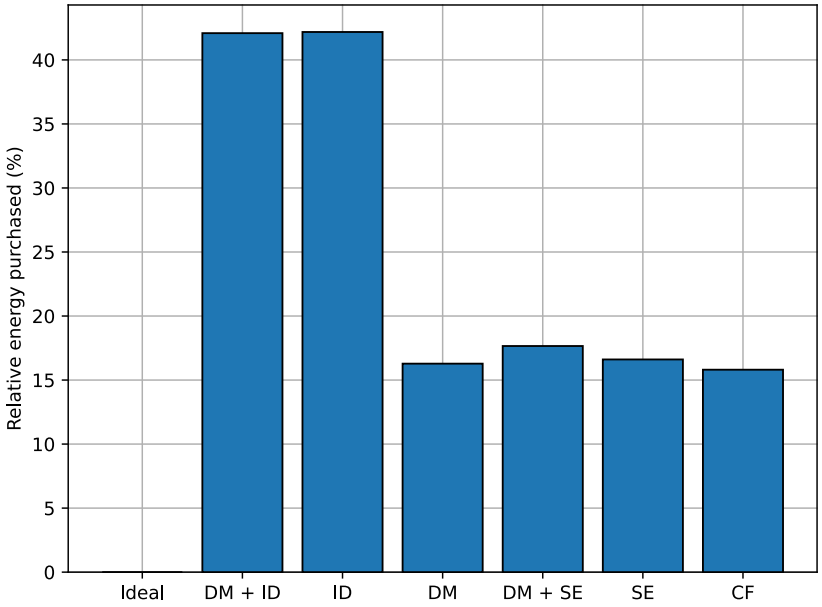

Figure 5.9: Committed energy covered with purchases on intraday markets.

provides the most services, it tends to be emptier, which reduces calendar degradation and results in lower overall aging of the ESS.

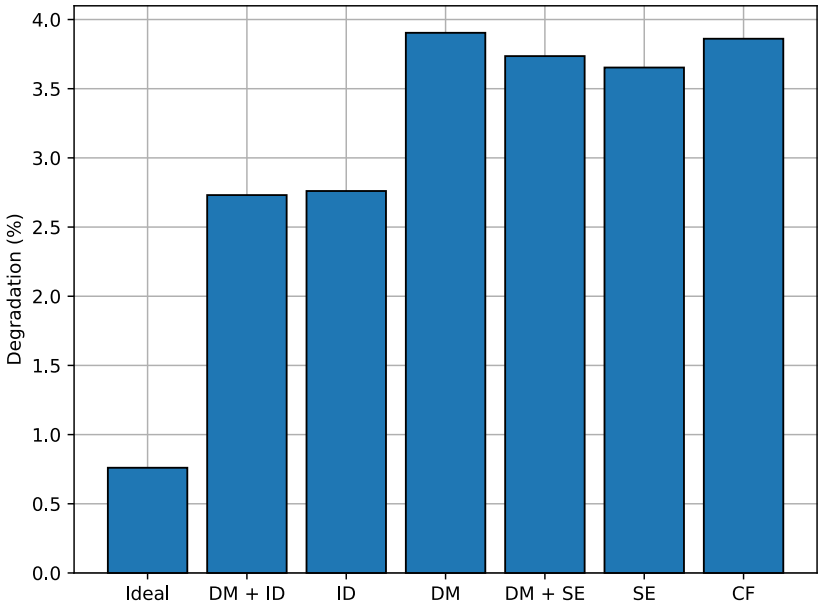

Figure 5.10: Degradation under each case.

Figure 5.11 shows the comparison between real profits and degradation. As it can be seen, the case in which the BESS solely performs the proposed SE service and real-time deviation management yields the best benefits per degradation. This indicates that that reserving the ESS for SOC emptying and capacity firming yields the best outcome when profits are compared to capacity loss, which is a more efficient usage of the ESS.

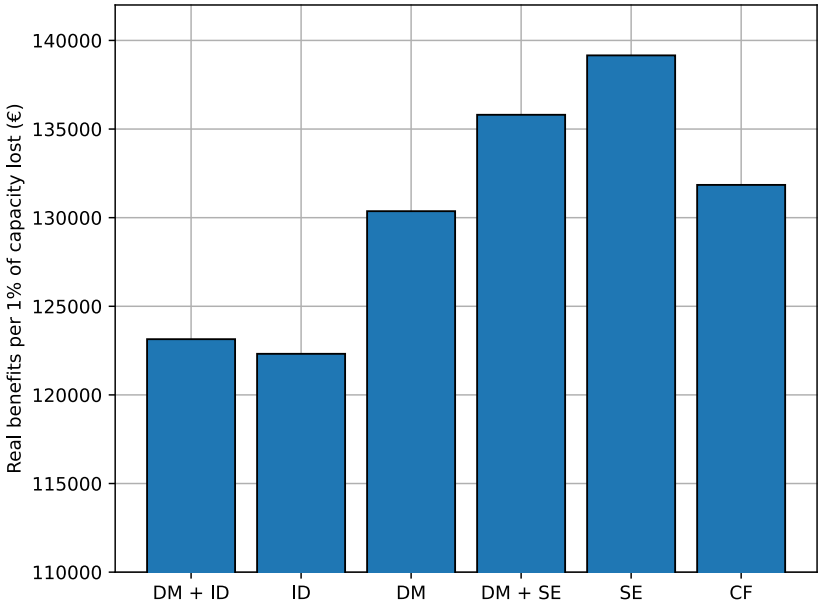

Figure 5.11: Real profits per 1% of capacity lost.

5.4.3. Full project extrapolation results.

The trade-off between maximizing short-term profits and stretching the life of the energy storage system is a crucial factor to consider. The NPV is a useful metric that takes into account future cash flows and discount rate to determine a project's overall profitability.

In the table, NPV of each case is calculated, discounting daily cash flow and the purchase cost of the ESS. The results show that the best NPV is achieved when the ESS is reserved for SE and capacity firming. When only participating on day-ahead market, NPV is not very different, but participating on intraday market s significantly lowers the NPV, indicating lower project profitability.

The results of each simulation scenario are extrapolated for the entire project. The average daily cash flow is determined from the average daily results of 2018, and daily degradation is similarly calculated to estimate project completion. The project ends when the accumulated degradation of the ESS reaches 20%, a commonly used value in relevant literature (e.g. [34], [35]). The average values and estimated project lifetimes for each case are presented in Table 5.4.

It is worth noting that the ESS is not operated in the ideal scenario. In this case, the ESS is only utilized for allocating generated energy when prices are the highest. However, due to degradation costs and the ESS efficiency, this operation is not profitable

The SE has lower daily profits but higher NPV compared to the case with CF. The NPV of each project is calculated using a 7.5% discount rate and presented in Table 5.5. The results show that using the ESS for SE service and capacity firming provides the highest NPV.

Table 5.4: Project extrapolation under each case.

Case	Average daily capacity loss (%)	Average daily profits (€)	Lifetime (years)
Ideal	$2.08 \cdot 10^{-3}$	1682.28	26.31
DM + ID	$7.48 \cdot 10^{-3}$	921.44	7.32
ID	$7.56 \cdot 10^{-3}$	925.11	7.25
DM	$1.06 \cdot 10^{-2}$	1394.37	5.12
DM + SE	$1.02 \cdot 10^{-2}$	1389.89	5.36
SE	$1 \cdot 10^{-2}$	1392.7	5.48
CF	$1.05 \cdot 10^{-2}$	1394.74	5.18

Table 5.5: Project extrapolation under each case.

Case	NPV (M€)
Ideal	7.226
DM + intraday market	1.912
intraday market	1.905
DM	2.179
DM + SE	2.253
SE	2.299
CF	2.2

5.5. Chapter conclusion

An HF model formulation has been presented in this chapter. This model is made for operating in multiple electricity markets. A three-level control system has been proposed for market bids origination in the market sessions, as well as real-time deviation management. A novel control algorithm for mitigating the effect of market overlapping has been proposed.

In the next chapter, the fundamentals of green hydrogen production are presented. A green hydrogen production system model is incorporating into the HF model. This new system enables participation in the hydrogen market. The effect of uncertainties is studied, as well as different future scenarios of hydrogen market and supply chain which are evaluated with a proposed simulation framework.

6. USE OF ALKALINE ELECTROLYZERS IN HYBRID WIND AND ENERGY STORAGE SYSTEMS

The incorporation of an electrolyzer into the HF enables the participation in the hydrogen market. This device is used for generating hydrogen whenever electricity prices are low or there is a surplus. The incorporation of a green hydrogen production system increases complexity and requires the implementation of more advanced EMS control algorithms.

This chapter introduces the fundamentals of green hydrogen production, specifically with AELs. The formulation for an AEL for EMS applications is introduced. Day-ahead market participation and real-time management is proposed as a MILP optimization problem, the effect of uncertainties is incorporated into a two-stage stochastic algorithm. The comparison of different approaches, with the proposal of a novel one, is evaluated in an implementation.

6.1. Green hydrogen production

The term *Green Hydrogen* refers to the hydrogen generated by low-emission energy sources. This is achieved by splitting water molecules using electricity. This process is called *water electrolysis*, and it is performed by a device called *electrolyzer*.

This section describes the electrolysis process. Afterwards, AELs working principles are presented. This technology has been chosen over Polymer Electrolyte Membrane (PEM) and Solid Oxide Electrolyzers (SOE) due its maturity [87].

6.1.1. Water electrolysis

The process of water electrolysis, consists in applying a voltage to water. This is performed in an electrochemical cell, as the one illustrated in Figure 6.1. Hydrogen and oxygen gas bubbles evolve at the cathode and anode respectively [88].

When an electric current is applied across the electrodes, the water molecules at the anode are oxidized, releasing oxygen gas and protons. These protons then migrate through the diaphragm to the cathode, where they combine with electrons to form hydrogen gas [89]. The reactions involved are [90]:

$$\begin{aligned} \text{Anode: } & 4\,OH^- \longrightarrow O_2 + 2\,H_2O + 4\,e^- \\ \text{Cathode: } & 4\,H_2O^- + 4\,e^- \longrightarrow 2\,H_2 + 4\,OH^- \\ \text{Overall: } & 2\,H_2O \longrightarrow 2\,H_2 + O_2 \end{aligned}$$

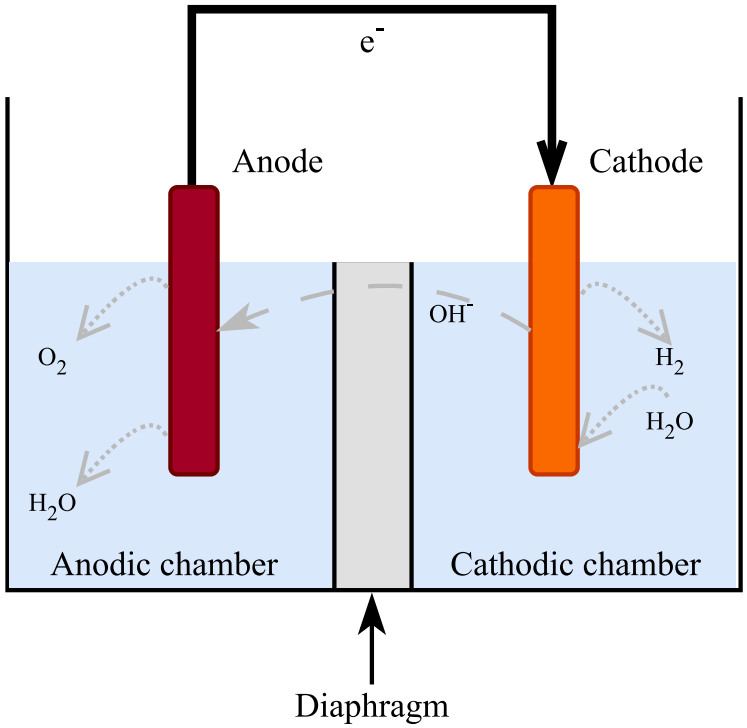

Figure 6.1: Water electrolysis.

The efficiency of the electrolysis depends on the electrode materials, current density and temperature, among other factors. This is a well-established process which has been used over two centuries, the device in which this process occurs is called *electrolyzer*. There are three main water electrolyzer technologies:

- AELs: Using an alkaline electrolyte solution [89].
- Proton Exchange Membrane (PEM) electrolyzers: Using a solid polymer electrolyte membrane at low temperatures and pressures [91].
- Solid Oxide Electrolyzers (SOE): Using a solid oxide electrolyte at high temperatures [92].

AEL are the most widespread technology for industrial applications. They operate at relatively low temperatures and pressures and use economical materials. This technology has been applied at large scales and it is considered as the most mature [87].

6.1.2. Alkaline electrolyzers working principles

AEL electrolyzers use an alkaline electrolyte solution, usually potassium hydroxide (KOH). The electrodes are typically made of nickel or steel. The hydroxide ions move from the cathodic to the anodic chamber through a diaphragm while the hydrogen protons are collected [93].

One of the main drawbacks of these devices is the effect of partial loads. Hydrogen purity in oxygen decreases at lower current densities. This leads to the formation of explosive gases, as reported in [94]. After reaching a 2% of H_2 concentration in O_2, the AEL is shut down as a safety measure. After this shut down, the electrolyzer has to be purged with a noble gas, such as Argon [95].

Figure 6.2 illustrates the relationship between input power and H_2 concentration in O_2. This has been obtained empirically by authors on [94]. As it can be seen, at higher input powers such concentration remains stable.

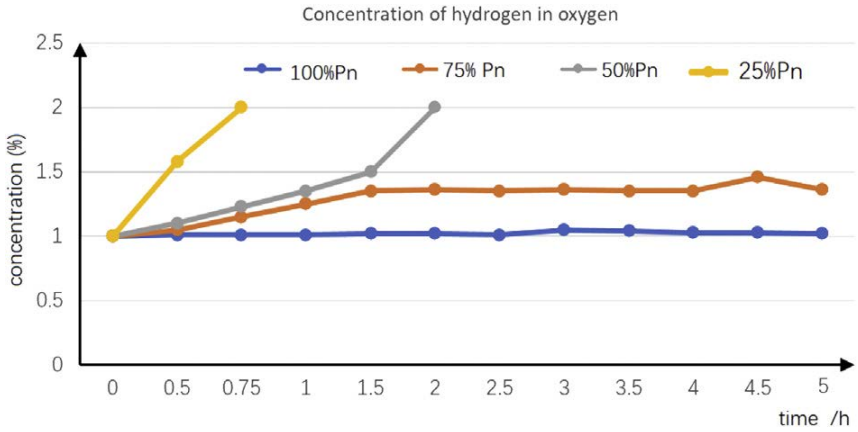

Figure 6.2: Relationship between oxygen contamination and active power [94].

Furthermore, an AEL can only generate hydrogen at nominal pressure and temperature conditions [96]. This requires to spend time and energy in switching on the electrolyzer into this state. Cold starts are possible, however it is common to also keep the electrolyzer in standby mode for a faster hot start [97].

Nevertheless, there is a lack of empirical data for examining the AEL operation impact in this ageing process. Authors in [98] argue that the deterioration of the electrolyte is a result of the dissolution of elements, as well as the detachment and coalescence of catalysts. The degradation process results in a decline in efficiency, as reported in [87].

6.2. Alkaline electrolyzer model

The literature on AEL modelling is limited in comparison to the literature on BESS. A common approach is the use of current-voltage models, as first proposed by Ulleberg in [99]. However, these models are not efficient for long-range simulations due to their non-linear nature and excessive complexity.

Authors in [100] introduce a model for mixed-integer dynamic optimization, with a high degree of nonlinearity. In [101], the nonlinearities caused by the relationship between the modelling of heat production caused by electrolysis. The framework uses an auxiliary advanced AEL model to update a fixed electrolysis efficiency in order to avoid non-linearities and improve accuracy.

A linear formulation, suitable for MILP, is presented in [96]. This model incorporates operational states and startup times, which are very important in alkaline electrolyzers. Authors study the effect of variable wind energy on Power-to-H2 using a fluctuating wind energy source.

The model presented in this work is linear, its input variable is active power and its output is hydrogen flow. This approach is based in an extension of the formulation presented in [96] that considers degradation caused by usage and start/stop cycles. The effect of partial loads in O_2 purity is also incorporated, as a contribution of this work.

Authors in [98] argue that the deterioration of the electrolyte is a result of the dissolution of elements, as well as the detachment and coalescence of catalysts. The degradation process results in a decline in efficiency, as reported in [87].

Nevertheless, there is a lack of empirical data for examining the AEL operation impact in this ageing process. This makes the incorporation of degradation into AEL modelling less common. A fixed rate of 1% efficiency loss per year is considered in [102]. Authors in [87] follow a similar strategy.

The degradation model proposed in this work follows a semi-empirical approach, which gives an approximation operation effect in useful life loss. To quantify the degradation caused by intermittent operation, a start-stop cycle counter is utilized, as a limited number of cycles have been reported in reference [103]. Additionally, a working hours model is taken into account, recognizing that the loss of efficiency is also proportional to the limited lifetime hours, as reported in reference [104].

This semi-empirical model integrates manufacturer's data in useful life into short-term operation analysis. As with the BESS model, the lost of useful lifetime by operation is computed using the units-of-production method, [105]:

$$\Delta Life_{AEL}(t) = \frac{Hours(t)}{EOL_{hours}} + \frac{Cycles(t)}{EOL_{Cycles}}, \tag{6.1}$$

where:

- $Life_{AEL}(t)$: AEL remaining useful lifetime t *(p.u.)*.
- $Hours(t)$: Hours of operation during hour t.
- EOL_{hours}: Lifetime hours.
- $Cycles(t)$: Start/stop cycles performed during hour t.
- EOL_{Cycles}: Start/stop lifetime cycles.

Finally, the effect of partial loads on operation is considered. Hydrogen purity in oxygen decreases at lower current densities. This leads to the formation of explosive

gases, as reported in [94]. After reaching a 2% of H_2 concentration in O_2, the AEL is shut down as a safety measure.

In the approach outlined in [106], a minimal load threshold is established to control the purity of hydrogen in oxygen. This approach does not consider the contamination process at variable loads, which results in a less flexible operation. In this work, empirical data from [94] is used to develop an oxygen contamination model.

The results obtained by experiments conducted by authors in [94] are depicted in Figure 6.2. As illustrated, at 25% of rated power the 2% safety limit is reached in less than one hour. It is worth noting that this process is not reversible, once the limit is reached, the AEL needs to be shut down for purging. The oxygen contamination model proposed in this work follows calculates the level of hydrogen purity present in oxygen based on the operational conditions, it is formulated as follows:

$$\Delta H_2(h) = \begin{cases} 3.5 - 5 \cdot P(t) & \text{if} \quad 0.3 \leq P(t) \leq 0.7 \\ 0 & \text{if} \quad P(t) > 0.7 \end{cases} \tag{6.2}$$

where:

- $\Delta H_2(h)$: Hydrogen contamination growth during hourly hour t *(p.u.)*.
- P: AEL input power during hourly hour t *(p.u.)*.

The current approach employs electrolyzer's input power as decision variable. The device generates hydrogen only in nominal pressure and temperature conditions [106]. Reaching and maintaining such conditions requires energy. In absence of this energy, the device begins to cool, ultimately reaching a fully cold state. Consequently, the system's operational modes are defined as follows:

- *On* mode: The AEL is producing hydrogen and operating at nominal conditions.
- *Idle* mode: Nominal conditions are maintained, but the AEL is not producing hydrogen.
- *Off* mode: The AEL is not generating hydrogen and no energy is being applied to maintain nominal conditions, resulting in a gradual cooling until reaching a fully cold state.

Transitioning from *off* mode to *on* mode necessitates a starting power proportional to the discrepancy between the electrolyzer's current pressure and temperature and the conditions required for hydrogen production [97]. Both *off* and *idle* modes entail active power consumption, although power usage during *off* mode is minimal, in this work such power consumption is neglected.

As with the BESS model, the optimization constraints align with the physical limitations of the device, limiting the solution space. These constraints are outlined as follows:

1. The total electrolyzer power output for each time period is derived from the sum of the various operating modes:

$$P_{on}(t) + P_{idle}(t) + P_{start}(t) = P_{AEL}(t) \ , \tag{6.3}$$

where:

- $P_{on}(t)$: Power employed in producing hydrogen during hour *t (MW)*.
- $P_{idle}(t)$: Power consumed in the *idle* mode during hour *t (MW)*.
- $P_{start}(t)$: Cold starting power consumed during hour *t (MW)*.
- $P_{AEL}(t)$: Total power consumption during hour *t (MW)*.

2. Binary variables are used to determine the AEL operation mode at each hour, only one mode is allowed at a time:

$$On(t) + Off(t) + Idle(t) = 1, \tag{6.4}$$

where:

- $On(t)$: Binary variable for *on* mode.
- $Off(t)$: Binary variable for *off* mode.
- $Idle(t)$: Binary variable for the *idle* mode.

Each binary variable takes value 1 when its respective mode is enabled.

3. An additional mode is used to define the cooling process, which appears only when the AEL is off:

$$Cool(t) \leq Off(t) \ , \tag{6.5}$$

where: $Cool(t)$ is a binary variable which defines *cool* mode. It equals 1 when its temperature and pressure state has gone colder.

4. The pressure & temperature state of the electrolyzer is updated at each hour as follows:

$$\tau(t) = \tau(t-1) + \upsilon(t) \cdot t_{off} - Cool(t), \tag{6.6}$$

where:

- $\tau(t)$: State at the end of hour t, this variable is limited between 0 and t_{off}.
- t_{off}: Number of hours it takes to get fully cold when off.
- $\upsilon(t)$: The fraction of the starting power required to a cold start.

5. The cooling process stops when it reaches a fully cold state:

$$\begin{cases} Cool(t) \leq \frac{\tau(t-1)}{t_{off}} + 0.9 \\ Cool(t) \geq \frac{\tau(t-1)}{t_{off}} - 1 + Off(t) \end{cases} , \tag{6.7}$$

the 0.9 in the first term prevents the binary variable $Cool(t)$ from reaching a value of 0 until $\frac{\tau(t-1)}{t_{off}}$ is 0.

6. *Idle* mode hourly power consumption is defined as:

$$P_{idle} = Idle\,(t) \cdot P_{idle}\ , \tag{6.8}$$

where P_{idle} is the hourly power consumption during idle mode in MW.

7. *On* mode hourly power consumption is limited as:

$$P_{on,min} \cdot On(t) \leq P_{on}\,(t)\ \leq P_{on,max} \cdot On(t)\ , \tag{6.9}$$

where:

- $P_{on,min}$: Minimum AEL *on* mode active power *(MW)*.
- $P_{on,max}$: Maximum AEL *on* mode active power *(MW)*.

8. The cold start power factor is defined as:

$$\upsilon(t) \leq \frac{t_{off}(t) - \tau\,(t-1)}{t_{off}}. \tag{6.10}$$

9. The cold start power consumption is defined as:

$$P_{start}\,(t) = Start_{factor}\,(t) \cdot t_{start} \cdot AEL_{Pmax}, \tag{6.11}$$

where:

- t_{start}: Cold start time in hours.
- AEL_{Pmax}: Maximum electrolyzer power *(MW)*.

10. The hydrogen generation process is defined as:

$$Q\,(t) = P_{on} \cdot \frac{AEL_{eff}}{HHV}, \tag{6.12}$$

where:

- $Q\,(t)$: Hydrogen flow during hour h *(kg)*.
- AEL_{eff}: AEL efficiency *(p.u.)*.
- HHV: Hydrogen high heating value *(kg/MWh)*.

11. The operation cost of the AEL, defined with the degradation models described above, is formulated as:

$$Deg_{Cost,AEL}(t) = \left(\frac{On\,(t)}{EOL_{hours}} + \frac{P_{start}(t)}{AEL_{Pmax} \cdot t_{start} \cdot EOL_{Cycles}}\right) \cdot K, \tag{6.13}$$

where:

- $Deg_{Cost,AEL}(t)$: Degradation cost during hour *t (€)*.
- K: Electrolyzer replacement cost *(€)*.

12. The oxygen contamination process is formulated as:

$$imp\,(t) = imp\,(t-1) + cont\,(t) - 2 \cdot purg(t), \tag{6.14}$$

where:

- $imp\,(t)$: Oxygen impurity level at the end of hour t *(%)*.
- $cont\,(t)$: Oxygen contamination during hour t *(%)*.
- $purg(t)$: A binary variable which defines the AEL purging.

13. The *purging* mode is enabled when no H_2 is being produced:

$$purg\,(t) \leq off\,(t) + idle(t). \tag{6.15}$$

An inequality constraint is applied to allow for the possibility of *off* and *idle* modes to be non-zero when no purge is in progress. This scenario occurs, for instance, when the AEL is in a clean state and does not intend to generate hydrogen, enabling the *off* or *idle* binary variables to have a value of 1.

14. When oxygen contamination reaches 2%, the AEL is shut down:

$$imp\,(t-1) - off\,(t) \leq 2. \tag{6.16}$$

15. Purging mode is disabled when contamination value reaches 0:

$$purg\,(t) \leq imp(t-1). \tag{6.17}$$

16. A piecewise constraint is used to regulate the contamination process, derived from (6.2):

$$cont(t) = \begin{cases} 0 & \text{if} \quad \frac{P_{on}(t)}{AEL_{Pmax}} < 0.3 \\ 3.5 - 5 \cdot \frac{P_{on}(t)}{AEL_{Pmax}} & \text{if} \quad 0.3 \leq \frac{P_{on}(t)}{AEL_{Pmax}} \leq 0.7 \\ 0 & \text{if} \quad \frac{P_{on}(t)}{AEL_{Pmax}} > 0.7 \end{cases} \tag{6.18}$$

Plant model

The plant model combines the previously formulated model constraints. Additional ones define the interactions between the plant components. Figure 6.3 illustrates the plant architecture.

As illustrated, the system operates within the hydrogen and electricity markets. Energy generated by the wind turbine can be sent to the AEL, the BESS, and the grid. The BESS can supply energy to both the AEL and the grid. The AEL can receive energy from all other agents.

These additional constraints are used to determine the aforementioned interactions. Active powers during each hourly period are considered constant, thus active power can be treated as energy. These constraints are defined as follows:

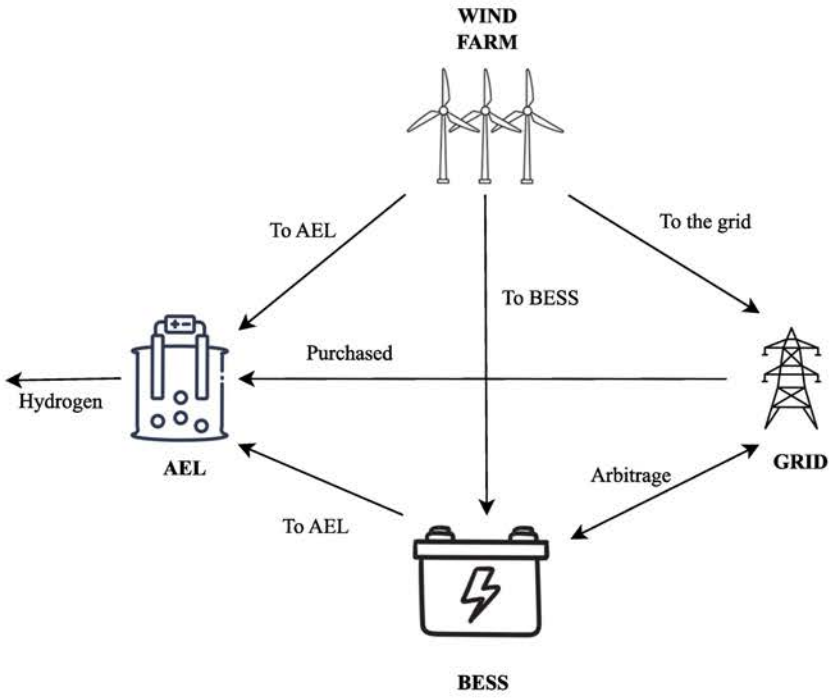

Figure 6.3: Plant architecture.

1. The generated power by the wind farm is defined as:

$$P_{Gen}(t) = P_{WTG,BESS}(t) + P_{WTG,Grid}(t) + P_{WTG,AEL}(t) + P_{WTG,Curt}(t), \tag{6.19}$$

where:

- $P_{Gen}(t)$: Generated power during hour t *(MW)*.
- $P_{WTG,BESS}(t)$: Generated power sent to the BESS during hour t *(MW)*.
- $P_{WTG,Grid}(t)$: Generated power sent to the grid during hour t *(MW)*.
- $P_{WTG,AEL}(t)$: Generated power sent to the AEL*(MW)*.
- $P_{WTG,Curt}(t)$: Curtailed power during hour t *(MW)*.

2. The BESS discharging power is divided as follows:

$$P_D(t) = P_{BESS,Grid}(t) + P_{BESS,AEL}(t) \ , \tag{6.20}$$

where:

- $P_{BESS,Grid}(t)$: BESS power sent to the grid during hour t *(MW)*.
- $P_{BESS,AEL}(t)$: BESS power sent to the AEL during hour t *(MW)*.

3. The AEL power flow is defined as follows:

$$P_{AEL}(t) = P_{BESS,AEL}(t) + P_{Grid,AEL}(t) + P_{WTG,AEL}(t) \ . \tag{6.21}$$

As it can be seen, these constraints formulation just relates the different plant components power flow. The assumption that no losses caused by power converters or lines is taken. The effect of such losses could be modelled by incorporating efficiency factors to this formulation, which is beyond the scope of this work.

6.3. Day-ahead operation optimization model

The constraints from the previous section are applied in two optimization models: one for generating day-ahead electricity market commitments and the other for reducing deviations and producing hydrogen from electricity. In this section, the formulation of the objective functions of both models are introduced. As example, the operation for a single day is shown.

6.3.1. Day-ahead market bidding

This optimization model receives as inputs hourly prices and wind speed forecasts. This model generates hourly day-ahead market commitments. Its objective function is formulated as follows:

$$\text{maximize} \sum_{t=1}^{24} \Big[\pi_{El,fore}(t) \cdot (P_{WTG,Grid}(t) + P_{BESS,Grid}(t) - P_{Grid,BESS}(t) - P_{Grid,AEL}(t)) + \pi_{H2} \cdot Q(t) - Deg_{Cost,AEL}(t) \Big] - Deg_{Cost,BESS}, \quad (6.22)$$

where:

- $\pi_{El,fore}(t)$: Hourly forecasted electricity price *(€/MWh)*.
- π_{H2}: Hydrogen price *(€/kg)*.

As it can be seen the objective function has two terms: one for the operation in the electricity market and other for the operation in the hydrogen market.

6.3.2. Real-time operation

Real-time operation is based on the assumption that actual electricity and wind speed are know and available at the start of the day. An optimization model is used to allocate resources to minimize deviation and maximize revenues by also producing hydrogen. An additional constraint, which calculates deviation costs, needs be added to this model:

$$Dev_{Costs}(t) = \Big[P_{Com,DM}(t) - (P_{WTG,Grid}(t) - P_{BESS,Grid}(t)) \Big] \cdot \lambda \cdot \pi_{El,real}(t) \quad , \quad (6.23)$$

where:

- $P_{Com,DM}(t)$: Day-ahead market power commitment for hour *t (MW)*.

- $\pi_{El,real}(t)$: Real electricity price for hour t *(€/MWh)*.
- λ: Deviation costs factor for hour t.

The objective function of this optimization problem is formulated as follows:

$$maximize \sum_{t=1}^{24} \left[\pi_{H2} \cdot Q(t) - Dev_{Costs}(t) \right] - Deg_{Cost}(t) \,. \tag{6.24}$$

The primary objective at this stage is to optimize profits through the implementation of measures aimed at minimizing deviation costs and utilizing surplus energy for the production of hydrogen.

6.4. Two-stage stochastic optimization algorithms

This section introduces the approaches of stochastic optimization for this application. The common Montecarlo approach is compared to a proposed Bootstrapping approach. The formulation for both strategies is presented.

6.4.1. Montecarlo approach

In this approach, 10 wind speed and electricity prices scenarios are generated for each day using a SARIMA model. Historical electricity prices from DKK1 are used as input. The authors in [70] statistically show that a SARIMA with order $(2,1,3)(1,0,1)_{24}$ is appropriate for forecasting such prices, and the same order is used here too. The previous 100 days of hourly electricity prices are used as training data.

Hourly wind speed data, obtained for Merra-2 Database [107], located in Brande, Denmark, is used as input for wind speed prediction. In its first stage, a SARIMA of is used to generate a deterministic forecast of wind speed, which is then computed as wind power using the curve of the Siemens SWT-3.0-113 wind turbine generator. The SARIMA model has an order of $(2,0,1)(2,0,3)_{12}$, which has been obtained through testing. Wind speed data from previous 5 days is used as training data.

In Figure 6.4, deterministic forecasts for price and wind speed on March the 25^{th} 2020 are shown, this day has been selected arbitrarily for illustration purposes. The figure shows that forecast errors grow over time, with electricity prices overestimated in later hours and wind speed underestimated for this specific day.

The scenarios, generated using historical data in the forecasting model, are used to obtain a probability density function of the realization of the uncertain parameters. A set of 10 wind speed and electricity prices scenarios for March the 25th 2020 is shown, for both wind speed and electricity prices is shown in 6.5.

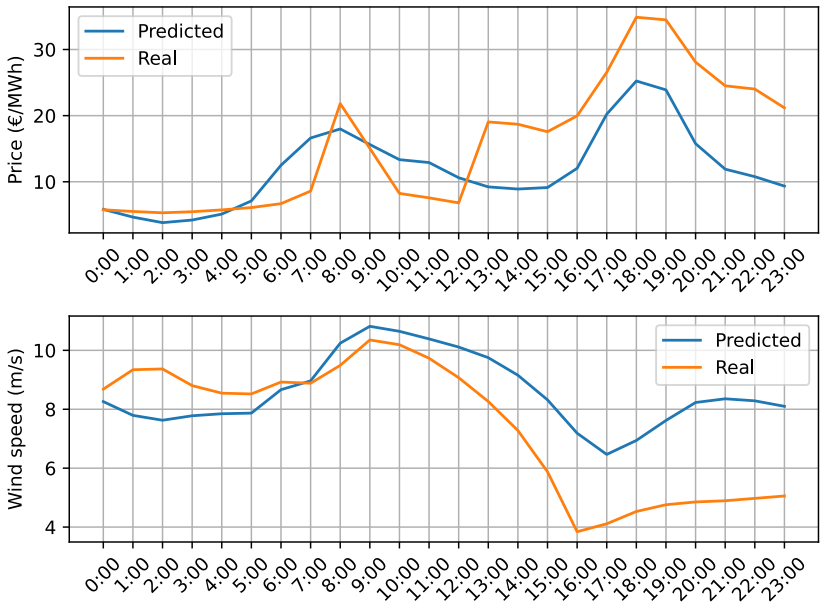

Figure 6.4: Deterministic forecasts for March the 25^{th} 2020.

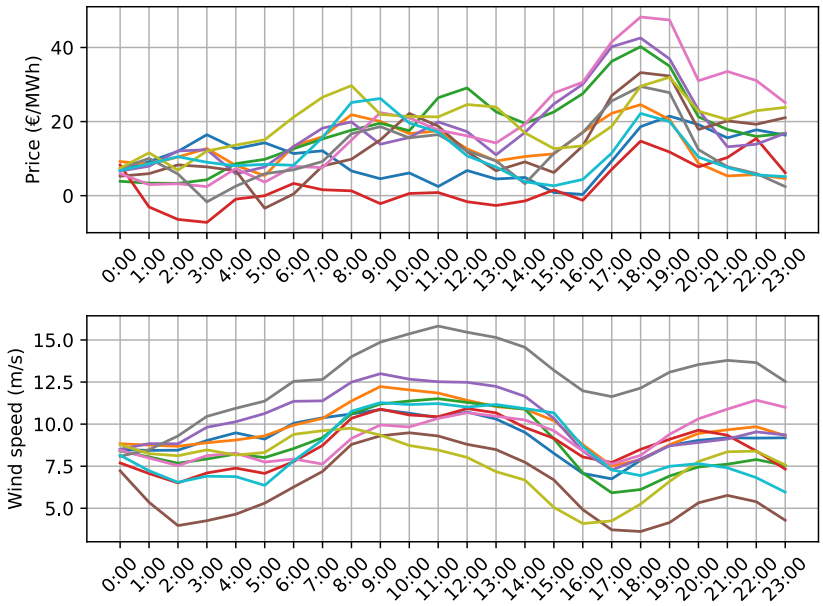

Figure 6.5: Probabilistic forecast example for March the 25^{th} 2020.

For each combination of scenarios, a candidate solution is generated using the day-ahead optimization model. Therefore, in the first stage 100 candidate solutions are generated. The power commitments of each candidate solution are sent to the real-time optimization model.

The real-stage optimization is solved for each candidate solution under each combination of wind and price scenario. This results in 100x100 evaluations for each day. The costs of each candidate under each combination of scenarios are calculated as follows:

$$Cost(i, j) = Dev_{Costs}(i, j) + \Delta E_{Ben}(i, j), \tag{6.25}$$

where:

- $Cost(i, j)$: The second-stage costs under wind speed scenario j and electricity price scenario i (€).
- $Dev_{Costs}(i, j)$: Deviation costs under wind speed scenario j and electricity price scenario i (€).
- $\Delta E_{Ben}(i, j)$: Difference between expected and real electricity market benefits under wind speed scenario j and electricity price scenario i (€).

A sample of 100 second-stage costs is generated for each candidate solution. Figure 6.6, illustrates an example.

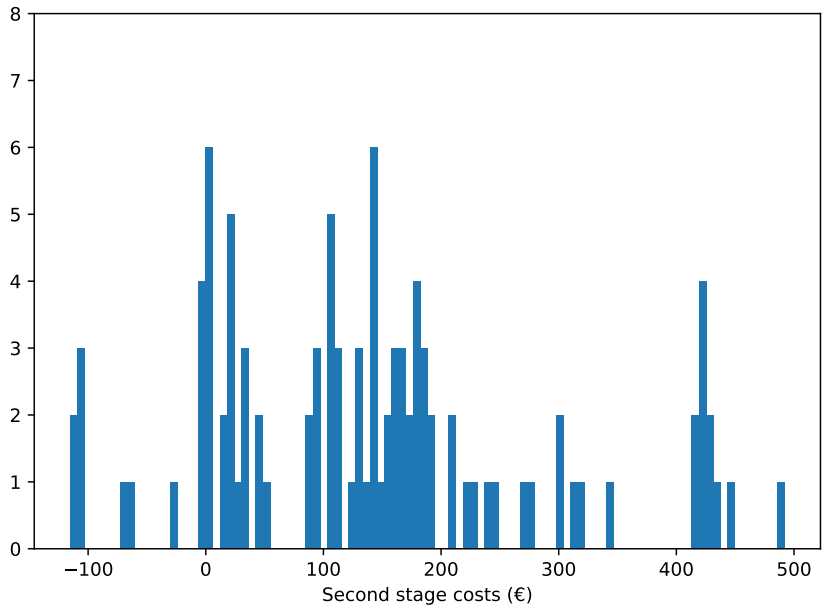

Figure 6.6: Sample of 100 second-stage costs.

Negative costs result from certain combinations of scenarios, indicating more energy was available than expected. The accuracy of Montecarlo-based stochastic algorithms depends on the number of simulations, so a large number of simulations should be performed to reduce uncertainty in the results. This stochastic optimization problem can be formulated as follows:

$$\max E_1(S) - CVaR_{1-\beta}(E_2(S)), \tag{6.26}$$

where:

- $E_1(S)$: Expected benefits for candidate solution S *(€)*.
- $CVaR_{1-\beta}(E_2(S))$: Conditional variance of the second-stage costs for candidate solution S, for the confidence interval β *(€)*.

The current implementation faces a challenge in regards to increasing the number of available samples. Each sample requires solving an additional optimization problem, and therefore, for 100 candidate solutions, 10.000 optimization problems must be solved for each day. This can result in the requirement to solve a million optimization problems in order to obtain 1000 samples for 1000 candidate solutions, which may render the problem computationally infeasible due to the amount of computational time required.

6.4.2. Bootstrapping approach

Bootstrapping is a re-sampling method which allows to estimate parameters using sampled data [108]. It is used when the sampling process is difficult, for example in clinical studies [109]. It is also used when the available input data is scarce, which is the common case in some forecasting applications [110].

This method involves re-sampling the original population randomly, generating a new sample. A statistical quantity of the new sample is calculated, such as the mean. By repeating this process, a distribution of estimates is obtained, which can be used to calculate variability measures.

Bootstrapping is often computationally simpler than Montecarlo. Besides, it can provide more accurate estimates when the sample size is small or the distribution is not normal [111]. Also, obtaining a confidence interval of a statistical quantity allows for a more robust approach with a smaller population of samples.

In this application, the second-stage costs are re-sampled with repetition, and the mean of each re-sample is stored. This process is repeated 10.000 times, creating new *bootstrap sample*. An example of a bootstrap sample obtained with this procedure is shown in Figure 6.7.

As it can be seen, this distribution presents a more normal shape. The formulation presented in (6.26) can be adapted to this approach as follows:

$$\max E_1(S) - CVaR_{1-\beta}(E_2(\overline{S})), \tag{6.27}$$

where $CVaR_{1-\beta}(E_2(\overline{S}))$ is the conditional variance of the second-stage costs means for candidate solution S, in € for the confidence interval β. A 95% confidence interval is used in this case.

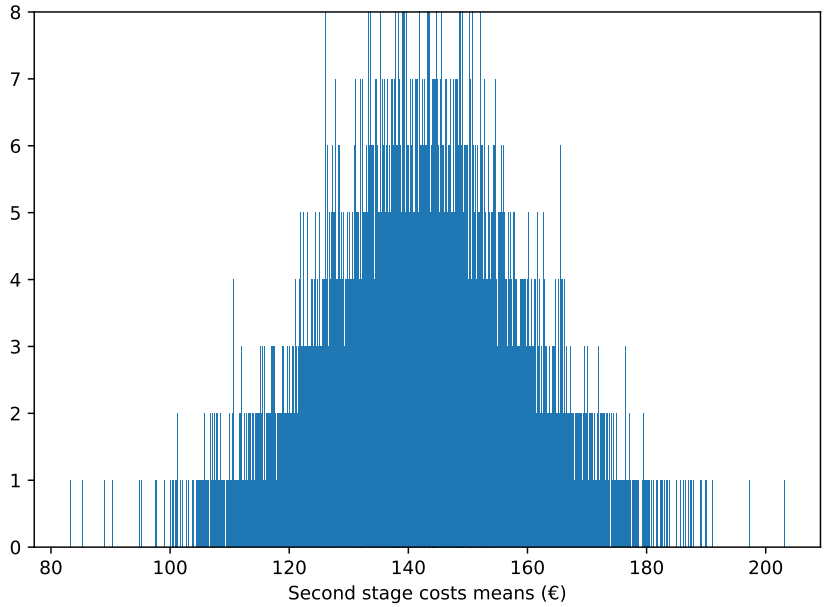

Figure 6.7: Second-stage costs means bootstrap sample.

6.5. Simulation results

A demonstration of the introduced model is presented in this section. Afterwards, the simulation framework for evaluating the performance of the proposed optimization method is described. Different simulation scenarios are run on the same plant model, in each case a different approach for generating day-ahead market commitments is considered. Results under each approach are presented and compared.

6.5.1. Single-day demonstration

This subsection presents a demonstration of the formulated plant model operation for March the 25^{th} 2020. The demonstration employs a deterministic forecast of electricity prices and generated power as input for the day-ahead stage. The power commitments are subsequently inputted into the real-time optimization problem, the primary objective of which is to minimize deviation resulting from forecasting errors.

The plant's components parameters are introduced in Table 6.1.

The inputs for the day-ahead scheduling optimization problem is the predicted wind and electricity prices, shown in Figure 6.4. The optimal solution is depicted in Figure 6.8, which shows the hourly active powers from the plant components and the power exchanges with the grid.

The electrolyzer starts at full power later in the first hour by taking cold start power from the grid and runs at full power all day. The battery schedules an arbitrage operation using price spread. When electricity prices are low, some power generated from the wind

Table 6.1: Plant parameters.

Parameter	Value	Parameter	Value
AEL Nominal Power	1 MW	AEL cooling time	5 hours
AEL Minimum Power	0.3 MW	Hydrogen HHV	0.0394 kg · MWh
AEL efficiency	75%	AEL Idle mode power	0.04 MW
AEL replacement cost	500 €/kW	BESS capacity	10 MWh
AEL Lifetime	100000 hours	BESS nominal power	2.5 MW
AEL Lifetime cycles	50000	BESS efficiency	90%
AEL cold start time	12 minutes	BESS replacement cost	50 €/KWh

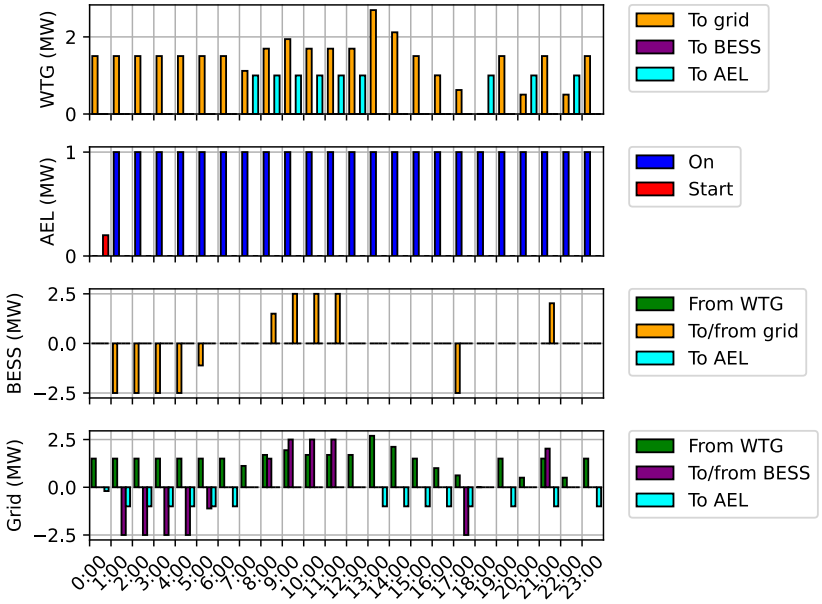

Figure 6.8: Day-ahead commitment example for March the 25^{th} 2020.

turbine is sent to the electrolyzer for hydrogen production.

The hourly commitments generated in this stage are sent to the real-time stage. The optimization problem takes as input the real electricity prices, wind speed from day and day-ahead hourly power commitments. Figure 6.9 illustrates the results:

The optimization problem uses the BESS to cover deviations since real generated power is lower than expected (as shown in Figure 6.4). Wind turbine generated power is stored during low electricity price hours, when deviation costs are low, and released by the BESS during price peaks at the end of the day. Hydrogen production is kept constant during the day.

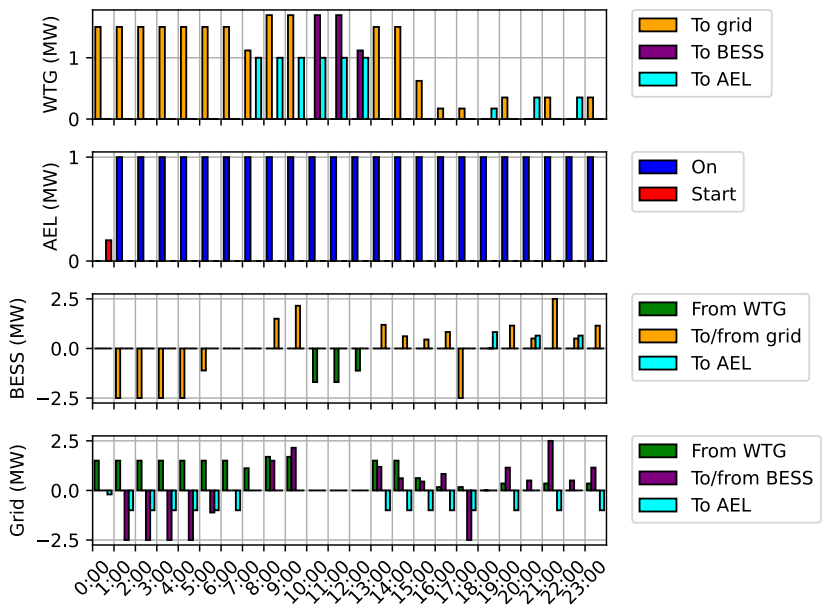

Figure 6.9: Real-time operation example for March the 25^{th} 2020.

6.5.2. Cases of study

Different cases of study are performed with the simulation framework. The simulation goes from January the 1^{st} 2020 to December the 31^{st} 2020. AEL and BESS states at the end of a day are considered as the initial for the next one. For simplicity, perfect price & wind power foresight are assumed.

The plant participates in two different markets, but future hydrogen prices are uncertain. The first case study examines the effects of various hydrogen prices. Figure 6.10 illustrates the accumulated benefits at the end of the year attained in both electricity and hydrogen market.

The figure shows that the hydrogen market benefits become noticeable only when hydrogen prices exceed 1.5€ per kg. As the hydrogen prices increase further, the plant starts to use more energy for hydrogen production and as a result, the electricity market participation decreases. When the hydrogen price reaches 3.5€/kg, the benefits from the hydrogen market surpass the ones from the electricity market.

Various green hydrogen supply chain configurations exist. One option involves a pipeline infrastructure, where the plant unloads the produced hydrogen in real-time [112]. Another option, particularly in the case of remote plant locations such as offshore, involves the storage of hydrogen in a tank, which is unloaded periodically using trucks or vessels [113], adding an extra constraint to green hydrogen production.

In this case of study, different tank capacities at and different tank unloading schedules are evaluated, both scenarios of low and high hydrogen prices are considered. Moreover, the scenario of a hydrogen pipeline is also evaluated. Figure 6.11 illustrates the accumu-

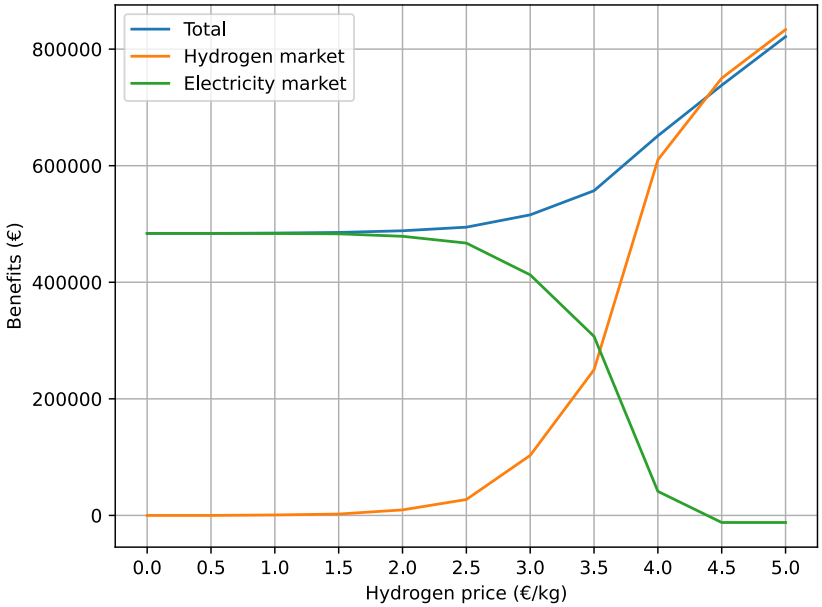

Figure 6.10: Hydrogen price effect on markets benefits.

lated benefits at the end of the year in each case.

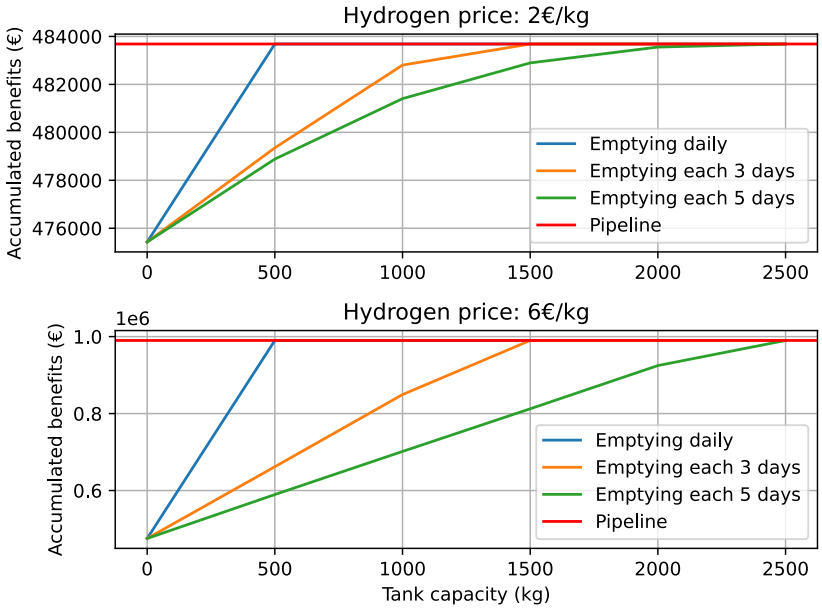

Figure 6.11: Hydrogen supply chain effect on benefits.

Results demonstrate how the pipeline scenario yields the best results. Increasing tank unloading regularity allows to operate with smaller tanks. This constraint needs to be carefully considered when sizing the plant, in order to attain the best balance between unloading schedule and tank capacity. This requirement is present in both low-price and high price scenarios.

6.5.3. Stochastic algorithms comparison

For validating the proposed stochastic optimization model, a simulation framework of the plant participating in hydrogen and day-ahead electricity markets is developed, a hydrogen price of 4€/kg is considered. The plant components parameters are the ones depicted in Table 6.1.

Four different simulation scenarios are considered:

- Ideal scenario: The plant receives perfect forecasts.
- Stochastic Montecarlo scenario: The Montecarlo algorithm is used.
- Stochastic Bootstrap scenario: The proposed bootstrap algorithm is used.
- Deterministic scenario: A direct approach, considering deterministic forecasts.

The total revenues for each simulation case are presented in Figure 6.12:

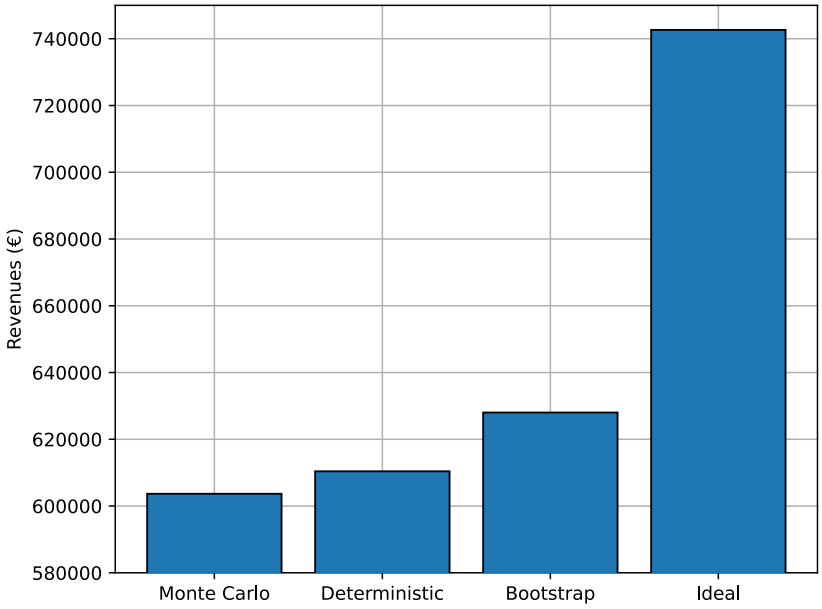

Figure 6.12: Final results for 2020 simulation.

As it can be seen, the Montecarlo approach yields the worst results, close to the deterministic case. This is caused by the low amount of samples used in the process, since this method performs better with higher populations. However, as mentioned above, the generation of samples with requires a high computational burden.

This issue is overcome with the use of bootstrap sampling in the second-stage samples. As it can be seen, by using the same original population and applying this re-sampling process, the results are improved. This proposed method has proven to outperform the Montecarlo and deterministic approaches used in the literature.

6.6. Chapter conclusion

A mathematical optimization model has been proposed for the integration of an AEL into the HF model outlined in Chapter 5. A linear formulation has been proposed to ensure its efficiency in EMS optimization applications, yet considering complex processes.

The effect of wind speed and energy price uncertainties has been addressed with the proposal of a two-stage stochastic optimization model. A comparison between a classical Montecarlo approach against the proposed Bootstrapping implementation demonstrate how this algorithm yields better outcome than the use of a Montecarlo strategy using the same data. Case studies of different plant configuration and hydrogen supply chain structures have been studied.

Results demonstrate how at low hydrogen prices, plant configuration must be carefully addressed in order to attain optimal income. Moreover, AEL interactions with the electrical market are detrimental at low hydrogen prices. As future works, authors propose the extension of this algorithm for intraday market participation. The BESS participation in frequency response services is also suggested.

7. CONCLUSIONS, CONTRIBUTIONS AND FUTURE WORKS

This chapter serves as the culminating point of this thesis dissertation, providing a summary of the conclusions and contributions made through the course of the research. Subsequently, it presents suggestions for future research and potential areas of expansion based on the findings of this study.

7.1. Conclusions & contributions

This research commenced with the implementation of degradation caused by operation into a standalone BESSs optimization framework. Two main approaches have been spotted in the literature for adapting the optimization problem formulation: implementing constraints to limit the operation or formulating the degradation as a cost in the objective function. It has been concluded that the methods based on using a degradation cost allow to better regulate the operation depending on the problem inputs.

The implementation of this degradation cost reduces short-term benefits increasing them in the long-term, by extending the BESS useful life. It has been demonstrated how the formulation of this degradation cost affects operation. Oversizing degradation impact in the operation can be detrimental, since it may prevent the BESS to operate in any scenario.

Risk-aware stochastic optimization strategies combined with this degradation cost have been compared in different use cases of BESS operating until reaching end of life. The importance of considering the full battery lifetime when evaluating these approaches has been demonstrated. The presence of a degradation cost has demonstrated to slightly improve the long-term profits, however these results have been found to be dependant on the stochastic approach.

By using an exogenous parameter, the robustness of the different stochastic strategies has been modulated. It has been found that a risk-averse approach does yields worst results for all values of that parameter, since income at the beginning of the lifetime is not as valuable as income at the end. Implementing a risk-prone approach to battery operation has demonstrated better results in the long-term, this is an important advantage found for risk measures-based stochastic strategies over deterministic schemes, which is a contribution of this work. Nevertheless, this requires to select the correct value for the exogenous parameter.

A three-level control system for a wind-storage hybrid system which participates in multiple Iberian electricity markets has been presented. The model has incorporated adjustments based on Iberian market regulations to account for committed power correction impacts. A simulation framework has been proposed to assess various market participa-

tion strategies.

The results show that using the ESS in all electricity markets not necessarily yields higher income, challenging the common belief that ESS revenue stacking is always beneficial. Market overlapping has been found to be the main cause of this issue. A new market participation strategy has been proposed, which has demonstrated to improve ESS benefits per degradation, this is an indicator of a more efficient usage.

Lastly, green hydrogen production has been incorporated into the hybrid system. A linear optimization model with an alkaline electrolyzer has been proposed. This formulation considers complex processes such as degradation and partial loading effect, along with the electrolyzer's operational states.

The effect of wind speed and energy price uncertainties has been addressed with the proposal of a two-stage stochastic optimization model. The state-of-the-art Montecarlo approach has been compared to a proposed Bootstrap-based algorithm. Results demonstrate how incorporating bootstrap sampling improve results using the same sampled data.

Case studies including different plant configurations and hydrogen supply chain structures have been studied. It has been found how at low hydrogen prices, plant configuration must be carefully addressed in order to attain optimal income. The structure of the hydrogen supply chain has shown to have more impact in project benefits at high hydrogen prices.

7.2. Future works

Future works should aim to improve current BESS degradation cost as a dynamic value, which changes over time and considers the remaining useful life. This dynamic approach, presented in Chapter 3, has been barely proposed in the literature.

Whilst revenue stacking in energy markets presents drawbacks, as outlined in Chapter 5, it is established that using BESSs for auxiliary services such as frequency response increases benefits. This topic has raised interest in recent literature and future research streams should explore control solutions for combining both applications.

Lastly, more data is required in understanding electrolyzer degradation caused by operation. The degradation model formulation presented in this article is a simplistic application of manufacturers data. Future researchers should develop more detailed degradation models, unfortunately, lack of available data causes a bottleneck in this topic.

BIBLIOGRAPHY

[1] F. Tanrisever, K. Derinkuyu, and G. Jongen, "Organization and functioning of liberalized electricity markets: An overview of the dutch market," *Renewable and Sustainable Energy Reviews*, vol. 51, pp. 1363–1374, 2015. DOI: https://doi.org/10.1016/j.rser.2015.07.019.

[2] D. Shah and S. Chatterjee, "A comprehensive review on day-ahead electricity market and important features of world's major electric power exchanges," *International Transactions on Electrical Energy Systems*, vol. 30, no. 7, e12360, 2020. DOI: https://doi.org/10.1002/2050-7038.12360.

[3] P. Shinde and M. Amelin, "A literature review of intraday electricity markets and prices," in *2019 IEEE Milan PowerTech*, 2019, pp. 1–6. DOI: 10.1109/PTC.2019.8810752.

[4] A. Lebedys *et al.*, "Renewable capacity statistics 2022," IRENA, 2022.

[5] L. Olatomiwa, S. Mekhilef, M. Ismail, and M. Moghavvemi, "Energy management strategies in hybrid renewable energy systems: A review," *Renewable and Sustainable Energy Reviews*, vol. 62, pp. 821–835, 2016. DOI: https://doi.org/10.1016/j.rser.2016.05.040.

[6] J. M. Morales, A. J. Conejo, H. Madsen, P. Pinson, and M. Zugno, *Integrating Renewables in Electricity Markets*. Springer, 2014.

[7] A. Olabi, C. Onumaegbu, T. Wilberforce, M. Ramadan, M. A. Abdelkareem, and A. H. Al – Alami, "Critical review of energy storage systems," *Energy*, vol. 214, p. 118 987, 2021. DOI: https://doi.org/10.1016/j.energy.2020.118987.

[8] J. Liu, C. Hu, A. Kimber, and Z. Wang, "Uses, cost-benefit analysis, and markets of energy storage systems for electric grid applications," *Journal of Energy Storage*, vol. 32, p. 101 731, 2020. DOI: https://doi.org/10.1016/j.est.2020.101731.

[9] L. Meng *et al.*, "Fast frequency response from energy storage systems—a review of grid standards, projects and technical issues," *IEEE Transactions on Smart Grid*, vol. 11, no. 2, pp. 1566–1581, 2020. DOI: 10.1109/TSG.2019.2940173.

[10] M. S. Rafaq, B. A. Basit, S. A. Q. Mohammed, and J.-W. Jung, "A comprehensive state-of-the-art review of power conditioning systems for energy storage systems: Topology and control applications in power systems," *IET Renewable Power Generation*, vol. 16, no. 10, pp. 1971–1991, 2022. DOI: https://doi.org/10.1049/rpg2.12498.

[11] R. Moreira, R. Moreno, and G. Strbac, "Synergies and conflicts among energy storage services," in *2016 IEEE International Energy Conference (ENERGYCON)*, 2016, pp. 1–6. DOI: http://dx.doi.org/10.1109/ENERGYCON.2016.7513945.

[12] M. Schoenfisch and A. Dasgupta, "Grid-scale storage," International Energy Agency (IEA), 2022.

[13] H. S. Hirsh, Y. Li, D. H. S. Tan, M. Zhang, E. Zhao, and Y. S. Meng, "Sodium-ion batteries paving the way for grid energy storage," *Advanced Energy Materials*, vol. 10, no. 32, p. 2 001 274, 2020. DOI: https://doi.org/10.1002/aenm.202001274.

[14] A. M. Oliveira, R. R. Beswick, and Y. Yan, "A green hydrogen economy for a renewable energy society," *Current Opinion in Chemical Engineering*, vol. 33, p. 100 701, 2021. DOI: https://doi.org/10.1016/j.coche.2021.100701.

[15] H. Wang *et al.*, "Research and demonstration on hydrogen compatibility of pipelines: A review of current status and challenges," *International Journal of Hydrogen Energy*, vol. 47, no. 66, pp. 28 585–28 604, 2022. DOI: https://doi.org/10.1016/j.ijhydene.2022.06.158.

[16] A. L. Santos, M.-J. Cebola, and D. M. F. Santos, "Towards the hydrogen economy—a review of the parameters that influence the efficiency of alkaline water electrolyzers," *Energies*, vol. 14, no. 11, 2021. DOI: https://doi.org/10.3390/en14113193.

[17] S. K. Rathor and D. Saxena, "Energy management system for smart grid: An overview and key issues," *International Journal of Energy Research*, vol. 44, no. 6, pp. 4067–4109, 2020. DOI: https://doi.org/10.1002/er.4883.

[18] B. Jyoti Saharia, H. Brahma, and N. Sarmah, "A review of algorithms for control and optimization for energy management of hybrid renewable energy systems," *Journal of Renewable and Sustainable Energy*, vol. 10, no. 5, p. 053 502, 2018. DOI: https://doi.org/10.1063/1.5032146.

[19] M. J., F. R. C., and R. J. K., *Chemistry*. Pearson, 2015.

[20] J. Hou, S. Qu, M. Yang, and J. Zhang, "Materials and electrode engineering of high capacity anodes in lithium ion batteries," *Journal of Power Sources*, vol. 450, p. 227 697, 2020. DOI: https://doi.org/10.1016/j.jpowsour.2019.227697.

[21] X. J., L. Q., and B. Y., "Understanding and applying coulombic efficiency in lithium metal batteries," *Nat Energy*, vol. 5, pp. 561–568, 2020. DOI: https://doi.org/10.1038/s41560-020-0648-z.

[22] X. Han *et al.*, "A review on the key issues of the lithium ion battery degradation among the whole life cycle," *eTransportation*, vol. 1, p. 100 005, 2019. DOI: https://doi.org/10.1016/j.etran.2019.100005.

[23] A. Barré, B. Deguilhem, S. Grolleau, M. Gérard, F. Suard, and D. Riu, "A review on lithium-ion battery ageing mechanisms and estimations for automotive applications," *Journal of Power Sources*, vol. 241, pp. 680–689, 2013. DOI: https://doi.org/10.1016/j.jpowsour.2013.05.040.

[24] D. M. Rosewater, D. A. Copp, T. A. Nguyen, R. H. Byrne, and S. Santoso, "Battery energy storage models for optimal control," *IEEE Access*, vol. 7, pp. 178 357–178 391, 2019. DOI: 10.1109/ACCESS.2019.2957698.

[25] "State of charge estimation of lithium-ion batteries using the open-circuit voltage at various ambient temperatures," *Applied Energy*, vol. 113, pp. 106–115, 2014. DOI: https://doi.org/10.1016/j.apenergy.2013.07.008.

[26] E. Namor, D. Torregrossa, R. Cherkaoui, and M. Paolone, "Parameter identification of a lithium-ion cell single-particle model through non-invasive testing," *Journal of Energy Storage*, vol. 12, pp. 138–148, 2017. DOI: https://doi.org/10.1016/j.est.2017.04.008.

[27] X. Han *et al.*, "A review on the key issues of the lithium ion battery degradation among the whole life cycle," *eTransportation*, vol. 1, p. 100 005, 2019. DOI: https://doi.org/10.1016/j.etran.2019.100005.

[28] M. Broussely, S. Herreyre, P. Biensan, P. Kasztejna, K. Nechev, and R. Staniewicz, "Aging mechanism in li ion cells and calendar life predictions," *Journal of Power Sources*, vol. 97-98, pp. 13–21, 2001, Proceedings of the 10th International Meeting on Lithium Batteries. DOI: https://doi.org/10.1016/S0378-7753(01)00722-4.

[29] A. Maheshwari, N. G. Paterakis, M. Santarelli, and M. Gibescu, "Optimizing the operation of energy storage using a non-linear lithium-ion battery degradation model," *Applied Energy*, vol. 261, p. 114 360, 2020. DOI: https://doi.org/10.1016/j.apenergy.2019.114360.

[30] J. Cao, D. Harrold, Z. Fan, T. Morstyn, D. Healey, and K. Li, "Deep reinforcement learning-based energy storage arbitrage with accurate lithium-ion battery degradation model," *IEEE Transactions on Smart Grid*, vol. 11, no. 5, pp. 4513–4521, 2020. DOI: 10.1109/TSG.2020.2986333.

[31] D. Ouyang, J. Weng, M. Chen, J. Liu, and J. Wang, "Experimental analysis on the degradation behavior of overdischarged lithium-ion battery combined with the effect of high-temperature environment," *International Journal of Energy Research*, vol. 44, no. 1, pp. 229–241, 2020. DOI: https://doi.org/10.1002/er.4898.

[32] A. Perez, R. Moreno, R. Moreira, M. Orchard, and G. Strbac, "Effect of battery degradation on multi-service portfolios of energy storage," *IEEE Transactions on Sustainable Energy*, vol. 7, pp. 1718–1729, Oct. 2016. DOI: 10.1109/TSTE.2016.2589943.

[33] D. Doerffel and S. A. Sharkh, "A critical review of using the peukert equation for determining the remaining capacity of lead-acid and lithium-ion batteries," *Journal of Power Sources*, vol. 155, no. 2, pp. 395–400, 2006. DOI: https://doi.org/10.1016/j.jpowsour.2005.04.030.

[34] K. Smith, A. Saxon, M. Keyser, B. Lundstrom, Ziwei Cao, and A. Roc, "Life prediction model for grid-connected li-ion battery energy storage system," in *2017 American Control Conference (ACC)*, 2017, pp. 4062–4068.

[35] A. Maheshwari, N. G. Paterakis, M. Santarelli, and M. Gibescu, "Optimizing the operation of energy storage using a non-linear lithium-ion battery degradation model," *Applied Energy*, vol. 261, p. 114 360, 2020.

[36] D. Haifeng, W. Xuezhe, and S. Zechang, "A new soh prediction concept for the power lithium-ion battery used on hevs," in *2009 IEEE Vehicle Power and Propulsion Conference*, 2009, pp. 1649–1653.

[37] T. Baumhöfer, M. Brühl, S. Rothgang, and D. U. Sauer, "Production caused variation in capacity aging trend and correlation to initial cell performance," *Journal of Power Sources*, vol. 247, pp. 332–338, 2014.

[38] J. M. Reniers, G. Mulder, S. Ober-Blöbaum, and D. A. Howey, "Improving optimal control of grid-connected lithium-ion batteries through more accurate battery and degradation modelling," *Journal of Power Sources*, vol. 379, pp. 91–102, 2018. DOI: https://doi.org/10.1016/j.jpowsour.2018.01.004.

[39] H. Farzin, M. Fotuhi-Firuzabad, and M. Moeini-Aghtaie, "A practical scheme to involve degradation cost of lithium-ion batteries in vehicle-to-grid applications," *IEEE Transactions on Sustainable Energy*, vol. 7, no. 4, pp. 1730–1738, 2016. DOI: 10.1109/TSTE.2016.2558500.

[40] G. Yan, D. Liu, J. Li, and G. Mu, "A cost accounting method of the li-ion battery energy storage system for frequency regulation considering the effect of life degradation," *Protection and Control of Modern Power Systems*, vol. 3, Dec. 2018. DOI: 10.1186/s41601-018-0076-2.

[41] S. Cheng, Y.-H. Liu, H. Hesse, M. Naumann, C. Truong, and A. Jossen, "A pso-optimized fuzzy logic control-based charging method for individual household battery storage systems within a community," Ph.D. dissertation, Feb. 2018, p. 469.

[42] A. F. Peñaranda, D. Romero-Quete, and C. A. Cortés, "Grid-scale battery energy storage for arbitrage purposes: A colombian case," *Batteries*, vol. 7, no. 3, 2021. DOI: 10.3390/batteries7030059.

[43] A. Akbari-Dibavar *et al.*, "Optimal battery storage arbitrage considering degradation cost in energy markets," in *2020 IEEE 29th International Symposium on Industrial Electronics (ISIE)*, 2020, pp. 929–934. DOI: 10.1109/ISIE45063.2020.9152498.

[44] M. Baggu, A. Nagarajan, D. Cutler, D. Olis, T. Bialek, and M. Symko-Davies, "Coordinated optimization of multiservice dispatch for energy storage systems with degradation model for utility applications," *IEEE Transactions on Sustainable Energy*, vol. PP, pp. 1–1, Jul. 2018. DOI: 10.1109/TSTE.2018.2853673.

[45] J.-O. Lee and Y.-S. Kim, "Novel battery degradation cost formulation for optimal scheduling of battery energy storage systems," *International Journal of Electrical Power & Energy Systems*, vol. 137, p. 107 795, 2022. DOI: https://doi.org/10.1016/j.ijepes.2021.107795.

[46] Y. Li *et al.*, "Design of minimum cost degradation-conscious lithium-ion battery energy storage system to achieve renewable power dispatchability," *Applied Energy*, vol. 260, p. 114 282, 2020. DOI: https://doi.org/10.1016/j.apenergy.2019.114282.

[47] J. Li, R. Landers, and J. Park, "A comprehensive single-particle-degradation model for battery state-of-health prediction," *Journal of Power Sources*, vol. 456, p. 227 950, 2020. DOI: https://doi.org/10.1016/j.jpowsour.2020.227950.

[48] X. Li and S. Wang, "Energy management and operational control methods for grid battery energy storage systems," *CSEE Journal of Power and Energy Systems*, vol. 7, no. 5, pp. 1026–1040, 2021. DOI: 10.17775/CSEEJPES.2019.00160.

[49] S. Pelletier, O. Jabali, G. Laporte, and M. Veneroni, "Battery degradation and behaviour for electric vehicles: Review and numerical analyses of several models," *Transportation Research Part B: Methodological*, vol. 103, pp. 158–187, 2017, Green Urban Transportation. DOI: https://doi.org/10.1016/j.trb.2017.01.020.

[50] R. L. Fares and M. E. Webber, "What are the tradeoffs between battery energy storage cycle life and calendar life in the energy arbitrage application?" *Journal of Energy Storage*, vol. 16, pp. 37–45, 2018. DOI: https://doi.org/10.1016/j.est.2018.01.002.

[51] T. Terlouw, T. AlSkaif, C. Bauer, and W. van Sark, "Multi-objective optimization of energy arbitrage in community energy storage systems using different battery technologies," *Applied Energy*, vol. 239, pp. 356–372, 2019. DOI: https://doi.org/10.1016/j.apenergy.2019.01.227.

[52] F. Wankmüller, P. R. Thimmapuram, K. G. Gallagher, and A. Botterud, "Impact of battery degradation on energy arbitrage revenue of grid-level energy storage," *Journal of Energy Storage*, vol. 10, pp. 56–66, 2017. DOI: https://doi.org/10.1016/j.est.2016.12.004.

[53] C. S. Lai *et al.*, "Levelized cost of electricity for photovoltaic/biogas power plant hybrid system with electrical energy storage degradation costs," *Energy Conversion and Management*, vol. 153, pp. 34–47, 2017. DOI: https://doi.org/10.1016/j.enconman.2017.09.076.

[54] A. Ahmadian, M. Sedghi, B. Mohammadi-ivatloo, A. Elkamel, M. Aliakbar Golkar, and M. Fowler, "Cost-benefit analysis of v2g implementation in distribution networks considering pevs battery degradation," *IEEE Transactions on Sustainable Energy*, vol. PP, pp. 1–1, Nov. 2017. DOI: 10.1109/TSTE.2017.2768437.

[55] Y. Wang, Z. Zhou, A. Botterud, K. Zhang, and Q. Ding, "Stochastic coordinated operation of wind and battery energy storage system considering battery degradation," *Journal of Modern Power Systems and Clean Energy*, vol. 4, no. 4, pp. 581–592, 2016. DOI: 10.1007/s40565-016-0238-z.

[56] W. Cole and A. W. Frazier, "Cost projections for utility-scale battery storage," National Renewable Energy Laboratory., Tech. Rep., 2021.

[57] W. Gorman, C. C. Montañés, A. Mills, J. H. Kim, D. Millstein, and R. Wiser, "Are coupled renewable-battery power plants more valuable than independently sited installations?" *Energy Economics*, vol. 107, p. 105 832, 2022. DOI: https://doi.org/10.1016/j.eneco.2022.105832.

[58] K. Abdulla *et al.*, "Optimal operation of energy storage systems considering forecasts and battery degradation," *IEEE Transactions on Smart Grid*, vol. 9, no. 3, pp. 2086–2096, 2018. DOI: 10.1109/TSG.2016.2606490.

[59] A. Akbari-Dibavar, K. Zare, and S. Nojavan, "A hybrid stochastic-robust optimization approach for energy storage arbitrage in day-ahead and real-time markets," *Sustainable Cities and Society*, vol. 49, p. 101 600, 2019. DOI: https://doi.org/10.1016/j.scs.2019.101600.

[60] L. A. Roald, D. Pozo, A. Papavasiliou, D. K. Molzahn, J. Kazempour, and A. Conejo, "Power systems optimization under uncertainty: A review of methods and applications," *Electric Power Systems Research*, vol. 214, p. 108 725, 2023. DOI: https://doi.org/10.1016/j.epsr.2022.108725.

[61] "Stochastic optimization: A review," *International Statistical Review*, vol. 70, no. 3, pp. 315–349, 2002. DOI: https://doi.org/10.2307/1403861.

[62] A. Zakaria, F. B. Ismail, M. H. Lipu, and M. Hannan, "Uncertainty models for stochastic optimization in renewable energy applications," *Renewable Energy*, vol. 145, pp. 1543–1571, 2020. DOI: https://doi.org/10.1016/j.renene.2019.07.081.

[63] M. Alipour, B. Mohammadi-Ivatloo, and K. Zare, "Stochastic scheduling of renewable and chp-based microgrids," *IEEE Transactions on Industrial Informatics*, vol. 11, no. 5, pp. 1049–1058, 2015. DOI: 10.1109/TII.2015.2462296.

[64] P. Krokhmal, M. Zabarankin, and S. Uryasev, "Modeling and optimization of risk," *Surveys in Operations Research and Management Science*, vol. 16, no. 2, pp. 49–66, 2011. DOI: https://doi.org/10.1016/j.sorms.2010.08.001.

[65] D. P. Kroese, T. J. Brereton, T. Taimre, and Z. I. Botev, "Why the monte carlo method is so important today," *Wiley Interdisciplinary Reviews: Computational Statistics*, vol. 6, 2014.

[66] R. L. Harrison, "Introduction to monte carlo simulation," *AIP Conference Proceedings*, vol. 1204, no. 1, pp. 17–21, 2010. DOI: 10.1063/1.3295638.

[67] T. Homem-de-Mello and G. Bayraksan, "Monte carlo sampling-based methods for stochastic optimization," *Surveys in Operations Research and Management Science*, vol. 19, no. 1, pp. 56–85, 2014. DOI: https://doi.org/10.1016/j.sorms.2014.05.001.

[68] R. J. Bessa, V. Miranda, A. Botterud, Z. Zhou, and J. Wang, "Time-adaptive quantile-copula for wind power probabilistic forecasting," *Renewable Energy*, vol. 40, no. 1, pp. 29–39, 2012. DOI: https://doi.org/10.1016/j.renene.2011.08.015.

[69] Growe-Kuska, N., Heitsch, H., and W. Romisch, "Scenario reduction and scenario tree construction for power management problems," in *2003 IEEE Bologna Power Tech Conference Proceedings,*, vol. 3, 2003. DOI: 10.1109/PTC.2003.1304379.

[70] C. McHugh, S. Coleman, D. Kerr, and D. McGlynn, "Forecasting day-ahead electricity prices with a sarimax model," *2019 IEEE Symposium Series on Computational Intelligence (SSCI)*, pp. 1523–1529, 2019. DOI: 10.1109/SSCI44817.2019.9002930.

[71] M. Salehi Borujeni, A. Akbari Foroud, and A. Dideban, "Wind speed scenario generation based on dependency structure analysis," *Journal of Wind Engineering and Industrial Aerodynamics*, vol. 172, pp. 453–465, 2018. DOI: https://doi.org/10.1016/j.jweia.2017.11.023.

[72] D. Krishnamurthy, C. Uckun, Z. Zhou, P. R. Thimmapuram, and A. Botterud, "Energy storage arbitrage under day-ahead and real-time price uncertainty," *IEEE Transactions on Power Systems*, vol. 33, no. 1, pp. 84–93, 2018. DOI: 10.1109/TPWRS.2017.2685347.

[73] M. K. Zanjani, M. Nourelfath, and D. Ait-Kadi, "A multi-stage stochastic programming approach for production planning with uncertainty in the quality of raw materials and demand," *International Journal of Production Research*, vol. 48, no. 16, pp. 4701–4723, 2010. DOI: 10.1080/00207540903055727.

[74] M. Khosravi, S. Afsharnia, and S. Farhangi, "Stochastic power management strategy for optimal day-ahead scheduling of wind-hess considering wind power generation and market price uncertainties," *International Journal of Electrical Power & Energy Systems*, vol. 134, p. 107 429, 2022. DOI: https://doi.org/10.1016/j.ijepes.2021.107429.

[75] Y. Wang, H. Zhao, and P. Li, "Optimal offering and operating strategies for wind-storage system participating in spot electricity markets with progressive stochastic-robust hybrid optimization model series," *Mathematical Problems in Engineering*, vol. 2019, pp. 1–19, Jul. 2019. DOI: 10.1155/2019/2142050.

[76] M. Rosenblatt, "Remarks on Some Nonparametric Estimates of a Density Function," *The Annals of Mathematical Statistics*, vol. 27, no. 3, pp. 832–837, 1956. DOI: 10.1214/aoms/1177728190.

[77] B. Verweij, S. Ahmed, A. Kleywegt, G. Nemhauser, and A. Shapiro, "The sample average approximation method applied to stochastic routing problems: A computational study," *Computational Optimization and Applications*, vol. 24, pp. 289–333, Feb. 2003.

[78] M. Naumann, M. Schimpe, P. Keil, H. C. Hesse, and A. Jossen, "Analysis and modeling of calendar aging of a commercial lifepo4/graphite cell," *Journal of Energy Storage*, vol. 17, pp. 153–169, 2018. DOI: https://doi.org/10.1016/j.est.2018.01.019.

[79] "Informe de supervisión del mercado peninsular mayorista al contado de electricidad. año 2020," CNMC, 2021.

[80] *Day-ahead-market-operation*, https://www.omie.es/sites/default/files/inline-files/day_ahead_market.pdf, Accessed: 2022-05-30.

[81] D. Zheng, M. Shi, Y. Wang, A. T. Eseye, and J. Zhang, "Day-ahead wind power forecasting using a two-stage hybrid modeling approach based on scada and meteorological information, and evaluating the impact of input-data dependency on forecasting accuracy," *Energies*, vol. 10, no. 12, 2017. DOI: 10.3390/en10121988.

[82] *Sotavento experimental wind park*, https://www.sotaventogalicia.com/area-tecnica/datos-tiempo-real/instantaneos-parque/, Accessed: 2022-05-30.

[83] *The wind power*, https://www.thewindpower.net/turbines_manufacturers_es.php, Accessed: 2022-05-30.

[84] *Real decreto 960/2020, de 3 de noviembre, por el que se regula el régimen económico de energías renovables para instalaciones de producción de energía eléctrica.* https://www.boe.es/buscar/doc.php?lang=en&id=BOE-A-2020-13591, 2020.

[85] R.-K. Kim, M. Glick, K. Olson, and Y.-S. Kim, "Milp-pso combined optimization algorithm for an islanded microgrid scheduling with detailed battery ess efficiency model and policy considerations," *Energies*, vol. 13, p. 1898, Apr. 2020. DOI: 10.3390/en13081898.

[86] Y. Wang, H. Zhao, and P. Li, "Optimal offering and operating strategies for wind-storage system participating in spot electricity markets with progressive stochastic-robust hybrid optimization model series," *Mathematical Problems in Engineering*, vol. 2019, pp. 1–19, 2019. DOI: 10.1155/2019/2142050.

[87] M. David, C. Ocampo-Martínez, and R. Sánchez-Peña, "Advances in alkaline water electrolyzers: A review," *Journal of Energy Storage*, vol. 23, pp. 392–403, 2019. DOI: https://doi.org/10.1016/j.est.2019.03.001.

[88] M. Rashid, M. Al Mesfer, H. Naseem, and M. Danish, "Hydrogen production by water electrolysis: A review of alkaline water electrolysis, pem water electrolysis and high temperature water electrolysis," *International Journal of Engineering and Advanced Technology*, vol. ISSN, pp. 2249–8958, Feb. 2015.

[89] M. Bodner, A. Hofer, and V. Hacker, "H2 generation from alkaline electrolyzer," *WIREs Energy and Environment*, vol. 4, no. 4, pp. 365–381,

[90] Y. Zheng, S. You, H. W. Bindner, and M. Münster, "Optimal day-ahead dispatch of an alkaline electrolyser system concerning thermal–electric properties and state-transitional dynamics," *Applied Energy*, vol. 307, p. 118 091, 2022. DOI: https://doi.org/10.1016/j.apenergy.2021.118091.

[91] M. Carmo, D. L. Fritz, J. Mergel, and D. Stolten, "A comprehensive review on pem water electrolysis," *International Journal of Hydrogen Energy*, vol. 38, no. 12, pp. 4901–4934, 2013. DOI: https://doi.org/10.1016/j.ijhydene.2013.01.151.

[92] A. Pandiyan, A. Uthayakumar, R. Subrayan, S. W. Cha, and S. B. Krishna Moorthy, "Review of solid oxide electrolysis cells: A clean energy strategy for hydrogen generation," *Nanomaterials and Energy*, vol. 8, no. 1, pp. 2–22, 2019. DOI: 10.1680/jnaen.18.00009.

[93] M. Bodner, A. Hofer, and V. Hacker, "H2 generation from alkaline electrolyzer," *WIREs Energy and Environment*, vol. 4, no. 4, pp. 365–381, 2015. DOI: https://doi.org/10.1002/wene.150.

[94] R. Fang and Y. Liang, "Control strategy of electrolyzer in a wind-hydrogen system considering the constraints of switching times," *International Journal of Hydrogen Energy*, vol. 44, no. 46, pp. 25 104–25 111, 2019, Special Issue on International Conference on Novel Functional Materials 2018. DOI: https://doi.org/10.1016/j.ijhydene.2019.03.033.

[95] L. Chen, X. Dong, Y. Wang, and et al., "Separating hydrogen and oxygen evolution in alkaline water electrolysis using nickel hydroxide," *Nature Communications*, vol. 7, p. 11 741, 2016. DOI: 10.1038/ncomms11741.

[96] C. Varela, M. Mostafa, and E. Zondervan, "Modeling alkaline water electrolysis for power-to-x applications: A scheduling approach," *International Journal of Hydrogen Energy*, vol. 46, no. 14, pp. 9303–9313, 2021. DOI: https://doi.org/10.1016/j.ijhydene.2020.12.111.

[97] G. Matute, J. Yusta, J. Beyza, and L. Correas, "Multi-state techno-economic model for optimal dispatch of grid connected hydrogen electrolysis systems operating under dynamic conditions," *International Journal of Hydrogen Energy*, vol. 46, no. 2, pp. 1449–1460, 2021. DOI: https://doi.org/10.1016/j.ijhydene.2020.10.019.

[98] C. Lafforgue, A. Zadick, L. Dubau, F. Maillard, and M. Chatenet, "Selected review of the degradation of pt and pd-based carbon-supported electrocatalysts for alkaline fuel cells: Towards mechanisms of degradation," *Fuel Cells*, vol. 18, no. 3, pp. 229–238, 2018. DOI: https://doi.org/10.1002/fuce.201700094.

[99] Ø. Ulleberg, "Modeling of advanced alkaline electrolyzers: A system simulation approach," *International Journal of Hydrogen Energy*, vol. 28, no. 1, pp. 21–33, 2003. DOI: https://doi.org/10.1016/S0360-3199(02)00033-2.

[100] H. Niaz and J. Liu, "A mixed integer dynamic optimization approach for a hybrid-stand alone solar and wind powered alkaline water electrolyser for renewable hydrogen," in *31st European Symposium on Computer Aided Process Engineering*, ser. Computer Aided Chemical Engineering, M. Türkay and R. Gani, Eds., vol. 50, Elsevier, 2021, pp. 1285–1291. DOI: https://doi.org/10.1016/B978-0-323-88506-5.50198-4.

[101] C. Huang, Y. Zong, S. You, and C. Træholt, "Economic model predictive control for multi-energy system considering hydrogen-thermal-electric dynamics and waste heat recovery of mw-level alkaline electrolyzer," *Energy Conversion and Management*, vol. 265, p. 115 697, 2022. DOI: https://doi.org/10.1016/j.enconman.2022.115697.

[102] M. H. Ali Khan *et al.*, "Designing optimal integrated electricity supply configurations for renewable hydrogen generation in australia," *iScience*, vol. 24, no. 6, p. 102 539, 2021. DOI: https://doi.org/10.1016/j.isci.2021.102539.

[103] J. Brauns and T. Turek, "Alkaline water electrolysis powered by renewable energy: A review," *Processes*, vol. 8, no. 2, 2020. DOI: 10.3390/pr8020248.

[104] O. Schmidt, A. Gambhir, I. Staffell, A. Hawkes, J. Nelson, and S. Few, "Future cost and performance of water electrolysis: An expert elicitation study," *International Journal of Hydrogen Energy*, vol. 42, no. 52, pp. 30 470–30 492, 2017. DOI: https://doi.org/10.1016/j.ijhydene.2017.10.045.

[105] Y. Wang, Z. Zhou, A. Botterud, K. Zhang, and Q. Ding, "Stochastic coordinated operation of wind and battery energy storage system considering battery degradation," *Journal of Modern Power Systems and Clean Energy*, vol. 4, no. 4, pp. 581–592, 2016.

[106] C. Varela, M. Mostafa, and E. Zondervan, "Modeling alkaline water electrolysis for power-to-x applications: A scheduling approach," *International Journal of Hydrogen Energy*, vol. 46, no. 14, pp. 9303–9313, 2021.

[107] Global Modeling and Assimilation Office, *inst3_3d_asm_Cp: MERRA-2 3D IAU State, Meteorology Instantaneous 3-hourly (p-coord, 0.625x0.5L42), version 5.12.4*, Accessed 11-21-2022, Greenbelt, MD, USA, 2015. DOI: 10.5067/VJAFPLI1CSIV.

[108] B. Efron and R. Tibshirani, *An Introduction to the Bootstrap*. Boca Raton, FL: Chapman & Hall/CRC, 1993, Software Archived 2012-07-12 at archive.today.

[109] J. P. Rosenfeld and E. Donchin, "Resampling (bootstrapping) the mean: A definite do," *Psychophysiology*, vol. 52, no. 7, pp. 969–972, 2015. DOI: https://doi.org/10.1111/psyp.12421.

[110] M. Hasni, M. Aguir, M. Babai, and Z. Jemai, "Spare parts demand forecasting: A review on bootstrapping methods," *International Journal of Production Research*, vol. 57, no. 15-16, pp. 4791–4804, 2019. DOI: 10.1080/00207543.2018.1424375.

[111] W. H. Beasley and J. L. Rodgers, "Bootstrapping and Monte Carlo methods," in *APA Handbook of Research Methods in Psychology, Vol. 2. Research Designs: Quantitative, Qualitative, Neuropsychological, and Biological*, H. Cooper, P. M. Camic, D. L. Long, A. T. Panter, D. Rindskopf, and K. J. Sher, Eds., American Psychological Association, 2012, pp. 407–425. DOI: 10.1037/13620-022.

[112] M. Ball and M. Wietschel, "The future of hydrogen – opportunities and challenges," *International Journal of Hydrogen Energy*, vol. 34, no. 2, pp. 615–627, 2009. DOI: https://doi.org/10.1016/j.ijhydene.2008.11.014.

[113] Y. Seo, H. Park, S. Lee, J. Kim, and S. Han, "Design concepts of hydrogen supply chain to bring consumers offshore green hydrogen," *International Journal of Hydrogen Energy*, 2023. DOI: https://doi.org/10.1016/j.ijhydene.2023.01.030.